# An effect of *miR-142* on mouse lung alveolar epithelial lineage formation during development

Inaugural Dissertation
Submitted to the
Faculty of Medicine
In partial fulfillment of the requirements
for the **Dr. biol. hom.** – Degree
Of the Faculty of Medicine of the
Justus Liebig University Giessen
Germany

by
Amit Shrestha
of
Bhaktapur, Nepal

Giessen, 2018

From the Department of Internal Medicine II and
Excellence Cluster Cardio-Pulmonary System (ECCPS)
of the Faculty of Medicine of the Justus Liebig University Giessen
Director/Chairman: Prof. Dr. Werner Seeger

First Supervisor : Prof. Dr. Saverio Bellusci

Second Supervisor : Prof. Dr. Christos Samakovlis

Date of Defense : 17.07.2018

## Declaration

“I declare that I have completed this dissertation single-handedly without the unauthorized help of a second party and only with the assistance acknowledged therein. I have appropriately acknowledged and referenced all text passages that are derived literally from or are based on the context of published or unpublished work of others, and all the information that relates to verbal communications. I have abided by the principles of good scientific practice laid down in the charter of Justus Liebig University of Giessen in carrying out the investigations described in the dissertation.”

Amit Shrestha

# Table of Contents

# List of Tables

# List of Figures

## Abbreviations and Acronyms

| | |
|---|---|
| 3' UTR | 3' Untranslated Region |
| 7AAD | 7-Aminoactinomycin D |
| AML | Acute myeloid leukemia |
| Apc | Adenomatous polyposis coli |
| APC - cy7 | Allophycoocyanin – cycnine 7 |
| Aqp5 | Aquaporin5 |
| AT1 | Type 1 alveolar epithelial cells |
| AT2 | Type 2 alveolar epithelial cells |
| BASC | Bronchoalveolar stem cells |
| Bmp | Bone morphogenetic protein |
| BP | Bipotent progenitor |
| BPD | Bronchopulmonary Dysplasia |
| Bzrap1 | Benzodiazepine receptor associated protein 1 |
| CD 31 | Cluster of differentiation 31 |
| CD 45 | Cluster of differentiation 45 |
| CD49f | Integrin alpha 6 |
| CMV | Cytomegalovirus |
| COPD | Chronic Obstructive Pulmonary Disease |
| CreErt2 | Fusion protein between Cyclization recombinase and triple mutated human estrogen receptor ligand binding domain |
| CTNNB1 | catenin beta 1 |
| Cy7 | Cyanine 7 |
| DAPI | 4′,6-diamidino-2-phenylindole, dihydrochloride |
| Dex | Dexamethasone |
| DMEM | Dulbecco's Modified Eagle's Medium |
| DNA | Deoxyribonucleic acid |

| | |
|---|---|
| dNTP | Deoxyribonucleotide triphosphate |
| E | Embryonic |
| Ecad | Cadherin 1 |
| ECL | Enhanced Chemiluminescence |
| EDTA | Ethylenediaminetetraacetic acid |
| EGFR | Epidermal growth factor receptor |
| Ep300 | Histone acetyltransferase p300 |
| Epcam | Epithelial cell adhesion molecule |
| ERK | Extracellular receptor kinase |
| ES | Embryonic stem cells |
| ESCC | Esophageal squamous-cell carcinoma |
| EtOH | Ethanol |
| Etv5 | Ets variant 5 |
| FACS | Fluorescence-activated cell sorting |
| FBS | Fetal bovine serum |
| Fgf | Fibroblast growth factor |
| Fgf10 | Fibroblast growth factor 10 |
| Fgfr | Fibroblast growth factor receptor |
| FITC | Fluorescein isothiocyanate |
| Fli1 | Friend leukemia integration 1 transcription factor |
| Fzd7 | Frizzled class receptor 7 |
| Gata2 | GATA binding protein 2 |
| GFP | Green Fluorescent Protein |
| Gli | Glioma-associated oncogene |
| gp130 | Glycoprotein 130/Interleukin 6 signal transducer |
| GSK3ß | Glycogen synthase kinase 3 beta |
| H/E | Hematoxylin/Eosin |

| | |
|---|---|
| HBSS | Hanks' Balanced Salt solution |
| HDAC3 | Histone deacetylase 3 |
| HMGA2 | High mobility group AT-hook 2 |
| Hprt | Hypoxanthine guanine phosphoribosyl transferase |
| HRP | Horseradish peroxidase |
| IF | Immunofluorescence |
| Id2 | Inhibitor of differentiation 2 |
| IP | Intraperitoneal |
| IPF | Idiopathic Pulmonary Fibrosis |
| ISL1 | Insulin gene enhancer protein ISL-1 |
| Kras | Kirsten Rat Sarcoma oncogene |
| Lef1 | Lymphoid enhancer binding factor 1 |
| Mapk | Mitogen activated protein kinases |
| mESCs | Mouse embryonic stem cells |
| miRs | microRNA |
| Oct4 | Octamer Binding transcription factor 4 |
| P63 | Tumor protein63 |
| PAH | Pulmonary Arterial Hypertension |
| PBS | Phosphate Buffered saline |
| PCR | Polymerase Chain Reaction |
| Pdfr | Platelet derived growth factor |
| Pdpn | Podoplanin |
| pErk | phosphoERK |
| PFA | Paraformaldehyde |
| PI3K-Akt | Phosphoinositide-3 kinase-Protein kinase B |
| Prox1 | Prospero Homeobox 1 |
| PVDF | Polyvinylidene difluoride membrane |

| | |
|---|---|
| qPCR | Quantitative Polymerase Chain Reaction |
| Ras | Rat sarcoma |
| Ret | Receptor tyrosine kinase |
| RISC | RNA induced silencing complex |
| RT | Room temperature |
| SCGB1A1 | Secretoglobin family 1A member 1 (Club cells) |
| Scl (TAL1) | TAL bHLH transcription factor 1, erythroid differentiation factor |
| SDS | Sodium dodecyl sulphate |
| SEM | Sub-mesothelial mesenchyme |
| SftpC | Surfactant Protein C |
| SHH | Sonic Hedgehog |
| SMM | Sub-mesothelial mesenchyme |
| Sox2 | SRY (Sex determining region Y)-box 2 |
| Sox9 | SRY (Sex-Determining Region Y)-Box 9 |
| Spry2 | Sprouty RTK signaling antagonist 2 |
| TAE | Tris Acetate buffer |
| Tam | Tamoxifen |
| TBST | Tris- Buffered Saline-Tween |
| Tgfβ | Transforming growth factor beta |
| Tgfβr1 | Transforming growth factor beta receptor 1 |
| Tom | Tomato |
| TTF-1 | Thyroid transcription factor 1 or NKX2.1 |
| Vegfr2 | Vascular endothelial growth factor receptor 2 |
| WB | Western blot |
| Wnt | Wingless and Int |

# 1. Introduction

## 1.1 Introduction to microRNAs

MicroRNAs (miRs) are small regulatory RNAs that account for approximately 1% of the genome. These are 21-25 nucleotide-long, single-stranded non-coding RNA molecules that regulate post-transcriptional gene regulation in eukaryotes by binding to the 3' untranslated region (UTR) of the target mRNA, leading to mRNA cleavage, degradation or translational repression (Ambros, 2004; Bartel, 2004; Huntzinger and Izaurralde, 2011).

The maturation of the hairpin transcript of the miRNA can give rise to a 5p strand (present in the forward 5'-3' position) and 3p (complementary to the 5p strand), both of which allow the silencing of specific sets of genes through base pairing to a minimal recognition sequence (Ambros and Lee, 2004). It is believed that more than 60% of protein-coding genes in mammals are controlled by miRs (Esteller, 2011). From the discovery of *Lin-4* as the first miR to be identified in C.elegans**,** more than two thousand miRs have been discovered up to now (miRBase.org). Each miR has the potential to regulate hundreds of mRNAs, and in-turn, a single mRNA can be targeted by many miRs (Friedman et al., 2009; Wu et al., 2011)). These small RNAs are now recognized as a major class of gene expression regulators with a crucial function in numerous biological processes, such as cell development, differentiation, proliferation, stress response and apoptosis (Ameres and Zamore, 2013).

### 1.1.1 MicroRNA biogenesis

The biogenesis of miRs starts with the transcription of independent miR genes or introns of protein-coding genes into primary-miRs (Pri-miRs) by RNA polymerase II. The transcripts are polyadenylated and capped, a characteristic of RNA polymerase II transcription. The Pri-miRs then fold into a hairpin loop, acting as a substrate for two members of the RNase III family of enzymes, Drosha and Dicer (Krol et al., 2010). The 5' and 3' arm of the Pri-miR hairpin loop is then endo-nucleolytically cleaved by the Drosha/DGCR8 (DiGeorge critical region 8) complex in mammals, or by Pasha in Drosophila melanogaster into precursor miRNA (pre-miR) in the nucleus. After the nuclear processing, the pre-miR is recognized and exported into the cytoplasm by Exportin 5. In the cytoplasm, a second RNase III enzyme, Dicer, cleaves the loop region and forms a

21-25 nucleotide miRNA-miRNA* duplex from pre-miRNA. Dicer interacts with the TRBP (Transactivation-response RNA binding protein) and PCAT (Protein Kinase R-activating protein) (Ameres and Zamore, 2013; Jonas and Izaurralde, 2015) that facilitates the Dicer-mediated cleavage of pre-miRNA. After the cleavage, the interaction between Dicer, TRBP, and PCAT is dissociated. Subsequently, the double-stranded duplexes are separated by helicase, and one of the strands in the duplex with the thermodynamically less stable 5' end will become mature miRNA, also referred to as the guide strand (i.e. both the 3p and 5p strand could be functional mature miRNAs). The functional guide strand, which is complementary to the target mRNA, is loaded to the Argonaute effector complex – also known as the RNA induced silencing complex (RISC) – leading to target mRNA degradation, translational repression or mRNA deadenylation. The particular effect of an miRNA is based on the degree of complementarity between the miRNA and the target mRNA, in combination with the Argonaute proteins in a RISC complex. The other strand, also termed the passenger strand, is subsequently degraded (He and Hannon, 2004; Krol et al., 2010; Winter et al., 2009).Schematic representation of microRNA biogenesis is shown in Fig. 1.

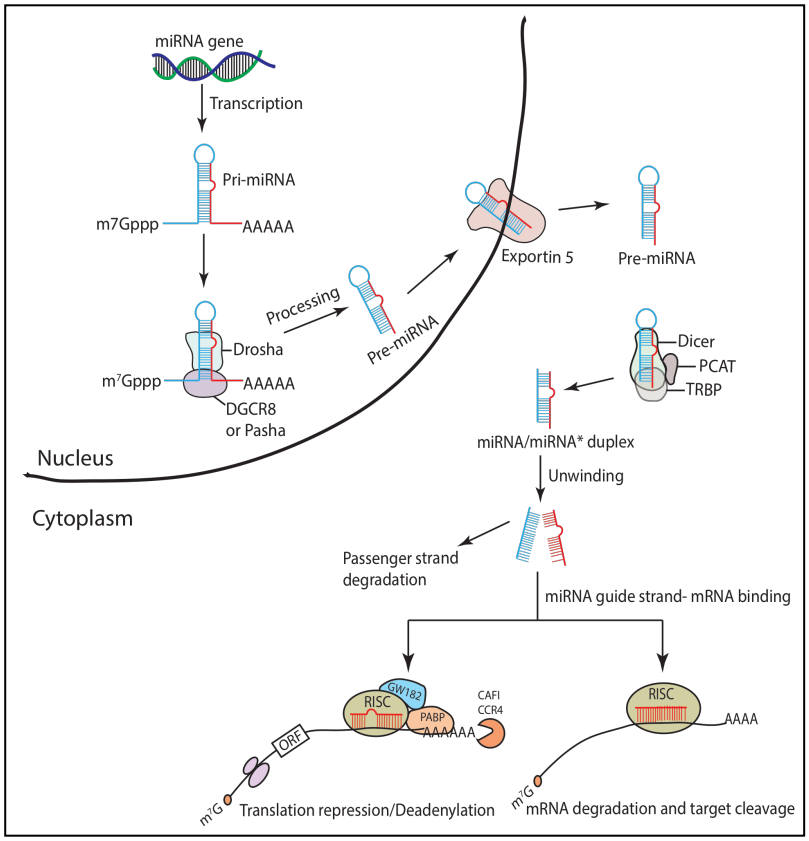


**Figure 1. Schematic representation of microRNA biogenesis** (adapted from Ameres and Zamore, 2013; He and Hannon, 2004; Krol et al., 2010)

## 1.2 Lung development

During mouse embryonic lung development, the respiratory system starts to develop from embryonic day 9.5 (E9.5) from ventral foregut endoderm. The expression of the transcription factor Nkx2.1 (also termed as thyroid transcription factor1 or T/EBP1) in the endodermal cells identifies the lung and tracheal progenitors in the foregut endoderm at E9 (Morrisey and Hogan, 2010).

At E9.5, two lateral buds from the ventral foregut endoderm evaginate, forming the primary bronchial buds of the right and left lungs. In subsequent stages of lung development, these primary lung buds undergo continuous branching morphogenesis, leading to the formation of one unique left lobe and four right lobes (cranial or rostral, medial, caudal and accessory) in the mouse, constituting the complete respiratory tree (Cardoso and Lu, 2006; Kimura and Deutsch, 2007; Warburton et al., 2010).

### 1.2.1 Stages of mouse lung development

Lung development can be categorized histologically into four stages.

**a) Pseudoglandular stage (mouse E9.5-E16.5; human week 4-17):**
During this stage, the primary lung buds undergo the process of branching morphogenesis to form a tree-like network of airways, which later become conducting airways. Simultaneously, many of the mesenchymal progenitor cells differentiate into smooth muscle cells, endothelial cells, nerve cells, and chondrocytes; whereas the epithelial progenitor cells differentiate into basal cells, neuroendocrine cells, ciliated cells and secretory cells.

**b) Canalicular stage (mouse E16.5-E17.5; human week 17-26):**
In this stage, double-layered blood capillaries are formed. In addition to this, AT1 and AT2 start to arise from the bipotent alveolar progenitor cells, which first form a primitive respiratory epithelium capable of gas exchange. Furthermore, the lipofibroblasts that are involved in the production of surfactants start to emerge during the canalicular stage (Chao et al., 2015; El Agha and Bellusci, 2014).

**c) Saccular stage (E17.5-P5; human week 26-36):**

The characteristic feature of this stage is the formation of alveolar sacs (primitive alveoli), surfactant production, and expansion of the capillary and lymphatic networks.

**d) Alveolar stage (mouse P5-P30; human 36 weeks-8yrs):**

During the alveolar stage of lung development, the terminal sacs develop into mature alveoli which are characterized by the formation of secondary septae, alveolar myofibroblast formation, and microvascular maturation, as well as a massive increase in alveolar surface area (El Agha and Bellusci, 2014). The adult mouse lung consists of about 2.3 million alveoli with an alveolar surface area of 82 $cm^2$; in an adult human, the lung consists of about 300 million alveoli with an alveolar surface area of 72 $m^2$ (Chao et al., 2015).

Most of the epithelial and mesenchymal cells start to appear during the pseudoglandular stage. Every step during lung development relies on signaling mechanisms as well as mutual interaction between the pulmonary epithelium and surrounding endothelium and mesenchyme. Any developmental defects during this period can lead to severe impairment in lung function in the adult stages (El Agha and Bellusci, 2014; McCulley et al., 2015). Fig. 2 summarizes the stages of lung development.

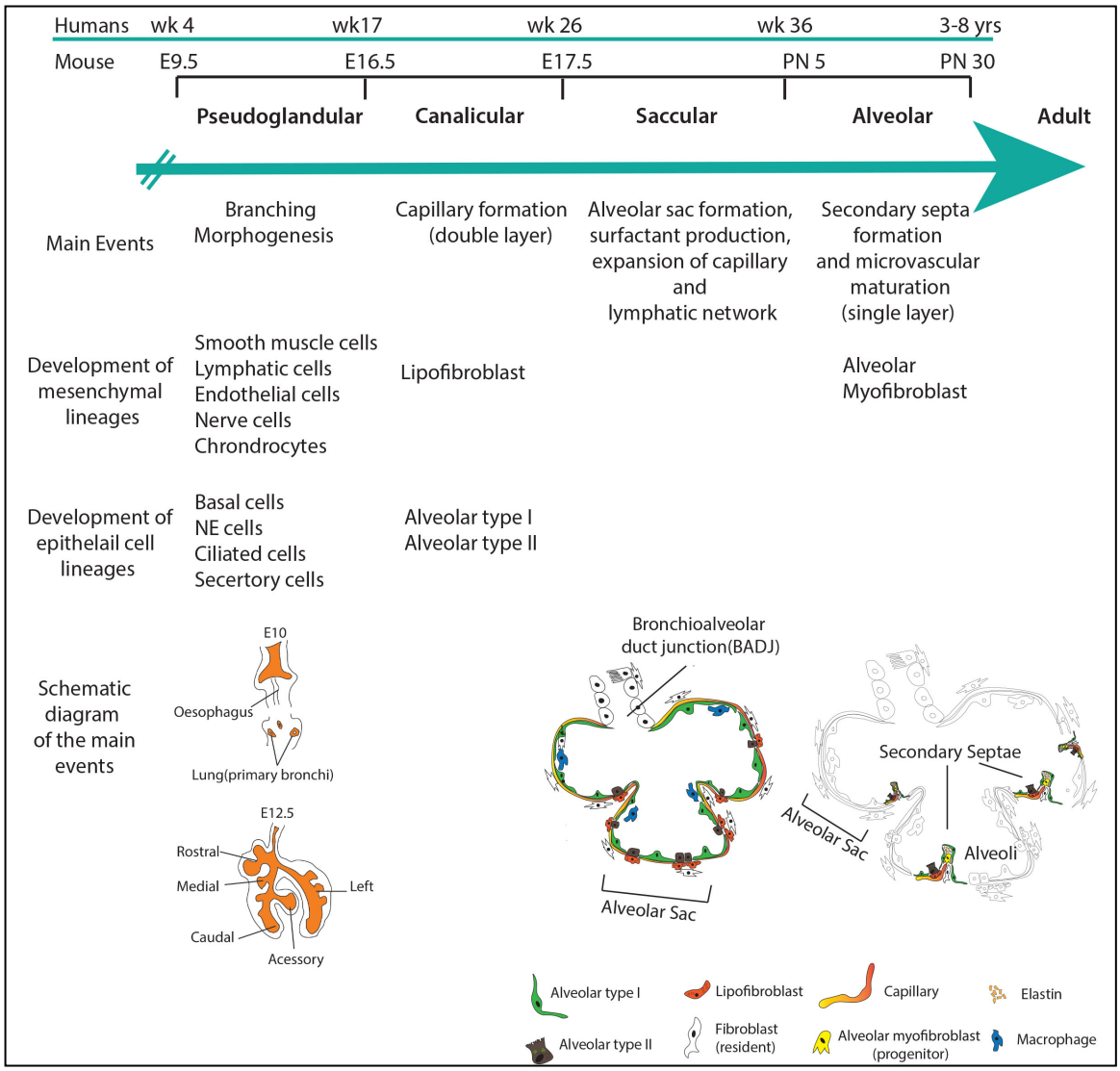


**Figure 2. Stages of murine and human lung development**
(adapted from Chao et al., 2015; El Agha and Bellusci, 2014).

### 1.2.2 Lung mesenchyme

The mesenchyme is an important source of morphogenetic specification and differentiation signals. However, it is also the host of surprisingly complex cell lineages that are critical for normal lung development and function (Herriges et al., 2014; McCulley et al., 2015). At the pseudoglandular stage, the embryonic distal lung bud is composed of three morphologically distinguishable layers: the mesothelium (outer layer), the mesenchyme (middle layer), and the epithelium (inner layer). The mesenchyme is further grouped into two domains, the submesothelial mesenchyme (SMM) and the sub-epithelial

mesenchyme (SEM). Wnt2, Gli, Isl1, Ret, Pdgf receptor alpha, Vegfr2, Prox1, Fgf10 and Tgfβ have been identified as specific markers for different mesenchymal progenitors. The mesenchymal compartment consists of a wide variety of cell types, such as airway smooth muscle cells, vascular smooth cells, resident mesenchymal cells, lipofibroblasts, endothelial cells, chrondocytes, nerve cells, alveolar myofibroblasts, lymphatic cells, and others. The mesenchyme is responsible for providing critical signals that control epithelial branching morphogenesis as well as epithelial differentiation. It is believed that mesenchymal progenitors play an important role not only during lung development but also in homeostasis, as well as repair after injury and regeneration (Chao et al., 2015; El Agha and Bellusci, 2014).

### 1.2.3 Lung epithelium

Most of the gas exchange processes take place across the epithelilal cells lining the distal lungs. These epithelial cells are derived from multipotent epithelial progenitors, located at the tips during pseudoglandular stages in the embryonic lung. These cells are cuboidal shaped and express the transcription factors Sox9 and Id2 (Rawlins et al., 2009). As lung development progresses, the lineage commitment of epithelial progenitor cells becomes restricted to specific cell types (Rock and Hogan, 2011).

During this stage, some distal epithelial progenitor cells start losing Sox9 and Id2 expression and express the proximal marker Sox2, thus giving rise to proximal bronchiolar progenitor cells, whereas the cells retaining both Sox9 and Id2 expression become distal alveolar progenitor cells (El Agha and Bellusci, 2014). Distal epithelial progenitors remain at the periphery of the lungs until late E17.5 or early E18.5 (Laresgoiti et al., 2016). Various pathways like Notch, Wnt, Bmp and Fgf signaling have been shown to be involved in epithelial progenitor cell fate determination during lung development (Rock and Hogan, 2011)

#### 1.2.3.1 Alveolar lung epithelium

The canalicular and saccular stages, extending from E16.5 to E18.5, provide the framework for future alveolar development during mouse lung development, and are considered a vital stage towards alveologenesis, as the formation of distal airspace saccules as well as the differentiation of alveolar epithelial cells occurs. Any interruption in this step during lung development can severely damage the lungs of neonates, leading to

various serious diseases like bronchopulmonary dysplasia (BPD). Meanwhile, at E17.5, an alveolar epithelial differentiation occurs at the bronchio-alveolar junction, which later proceeds towards the distal airway tip by E18.5. This leads to the formation of the alveolar type I (AT1) and the alveolar type II (AT2) cells, two of the major epithelial cell lineages lining the alveolar sacs (Laresgoiti et al., 2016; Wang et al., 2016b). AT1 are flat squamous cells that are the primary site for gas exchange and fluid homeostasis. They cover approximately 95% of the luminal surface of the alveoli. On the other hand, AT2 cells are cuboidal in shape and are usually observed at the corner of the alveoli. AT2 cells are rich in lamellar bodies that primarily secrete surfactant protein C (Sftpc), which helps in preventing alveolar collapse by decreasing lung surface tension and contributing to the host defense mechanism (Rock and Hogan, 2011; Whitsett et al., 2010).

The mechanisms regulating alveolar epithelial cell proliferation and differentiation, as well as the advancement of distinct lung progenitor cells towards given mature alveolar cell types, are poorly understood (McQualter et al., 2010; Weiss et al., 2008; Zemke et al., 2009). It has been proposed that AT2 cells can function as progenitors for AT1 cells, thus contributing to alveolar repair after lung injury. Recent studies on the lung epithelium using cell-specific markers, as well as single-cell transcriptomics during lung development, demonstrated that AT1 and AT2 cells are derived from common bipotent progenitor cells (Desai et al., 2014; Treutlein et al., 2014), and that weeks after birth, new AT1 and AT2 cells can be regenerated from rare, self-renewing, long-lived, mature AT2 cells. Approximately 1% of the mature AT2 cells show this stem cell capacity. This stem cell function is widely activated by AT1 cell injury, EGFR (epidermal growth factor receptor) ligand treatment *in vitro*, and oncogenic Kras (G12D) treatment *in vivo*, indicating that AT2 cells can contribute to lung repair after injury, and function as progenitors for AT1 cells (Desai et al., 2014). On the contrary, post-natally, AT1 are terminally differentiated cells that can be reactivated to proliferate and trans-differentiate to AT2 during lung regeneration induced by pneumonectomy (Jain et al., 2015). It is still possible that immature AT1 cells also exist in the AT1 lineage postnatally and that these cells have the capacity to proliferate and give rise to AT2 cells. Until better markers for pre-AT1 or mature AT1 have been characterized, it will be difficult to make conclusions about the exact nature of the cells contributing to the repair process. Recently, the role of histone deacetylase 3 (HDAC3) in the spreading of AT1 and a disruption of lung sacculation was reported. It was shown that *Hdac3* expressed in alveolar progenitors represses the expression of *miR-17-92*, thus allowing proper Tgfβ signaling during lung sacculation (Wang et al., 2016b). Interestingly, specific deletion of *Hdac3* in the developing lung mesenchyme also

displayed impairment in AT1 differentiation, correlating with decreased Ctnnb1 signaling in the epithelium, whereas rescue of Ctnnb1 signaling in the mutant lung partially rescues AT1 cell differentiation defects (Wang et al., 2016a).

A defect in epithelial differentiation and proliferation was also observed in Fgf10 hypomorphic lungs, which showed impairment in AT2 lineages (Ramasamy et al., 2007). Using *Fgf10* heterozygous (*Fgf10*$^{+/-}$) lungs, Chao and colleagues also demonstrated a decrease in the AT2/AT1 cell number ratio, suggesting that Fgf10 represents a crucial molecule regulating the differentiation of the bipotent progenitor cells towards the AT2 lineage (Chao et al., 2017). In addition, *Etv5*, a downstream target of Fgf10, has been recently reported to be important for the maintenance and differentiation of the AT2 cells. Conditional deletion of *Etv5* expression in differentiated AT2 cells postnatally leads to the decrease in the AT2 signature, and an associated increase in the AT1 signature (Zhang et al., 2017).

### 1.3 MicroRNA in lung development and diseases

A complex network of signaling pathways, such as Fgf, Tgfβ, Shh and Wnt pathways, are involved in lung development processes (Cardoso and Lu, 2006; Warburton et al., 2010). MicroRNAs are known to target genes involved in various signaling pathways. Therefore, it is likely that microRNAs regulate the multiple signaling mechanisms controlling lung development (Bhaskaran et al., 2009).

In recent years, miRNAs have been shown to regulate lung development, homeostasis, maintenance and disease (Ornitz and Yin, 2012). Conditional deletion of Dicer, an enzyme vital for miR processing, in mouse lung epithelial cells using a Cre/LoxP based approach, exhibited defects in epithelial lung branching morphogenesis, revealing the importance of miRNAs in epithelial morphogenesis (Harris et al., 2006). Many of the miRs are differentially expressed during different phases of lung development (Bhaskaran et al., 2009; Williams et al., 2007). The expression of the *miR-17-92* cluster has been observed in the epithelium and mesenchyme during the pseudoglandular stage of lung development (Carraro et al., 2009). Targeted deletion of members of the *miR-17-92* cluster showed early lethality, smaller embryos, and a severe hypoplastic lung phenotype without specific defects in branching morphogenesis; in contrast, overexpression results in hyperproliferation and inhibition of differentiation of embryonic lung epithelial progenitor cells (Lu et al., 2007; Ventura et al., 2008).

During the early stages of lung development, lower expression of *miR-127* and *miR-351* were detected. Overexpression of *miR-127* at the pseudoglandular stage showed decreased branching and enlarged terminal buds. However, both miRs exhibited higher expression during the saccular and alveolar stages. The expression pattern of these two miRs gradually shifted from the mesenchymal compartment towards the epithelial compartment lining the airways , suggesting their roles in cellular reorganization, differentiation of alveolar epithelial cells and or mesenchymal to epithelial transition (Bhaskaran et al., 2009). Growing evidence indicates that miRs are not only involved during lung development but also implicated in various pulmonary diseases like COPD, asthma, IPF, BPD, cystic fibrosis, and lung cancer. Abnormal expression of certain microRNAs in the lungs can contribute to the pathogenesis of lung disease (Angulo et al., 2012; Johar et al., 2015; Sessa and Hata, 2013). Table 1 summarizes the list of miRs involved in various pulmonary diseases.

**Table 1. Lists of microRNAs involved in various pulmonary diseases** (Compiled from Angulo et al., 2012; Johar et al., 2015; Sessa and Hata, 2013)

| Lung Disease | microRNAs differentially expressed in lung diseases |
|---|---|
| Lung Cancer | *miR-17-92 cluster, miR-21, miR-146b, miR-155, miR218,miR-200 family,miR-31,let-7, miR-1, miR-34,miR-133b,miR218* |
| Asthama | *miR126, miR-133a, miR-145a, miR-146a, miR-146b, miR-181, let-7, miR-21, miR-221, miR-222, miR-106a, miR-20b, miR-155* |
| Idiopathic Pulmonary Fibrosis (IPF) | *miR29, miR-2, miR-154, let-7d, miR-17,miR-155, miR-125b; miR-200* |
| Chronic Obstructive Pulmonary Disease (COPD) | *miR-17-92 cluster ,miR-206,miR-143,miR-145, miR-21,miR-27a,miR-204,miR-210,miR-424, miR-503,miR-150* |
| Cystic Fibrosis | *miR-155 ,miR-101,miR-494,miR-126,miR-138* |
| Pulmonary Arterial Hypertension (PAH) | *miR-17-92 cluster, miR-206, miR-143, miR-145, miR-21, miR-27a, miR-204, miR-210, miR-424, miR-503, miR-150* |
| Acute Lung Injury | *miR-127, miR-21, miR-155, miR-146, miR-32, miR-466-5p, miR-466-3p* |
| Hypercapnia | *miR-183* |

## 1.4 *miR-142*: a multifaceted regulator of organogenesis, homeostasis and disease

The *miR-142* gene is located on chromosome 11 of the mouse genome and on chromosome 17 of the human genome. *miR-142* encodes for two mature products, derived from the same precursor. The microRNA derived from the 3' arm is termed *miR-142-3p* and the one generated from the 5' arm is termed *miR-142-5p* (Fig.3). Both the miRNAs are evolutionarily conserved and functionally active. *miR-142* is emerging as a critical regulator of many biological processes and associated signaling pathways during embryonic development, homeostasis and disease. The diverse functions of this miRNA in various developmental and disease processes are summarized below.

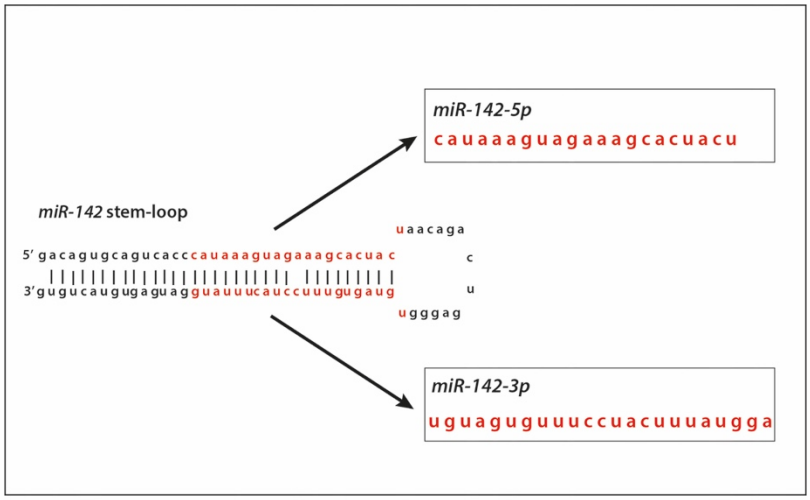


**Figure 3. *miR-142* hairpin loop structure**

### 1.4.1 *miR-142* in hematopoiesis

*miR-142-3p* was first identified in hematopoietic stem cells and is one of the highly expressed microRNAs in hematopoietic cell lineages (Chen et al., 2004), and has been shown to regulate the formation and differentiation of hematopoietic stem-progenitor lineages and heart development in zebrafish (Fan et al., 2014; Lu et al., 2013; Nishiyama et al., 2012). The earliest known regulator of the hematoendothelial lineages was pointed out to be *miR-142-3p,* which acts upstream of the hematopoietic transcription factors Fli-1, Gata2, Etv5 and Scl (Tal-1). *miR-142-3p* turns out to be essential for the specification

of the hemangioblast precursors of the hematopoietic stem cell lineages, suggesting that miRs can be instructive determinants of cell fate during development (Nimmo et al., 2013). Using *miR-142* general knock out mice, Krammer and colleagues demonstrated that loss of *miR-142* not only leads to abnormal hematopoietic lineage formation, but also to serious immunodeficiency. *miR-142* KO mice exhibit hypo-globulinemia and very low immune response against soluble antigens and viruses (Kramer et al., 2015). Furthermore, independent studies using gene-trapped-based *miR-142* KO mice also indicated impaired megakaryocyte maturation correlating with abnormal platelet formation and thrombocytopenia (Chapnik et al., 2014). We reported similar abnormalities in our classical *miR-142* knock out mice (Shrestha et al., 2015). Collectively, these findings suggest that *miR-142* is a master regulator of hematopoiesis.

### 1.4.2 Role of *miR-142* in stem cells

Stem cell decision to self-renew or differentiate is tightly regulated. Evidence shows that miRs play a key role in stem cell homeostasis. It was recently reported that *miR-142* is differentially expressed in mouse embryonic stem cells (mESCs). The authors reported the generation of a reporter cassette made of a bi-directional promoter driving the expression of a normalizer (H2B-mCherry) and a *miR* activity detector (H2B-Citrine), the latter containing a *miR-142* target sequence in its 3'UTR. This bi-directional reporter is made of a back-to-back arrangement of CAG promoters with four CMV enhancers allowing efficient expression in mESCs undergoing differentiation and the best signal-to-noise ratio for measurement of *miR* activity in single cells. The precise measurement of the H2B-Citrine over H2B-mCherry fluorescence is representative of *miR-142* activity. Using this reporter cassette, the authors confirmed that *miR-142-3p* is highly expressed in undifferentiated cells and downregulated in differentiated cells. In addition, they also demonstrated that the expressionof *miR-142* locks the mESCs in an undifferentiated state. Deletion of *miR-142* in embryonic stem cells leads to the differentiation of these cells along the neuroectoderm, mesoderm and endoderm fate with a complete absence of *Oct4* expression, which is a pluripotency marker. By contrast, overexpression of *miR-142* prevented the differentiation of the ES cells and maintained *Oct4* expression. A double negative feedback loop between KRas/ERK and *miR-142* levels has been suggested as a mechanism of action. Low level of *miR-142* induces KRas and Erk phosphorylation thus initiating differentiation and vice versa (Sladitschek and Neveu, 2015). This suggests a novel mechanism by which *miR-142* can play an important role in maintaining stem cell pluripotency during organogenesis.

### 1.4.3 Role of *miR-142* in cardiomyocyte hypertrophy

Postnatally, adaptive cardiomyocyte hypertrophy is a normal mechanism allowing an increase in heart size without requiring cell proliferation. However, in diseases such as hypertension, aortic valvular stenosis leads to an increase in cardiac workload, and a maladaptive cardiomyocyte hypertrophy has been observed. Prolonged maladaptive hypertrophy is likely to lead to heart failure. The molecular mechanisms controlling adaptive versus maladaptive cardiac growth are therefore critical from a therapeutic point of view. Interestingly, an inverse relationship has been observed between the levels of *miR-142* and cardiac hypertrophy. *miR-142-5p* and *miR-142-3p* were found to be down-regulated during cardiac hypertrophy, by mechanisms requiring *Ep300*, a transcription factor involved in cardiac growth and MAP kinase activity. *Ep300* is a direct target of *miR-142* (Sharma et al., 2012). The levels of Ep300 are sharply increased during hemodynamic stress, heart failure, and cardiac hypertrophy. However, a small increment or decrement in the level of Ep300 can drastically influence the extent of adaptive cardiac hypertrophy and risk of heart failure (Morimoto et al., 2008; Wei et al., 2008). In addition, *miR-142* can inhibit the cytokine signaling mechanism by targeting the cytokine receptor *gp130*, a critical receptor required for cardiac muscle cell survival. Down-regulation of *miR-142* in mice leads to increase in *Ep300* and *gp130*, ultimately increasing the rate of cytokine-mediated survival signals, reduction in apoptosis and heart failure during postnatal growth of the heart. These results suggest that *miR-142* is essential for the successful adaptation and survival of the heart due to changing hemodynamic demand *in vivo* (Sharma et al., 2012).

### 1.4.4 *miR-142* as a biomarker for the diseased state

miRs have emerged as biomarkers of various diseases such as cancer and heart disorders. In addition, miRs can represent potential gene-specific therapeutic targets in disease models (Schulte and Zeller, 2015). Circulating *miR-142-3p* in serum or plasma was found to be associated with a high risk of cancer recurrence in patients with early-stage lung adenocarcinoma (Kaduthanam et al., 2013). Another study showed that *miR-142-3p* was involved in the progression of esophageal squamous cell carcinoma (ESCC) and identified this miR as a potential prognostic biomarker for ESCC (Lin et al., 2012). Meanwhile, *miR-142-5p*, along with *miR-486-5p,* have been suggested as potential biomarkers for early detection of chronic antibody-mediated rejection in kidney transplantation (Iwasaki et al., 2016). Furthermore, the level of *miR-142-3p* and *-5p* are

significantly decreased in acute and chronic heart failure, respectively, indicating that these two miRs may act as specific biomarkers for heart failure (Vegter et al., 2016).

### 1.4.5 *miR-142* and immune tolerance

Autoimmune diseases are disorders of the immune system where the body's own immune response targets healthy cells for destruction due to decreased immunologic tolerance to auto reactive immune cells. Recent studies have shown that aberrant miR expression often correlates with the onset and prognosis of autoimmune disorders. This observation suggests that dysregulation in miR expression can elicit a serious effect on immune response and immune tolerance (Chen et al., 2013).

Developing a drug-free immune tolerance therapy or the successful use of a very low number of immunosuppressive drugs can make a huge impact in the field of human organ transplantation. A high level of *miR-142-3p* was observed in the peripheral blood mononuclear cells from immune-tolerant patients who underwent a kidney transplant. Further work suggested that a negative feedback loop involving Tgfβ signaling and *miR-142-3p* in peripheral blood mononuclear cells might be responsible for contributing to immune tolerance (Danger et al., 2012).

In addition, mice treated with a *miR-142*-regulated lentiviral vector encoding GFP and subsequently vaccinated with GFP are tolerant to the development of antibodies against GFP and display increased GFP-specific regulatory T cells. In control animals treated with the non-related *miR-122a*, a robust immune response to GFP is observed after vaccination. It was therefore proposed that *miR-142* can be used to induce immunologic tolerance to a gene-encoded antigen and could be used as a tool for gene therapy in patients with autoimmune disorders or patients requiring organ transplantation (Annoni et al., 2009).

### 1.4.6 *miR-142* in cancer

Cancer studies suggest that miRs are useful biomarkers of cancer development and tumor stages. Recent evidence has shown that miR mutations or mis-expressions correlate with various human cancer, indicating that miRs can function as tumor suppressors and/or oncogenes depending on the cellular function of their targets (Calin and Croce, 2006). The expression level of *miR-142-3p* in cervical cancer epithelial cells was significantly lower

than in healthy cervical epithelial cells, indicating a regulatory impact of *miR-142-3p* in cervical cancer. *miR-142-3p* inhibits cell proliferation and invasion via targeting Frizzled 7 (*Fzd7*) receptor in Hela and SiHa cells. *Fzd7* overexpression was able to reverse the effect induced by *miR-142-3p*. *miR-142-3p* is, therefore, a potential therapeutic target for cervical cancer (Deng et al., 2015). Similarly, *miR-142-3p* has been involved in inhibiting tumor progression and invasion in hepatocellular carcinoma cells (Tsang et al., 2015; Wu et al., 2011). Furthermore, in acute myeloid leukemia *miR-142-3p* has been found to be downregulated. Increasing the expression of *miR-142-3p* by promoting myeloid differentiation could therefore be a potential strategy for AML treatment (Wang et al., 2012).

Paradoxically, high levels of *miR-142-5p* expression correlate with cancer progression through regulating the Tgfβ-signaling pathway. In particular, *miR-142-5p* targets *Smad3*, thereby suppressing Tgfβ-induced growth inhibition in cancer cells. Overexpression of *miR-142-5p* leads to increased tumor cell proliferation and decreased apoptosis, while silencing of *miR-142-5p* leads to the opposite effects (Ma et al., 2016). Similarly, *miR-142-3p* can repress Tgfβ-induced growth inhibition by targeting the *Tgfβr1* receptor in non-small cell lung carcinoma cell lines (Lei et al., 2014).

A study performed by Isobe and colleagues demonstrated that *miR-142-3p* triggers the progression of tumors in human breast stem cells by targeting *Adenomatous Polyposis Coli* (*APC*). Loss of *APC* expression activates the canonical WNT/CTNNB1 signaling pathway leading to excessive cell growth in breast tissue (Isobe et al., 2014). Furthermore, studies in glioblastoma tumorigenesis showed that Interleukin 6 inhibits *miR-142-3p* expression via the increased methylation of the *miR-142-3p* promoter. In addition, high mobility group AT-hook2 (*HMGA2*), a target of *miR-142-3p,* is upregulated, leading to increased SOX2 expression, a transcription factor required to maintain stem cell-like properties in glioblastoma cells and associated with glioblastoma malignancy (Chiou et al., 2013).

### 1.4.7 Role of *miR-142* during lung development and disease

Increased levels of *miR-142-3p* in serum has been observed in patients with lung adenocarcinoma (Kaduthanam et al., 2013). *miR-142-3p* has also been shown to be upregulated in human breast cancer stem cells, which leads to the activation of the canonical Wnt signaling pathway by reducing the level of APC, thus resulting in enhanced

tumorigenicity (Isobe et al., 2014). Increased levels of *miR-142-3p* were observed in the sputum of patients suffering from severe inflammatory asthma (Maes et al., 2016). In the transgenic mouse model of lung cancer, the expression of *miR-142-5p* is down-regulated and over-expression of this microRNA markedly reduced proliferation in murine cancer cell lines (Liu et al., 2009). However, a study by Kee et al. observed that *miR-142-5p* enhances the vascular smooth muscle cell proliferation by down-regulating the B cell translocation gene (Kee et al., 2013).

During early embryonic lung development, *miR-142-3p* is highly expressed in the lung mesenchyme. Such restricted expression patterns suggest that *miR-142-3p* could play functions in controlling cell lineage formation in the lung mesenchyme. Using an *in vitro* embryonic mouse lung organ culture treated with morpholino (which inhibits microRNA expression and function) specific to *miR-142-3p*, a decreased proliferation of mesenchymal cells, as well as a premature differentiation of smooth muscle progenitor cells, was observed. Further evidence has shown that miR-*142-3p* controls Wnt/*Ctnnb1* (β-catenin) signaling in the mesenchyme by targeting *Adenomatous polyposis coli (APC)*. APC is a negative regulator of Wnt/*Ctnnb1* (β-catenin) signaling, which controls both cell proliferation and differentiation. In combination with Axin and GSK3β, APC induces ubiquitination and degradation of Ctnnb1.This results in decreased Wnt signaling and hence affects cell proliferation and differentiation. Therefore, *miR-142-3p* positively regulates Wnt/*Ctnnb1* signaling by targeting APC for its destruction (Carraro et al., 2014). On the other hand, *Ep300* is a target of *miR-142-5p*. A mutual inhibitory loop between *Ep300* and *miR-142-5p* has also been described, and under mechanical stress, Ep300 accumulates in the cardiac cells, which results in the down-regulation of *miR-142-5p*. This loss of *miR-142-5p* expression activates genes required for myocyte survival and function (Sharma et al., 2012). Ep300 is a positive regulator of β-catenin that synergistically activates β-catenin/TCF transcription (Sun et al., 2000). In conclusion, *miR-142* seems to display diverse biological activities depending on the cell type and the stage of development.

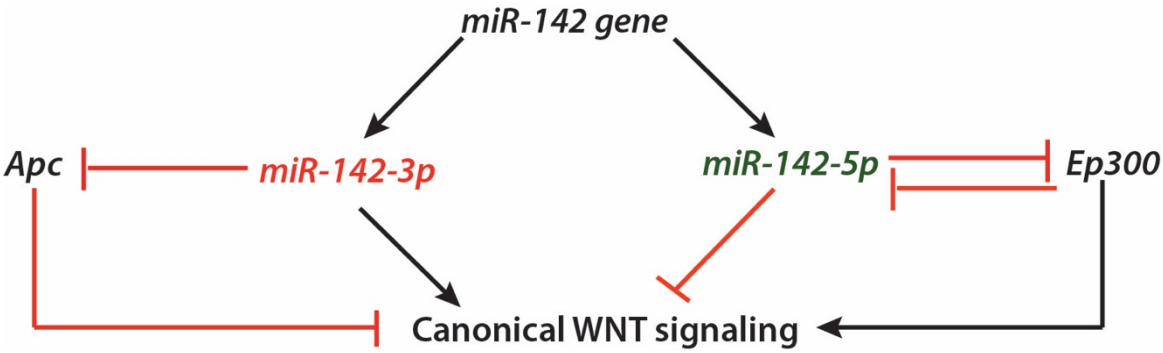


**Figure 4. Regulation of Wnt signaling by *miR-142*:** *miR-142-3p* regulates Wnt signaling by targeting *APC* whereas *miR-142-5p* regulates via targeting *Ep300*.

# 2 Objectives:

In order to determine, *in vivo*, the multiple roles played by *miR-142* in organogenesis, homeostasis and disease, we planned to use a *miR-142* classical knock out mouse line.

*miR-142-3p* targets *Apc*, leading to its destruction (Carraro et al., 2014). This results in the up-regulation of Wnt signaling, whereas miR-*142-5p* targets *Ep300* (Sharma et al., 2012), which leads to down-regulation of Wnt signaling. One being a negative regulator and the other being a positive regulator, we hypothesize that *miR-142* is a key regulator of Wnt signaling. Therefore, it would be interesting to understand how *miR-142* regulates the Wnt signaling pathway during lung development and disease via *Apc* and *Ep300*.

It has also been observed that *miR-142-3p* and *miR-142-5p* are up-regulated in the bronchioalveolar epithelial cells (BASCs) (Qian et al., 2008), which are suggested as a specific epithelial/stem progenitor cell pool in the lungs of mice and humans, that maintains brionchiolar epithelial (Clara) cells and Alveolar cells (AT1 and AT2) of the distal lung (Kotton and Morrisey, 2014). Proper formation of epithelial lineages is important for overall lung function. Hence, we further propose that *miR-142* regulates the formation and differentiation of epithelial progenitor cells.

**Aims:**

1. To understand the function of *miR-142* during *in vivo* lung development.
2. To investigate how *miR-142 regulates* the Wnt signaling pathway during lung development and disease via *Apc* and *Ep300*.
3. To study the role of *miR-142* in the formation and differentiation of epithelial progenitor cells.

# 3 Materials and Methods

## 3.1 Study approval

Animal experiments were approved by the Federal Authorities of Animal Research of the Regierungspräsidium Giessen, Hessen, Germany with approved protocol numbers 405_M, 423_M, 610_M, 613_M, G 47/2017 and G54/2017.

## 3.2 Generation and genotyping of mice

### 3.2.1 *miR-142* KO mouse line establishment

The *miR-142* KO mutant mouse line was established at the MCI/ICS (Institut Clinique de la Souris, iCS, Infrastructure Nationale PHENOMIN, 1 rue Laurent Fries, 67404 Illkirch, France). A MCI proprietary vector containing a floxed neomycin resistance cassette and Protamine-Cre cassette was used. The use of protamine-Cre cassette in the construction vector offers an efficient solution for the auto-excision of the floxed region in the male germ line of mice. In parallel, a 3.3kb fragment (corresponding to the 5' homology arm) and 2.6kb fragment (corresponding to the 3' homology arms) were amplified by PCR and sub-cloned in MCI proprietary vector to generate the final targeting construct. The linearized construct was electroporated in C57BL/6N mouse embryonic stem (ES) cells. After selection, targeted clones were identified by PCR using external primers and further confirmed by Southern blot with 3' external probe. Two positive recombinant ES clones were injected into Balb/CN blastocysts, and resulting male chimeras were crossed with wild type females. The genotype of mice with germ line transmission was confirmed using the primers described below.

### 3.2.2 Genotyping of *miR-142* KO mice

*miR-142* heterozygous and KO mutant mice were identified by performing PCR on tail genomic DNA with primers called P1, P2, P3 and P4. The P2/P3 primers couple allows detecting the *miR-142* wild type allele (174 bp). The P1/P4 primers couple allows detecting the presence of the LoxP cassette (105 bp). The P1/P3 primers couple allows detecting the deletion of the endogenous *miR-142* gene (254 bp).

(P1) forward: GAA GAA CGA GAT CAG CAG CCT CTG TTC C; (P2) forward: ACG CTA GCA CAG TGT GTG CCC A; (P3) reverse: ACC CAT ATG ATA CAC CAG CCA CGT C; (P4) reverse:GAA GTT ATA CTA GAG CGG CCG TTC AC.

The PCR program consists of a denaturation step at 95°C for 4 min, followed by 34 cycles of denaturation (94°C for 30 secs), annealing (62°C for 30 secs) and extension steps (72°C for 60 secs). The program ends with a completion step at 72°C for 420 secs. Each PCR tube contains 2.6 U of Taq polymerase in 5µl of reaction buffer (Qiagen Master Mix), 15 pmol of each primer, 0.5 mM dNTPs and 10 ng of genomic DNA in final volume of 10 µl.

### 3.2.3 Generation and genotyping of *Sftpc*$^{CreERT2/+;}$*Rosa26R*$^{miR142/+}$*; Tomato*$^{flox/+}$ mice

We also generated a knock-in of *miR-142* in the *Rosa26R* locus. The *Rosa26-LoxP-STOP-loxP-miR-142* (aka *Rosa26R*$^{miR-142/miR-142}$) mice were crossed with *Sftpc*$^{CreERT2/+}$; *Tomato*$^{flox/flox}$ mice to generate control (*Sftpc*$^{+/+;}$ *Rosa26R*$^{miR-142/+}$*; Tomato*$^{flox/+}$ ) and experimental (*Sftpc*$^{CreERT2/+;}$ *Rosa26R*$^{miR-142/+}$*; Tomato*$^{flox/+}$ ) embryos. The Cre-based recombination, allows an irreversible activation of *miR-142* expression in the epithelium. Table 2. summarizes the procedure and protocols for the detection of experimental *Sftpc*$^{CreERT2/+;}$ *Rosa26R*$^{miR-142/+}$*; Tomato*$^{flox/+}$ and control *Sftpc*$^{+/+;}$ *Rosa26R*$^{miR-142/+}$*; Tomato*$^{flox/+}$mice.

**Table 2. Primer sequences and genotyping protocol for mice.**

| Mouse line | Primer Sequence | PCR protocol | | |
|---|---|---|---|---|
| | | **Step** | **Temp°C** | **Time** |
| *Sftpc*$^{CreERT2/+}$ | *(P1) Fwd- CCC AGT CCC TCT CTG AAT TTG*<br>*(P2) Rev - GTT TCT ACC GAC CCT GTG AAG*<br>*(P3) WT - CAT CGC TCG ACC AGT TTA GTT A* | 1 | 95 | 3min |
| | | 2 | 95 | 30min |
| | | 3 | 50 | 30min |
| | | 4 (repeat step 2-4, 34 times) | 72 | 1 min |
| | | 5 | 72 | 5 min |
| | | 6 | 4 | Hold |
| *Tomato*$^{flox/+}$ | | **1** | 94 | 3 min |

| Mouse line | Primer Sequence | PCR protocol | | |
|---|---|---|---|---|
| | | **Step** | **Temp°C** | **Time** |
| | *(Tom) Fwd - CTG TTC CTG TAC GGC ATG G*<br><br>*(Tom) Rev - GGC ATT AAA GCA GCG TAT CC*<br><br>*(Wt) Fwd - CCG AAA ATC TGT GGG AAG TC*<br><br>*(Wt) Rev - AAG GGA GCT GCA GTG GAG TA* | **2** | 94 | 20 secs |
| | | **3** | 61 | 30 secs |
| | | **4** (repeat step 2-4, 34 times) | 72 | 30 secs |
| | | **5** | 72 | 2min |
| | | **6** | 4 | hold |
| *Rosa26R$^{miR-142/+}$* | (*Mut) Fwd - AAG CAC TAC TAA CAG CAC TGG AGG GTG*<br><br>*(Mut) Rev - CAC ACA CCA GGT TAG CCT TTA AGC CT*<br><br>*(Wt) Fwd - AGC ACG TTT CCG ACT TGA GTT GCC*<br><br>*(Wt) Rev - CAC ACA CCA GGT TAG CCT TTA AGC CT* | 1 | 95 | 4 min |
| | | 2 | 94 | 30secs |
| | | 3 | 70 | 30secs |
| | | 4 (repeat step 2-4, 34 times) | 72 | 1min |
| | | 5 | 72 | 7min |
| | | 6 | 20 | 5min |
| | | 7 | 4 | hold |

### 3.2.4 Gel electrophoresis

PCR products were analyzed using 1.5% agarose gel containing TAE buffer with Sybrsafe (50 µl Sybrsafe + 500ml 1x TAE buffer). 10 µl of PCR products were loaded with 2 µl loading dye (BioRad Nucleic Acid Sample loading dye, 5X). The gel was run with 120 V

for 60 min. A molecular ladder (QX Size Marker, 100bp-2,5kb Qiagen, Germany) was used to detect the expected band sizes.

**Table 3. Expected molecular size of genotyping products**

| Mouse line | Expected band size for Mutant | Expected band size for WT |
|---|---|---|
| *miR-142 KO* | 294 | 174 |
| *Rosa26R$^{miR-142/+}$* | 411bp | 386bp |
| *Sftpc$^{CreERT2/+}$* | 1000 bp | 500 bp |
| *Tomato$^{flox/+}$* | 196 bp | 297 bp |

### 3.2.5 Administration of Tamoxifen (I.P)

Tamoxifen stock solution was prepared by dissolving tamoxifen powder (T5648, Sigma, Schnelldorf, Germany) in corn oil at a concentration of 20 mg/mL at room temperature (RT).

Pregnant females received a double dose of intraperitoneal (IP) injection of 0.1 mg of tamoxifen per gram of body weight at E14.5 and E15.5 respectively. The embryos were collected and analyzed at E18.5. Dissected embryos and lungs were examined using Leica M205 FA fluorescence stereoscope (Leica, Wetzlar, Germany) and images were acquired using Leica DFC360 FX camera.

## 3.3 RNA extraction, Reverse Transcription-PCR, and Quantitative Real-time PCR Analysis

Freshly isolated embryonic lungs were placed in Qiazol lysis reagent, homogenized and lysed in GentleMACs (MACS) or Bullet blender (Next Advance). Total RNA was extracted using miRNeasy Mini or Micro kit (Qiagen, Hilden Germany) according to manufacturer's protocol. 200ng to 1 µg of RNA was used for cDNA synthesis. RT-PCR for mRNA was carried out using Quantitative Reverse Transcription kit (Qiagen).On the other hand,TaqMan MicroRNA Reverse Transcription kit (Applied Biosystem) was used to

synthesize cDNA for miRNA and 10 ng of total RNA was used. In both cases, reactions were assembled following the manufacturer's recommendations. qPCR was performed on a Light Cycler 480 system (Roche Applied Science). The TaqMan microRNA assay (Applied Biosystem) was used for screening the differential expression of miRNAs whereas SYBR Green (Platinum SYBR Green qPCR SuperMix-UDG Invitrogen) was used for the analysis of mRNA expression. *U6* and *Hprt* (Hypoxanthine phosphoribosyl transferase 1) were used as a reference for normalization of miRNA and mRNA respectively. Results were collected from at least three lung samples and each reaction was run in triplicate. Primers for *miR142-3p*, *miR142-5p* and *U6* were obtained from Applied Biosystems whereas primers (Table 4.) for regular genes were designed using Roche Applied Science Online Assay Design Tool. All primers were designed to span introns and blasted using NCBI software for specificity.

**Table 4. Primers used for Real Time-qPCR (Mouse Primers Forward/Reverse)**

| Gene | Forward sequence (5'-3') | Reverse sequence (5'-3') |
|---|---|---|
| *Hprt* | cctaagatgagcgcaagttgaa | ccacaggactagaacacctgctaa |
| *Fgf10* | atgactgttgacatcagactcctt | cactgttcagccttttgagga |
| *Fgfr2b* | cctacctcaaggtcctgaagc | catccatctccgtcacattg |
| *Fgfr2c* | tgcatggttgacagttctgc | tgcaggcgattaagaagacc |
| *Fgfr1b* | tgggtcggtgcggagatcgt | acggacaacaacaaaccaaaccct |
| β-*catenin* | gcagcagcagtttgtgga | tgtggagagctccagtacacc |
| *Lef1* | tcctgaaatccccaccttct | tgggataaacaggctgacct |
| *Etv5* | Gtggccgctcaggagta | gtgcttccaaagtctccgct |
| *Spry2* | gagaggggttggtgcaaag | ctccatcaggtcttggcagt |
| *Ep300* | acatgatgcctcggatgact | taggggctgtggcatatt |
| *Apc* | catggaccaggacaaaaacc | gaacacacacagcaggacaga |
| *gp130* | aggaccaaagatgcctcaac | tgaaggaagttcgaggagaca |
| *Kras* | tggatgagtacgaccctacga | tccctcattgcactgtactcc |
| *Pdpn* | ggatgaaacgcagacaacag | agctctttagggcgagaacc |
| *Sftpc* | ggtcctgatggagagtccac | gatgagaaggcgtttgaggt |
| *Scgb1a1* | gatcgccatcacaatcactg | cagatgtccgaagaagctga |
| *Epcam* | tgtcatttgctccaaactgg | gttctggatcgccccttc |
| *Aqp5* | taacctggccgtcaatgc | gccagctggaaagtcaagat |
| *Ecad* | gttgcagaaggcgctgtt | gtgttgacgtcatcgtctgc |

| Gene | Forward sequence (5'-3') | Reverse sequence (5'-3') |
|---|---|---|
| *P63* | agacctcagtgaccccatgt | ctgctggtccatgctgttc |
| *Bzrap1* | agagagccctgggtacagc | cccgaagcctatgttgaact |
| *LincRNA (A430104N18Rik)* | cttcctgacccctgatacttg | cccatatcctcacggacg |

### 3.4 *In-situ* hybridization and immunofluorescence staining

Freshly isolated lungs were washed in PBS, then fixed in 4% PFA, gradually dehydrated in ethanol, impregnated with xylene, embedded in paraffin and sectioned into 5 µm slices on poly-L-Lysine-coated slides. Antigen retrieval was performed by treating the sample with Proteinase K for 30 secs at 37°C. The slides were blocked 2 times 5 min with Dako (DAB Emission +Dual Linksystem HRP, Life Technologies) and then incubated with digoxygenin labeled LNA probes (Exiqon, miRCURY LNA Detection probe, Vedback, Denmark) specific for *miR142-3p* and *miR142-5p*. For immunofluorescence staining the slides were de-paraffinized blocked with 3% bovine serum albumin (BSA) and 0.4% Triton X-100 (in Tris-buffered saline (TBS) at room temperature (RT) for 1 hour and then incubated with primary antibodies against Apc (ab15270, Abcam; 1:200), phospho-$S^{552}$-β-catenin (9566,Cell Signaling; 1:200) Ep300 (sc-585,Santa Cruz; 1:200) ,Pro-Surfactant Protein C (AB3786, Millipore; 1:500), T1 alpha /Podoplanin (8.1.1,DSHB - Univ of Iowa;1:250),Cdh1/E-Cadherin (610181, BD Lab; 1:250), pErk (4376, Cell Signaling;1:250),Ki67 (NB600-1252, Novus Biologicals; 1;250) and Fgfr2-BEK (C-17) (sc-122, SantaCruz;1:250) at 4°C overnight. After incubation with primary antibodies, slides were washed three times in TBST (Tris buffer saline + 0.1% Tween 20) for 5 minutes, incubated with secondary antibodies at RT and washed three times with TBST before being mounted with Prolong Diamond Anti-fade Mountant with DAPI (4',6-diamidino2-phenylindole; Invitrogen). Photomicrographs of immunofluorescence staining were taken using a Leica DMRA fluorescence microscope with a Leica DFC360 FX camera (Leica, Wetzlar, Germany). Figures were assembled using Adobe Illustrator. The data are representative of at least three lungs from independent experiments. Antigen retrieval for some of the immuno-fluorescence staining was performed using citrate buffer for 10min at 100°C followed by cooling on ice for 15 min.

**Table 5. Probes and fluorescent antibodies/dyes used for fluorescence *in-situ* hybridization**

| Probes | Company (Catalog number) | Dilution |
|---|---|---|
| *hsa-miR-142-3p* | EXIQON mercury LNA™ microRNA Detection Probe,1nmol, 5'-DIG and 3'DIG labeled (18043-15) | 1:625 |
| *hsa-miR142-5p* | EXIQON mercury LNA™ microRNA Detection Probe, 1nmol, 5'-DIG and 3'DIG labeled (38514-15) | 1:625 |
| **Fluorescent antibody/dye/reagents** | **Company (Catalog number)** | |
| Anti-Dioxigenin-POD, Fab fragments | Roche Diagnostics (11207733910) | 1:400 |
| Dako EnVision® + Dual Link System-HRP (DAB+) | Dako Agilient Technologies K406511-2 | |
| Prolong Diamond Anti-fade Mountant with DAPI | Invitrogen (P369362) | |

**Table 6. Antibodies used for immunofluorescence.**

| Antibody | Company (Catalog number) | Dilution |
|---|---|---|
| Ki67 | Novus Biologicals (NB600-1252) | 1:250 |
| Cdh1/Ecad | BD Transduction Laboratories (610181) | 1:250 |
| Pro-Sftpc | Millipore (AB3786) | 1:500 |
| Podoplanin | Develpomental Studies Hybridoma Bank University of Iowa (8.1.1) | 1:250 |
| Apc | Abcam (ab15270) | 1:250 |
| Ep300 (c-20) | SantaCruz (sc-585) | 1:250 |
| β-catein pS-552 | Cell Signaling (9566s) | 1:250 |

| Antibody | Company (Catalog number) | Dilution |
|---|---|---|
| pErk | Cell Signaling (4376) | 1:250 |
| Fgfr2-BEK(C-17) | SantaCruz (sc-122) | 1:250 |

### 3.5 Murine peripheral blood counts

In the Mfd diagnostics facility, about 250 µl of whole blood was retro-orbitally drawn from 8 weeks-old sex-matched *miR-142* KO and wild type littermates into glass capillary tubes containing 5 µl of 0.5 M EDTA, to prevent coagulation. ADVIVA2120 Hematology System (Siemens Healthcare, Germany) was used to perform complete blood count measurements. Blood count measurement was performed at Justus-Liebig Universität Klinik fur Kleintiere (Central laboratory for small animals), Giessen Germany.

### 3.6 Hematoxylin and Eosin stain

3 – 5 um sections of the left lobe were deparaffinized, dipped in water and stained for Mayer's Hematoxylin solution for 1–3 min and washed under running tap water for up to 10min. Slides were monitored under the microscope for over and under staining. Slides were then incubated for 2 min in Eosin dye and brought back through increasing gradients of EtOH, xylene and cover slipped with pertex mounting media.

### 3.7 Flow cytometry analysis and fluorescence activated cell sorting

Lungs were dissected, washed with HBSS and kept on ice. Then, they were cut into fine pieces using a sharp blade before being digested with 0.5% Collagenase Type IV/HBSS (Life Technologies, Invitrogen) at 37°C for 45 min. Once homogenate was dissociated, the cell suspension was successively passed through 18, 21 and 24G syringes before being passed through 70 and 40 µm cell strainers (BD Biosciences, Heidelberg, Germany).One volume of HBSS buffer was added to the sample to dilute the collagenase and then centrifuged at 1200rpm for 10 minutes to remove the enzyme solution. Cells were then resuspended in cold FACS buffer (1xPBS;2%FBS;1mM EDTA;0.1% sodium azide: for FACS measurement), and or MACS buffer (1xPBS;2%FBS;1mM EDTA : for cell sorting). Cells were incubated with fluorochrome labeled antibodies (Table 6) for at least 15 min on ice in the dark and then centrifuged at 2000 rpm for 5 min and resuspended in FACS buffer or MACS buffer. FACS measurements were carried out using LSRFortessa equipped with

FACS DIVA™ software for analysis and FACSAria III cell sorter for isolation of epithelium and mesenchyme and isolation of AT2 cells (BD Biosciences).

### 3.7.1 Measurement of AT1 and AT2 cell number

Following antibodies were used for analysis of AT1 and AT2 cell number [488-CD31 (1:50), Biolegend, Cat-102513; FITC-CD45 (1:50), Biolegend, Cat-103108; Apc Cy7 EpCam (1:50), Biolegend, Cat-118217 or Apc–eFluor-780-EpCam (1:50), eBioscience, Cat-47-5791-80; proSPC (1:500), Millipore, Cat-AB3786; Apc-Podoplanin (1:20), Biolegend, Cat-127409; Apc Isotype Ctrl (1:20), Biolegend, Cat-402012] and samples were analysed using LSRFortessa equipped with FACS DIVA™ software.

### 3.7.2 Isolation of epithelium and mesenchymal cells as well as isolation of AT1 and AT2 cells from embryonic lungs

For the isolation of epithelium and mesenchyme we used following antibodies [488-CD31 (1:50); FITC-CD45 (1:50); Apc Cy7 EpCam (1:50)] whereas [488-CD31 (1:50); FITC-CD45 (1:50); Apc Cy7 EpCam(1:50), Apc-Podoplanin (1:20); Apc Isotype Ctrl(1:20)] antibodies were used for isolation of AT1 and AT2 cells.The samples were then passed through FACSAria III cell sorter.

**Table 7. Antibodies used for FACS.**

| Antibody | Company (Catalog number) | Dilution |
|---|---|---|
| Pro Surfactant Protein C (pro-*Sftpc*) Antibody | Millipore (AB3786) | 1:500 |
| T1alpha (Podoplanin) APC anti-mouse | Biolegend (127409) | 1:20 |
| Epcam (CD326) APC/Cy7 | Biolegend (118217) | 1:50 |
| Epcam (CD326) APC-eFlour780 | eBiosciences (553079) | 1:50 |
| Alexa Fluor 488 anti-mouse CD31 | Biolegend (102513) | 1:50 |
| BD Pharmingen FITC Rat Anti-Mouse CD45 (clone 30-F11) | Biolegend (103108) | 1:50 |
| PE anti-human/mouse CD49f Antibody | Biolegend (313611) | 1:50 |

| Antibody | Company (Catalog number) | Dilution |
|---|---|---|
| Rabbit serum | Sigma-Aldrich (R9133) | 1:500 |
| F(ab´)2-Goat anti-Rabbit IgG (H+L) Secondary Antibody, Alexa Fluor 555 conjugate | ThermoFisher Scientific (A-21430) | 1:1000 |
| Neg. control for T1alpha: APC Syrian Hamster IgG Isotype control | Biolegend (402012) | 1:20 |
| Fc Block Gamunex10% | Bayer (TAL-05-0002) | 1:10 |
| Saponin | Cabiochem (558255) | 0.02% |

### 3.8 Microarray experiments

RNA was isolated using the RNeasy Mini Kit (217004; Qiagen). Purified total RNA was amplified using the Ovation PicoSL WTA System V2 kit (NuGEN). Per sample, 2 µg amplified cDNA was Cy5-labeled using the SureTag DNA labeling kit (Agilent). 2 µg of the labeled cDNA were hybridized on Agilent-074809 SurePrint G3 Mouse GE v2 8x60K Microarrays for 22h at 65°C in Agilent hybridization chambers. The cDNA was not fragmented before hybridization. Dried slides were scanned at 2 µm/pixel resolution using the InnoScan IS900 (Innopsys). The analysis was performed with R and the Limma package. Gene set analyses were done using the Wilcoxon-tests of the t-statistics. The data are deposited in GEO and are available through the accession number GSE106411.

### 3.9 Embryonic lung explant culture

Timed-pregnant wild-type mice were sacrificed on E14.5, the embryonic lungs were harvested and placed on 8 µm Nucleopore Track-Etch membranes (110414; Whatman). Vivo-morpholinos specific for *miR-142-3p* and/or *miR-142-5p* (Gene Tools LLC) were added at 5 µM to E14.5 lung explants. Lungs were grown for 96 hours at 37°C with 5% CO2 prior to analysis. In a second set of experiments, 100 µM Dexamethasone (Dex, D1756; Sigma Aldrich), 10 µM IQ-1 (Ep300-Ctnnb1 inhibitor, S8248; Selleckchem), 10 µM SCH772984 (Erk inhibitor, 19166; CayMan Chemical) either alone or in combination with morpholinos were added to the E14.5 lung explants.

### 3.10 Western blotting

Protein samples from either E18.5 embryonic lung samples or cultured lung explants were isolated using RIPA buffer (Santa Cruz) containing protease inhibitor cocktails. Equal amounts of total protein from each assayed sample were used for chemiluminescent Loading buffer (5% SDS in bromophenol blue and β- mercaptoethanol- Biorad) was added to protein samples, denatured 5 min at 95°C and cooled on ice. 15 μg of protein sample was loaded on a 12% polyacrylamide gel and run at 35mA, 100volt for 1hour. Samples were then electrically transferred to a polyvinylidene fluoride (PVDF) membrane (MilliQ)- by semi-dry electro blotting (100mA, 24 volts per Gel, Gel size: 7x9 cm) for 90 minutes. The membrane was blocked with 5% Bovine Serum Albumin or 5% Milk in TBS-T at room temperature on a shaker for 1 hour followed by incubation with primary antibody (Table 8.) and overnight at 4°C. After washing the membrane with TBS-T five times for 5 minutes each, the membrane was incubated with the respective HRP-labeled secondary antibody (1:1000) at room temperature for 1 hour followed by 5 times washing with TBS-T for 5 minutes each. The protein bands were detected by ECL (Enhanced Chemi-luminescence, Amersham, Germany) treatment followed by exposure to the membrane. Immunoblotting was performed using antibodies against proSPCP (1:500) 9 (Millipore) and beta-actin (1:50000) (Abcam).

**Table 8. Antibodies used for Western blotting.**

| Primary antibody (rabbit) | Company (Catalog number) | Dilution | Secondary antibody | Company (Catalog number) | Dilution |
|---|---|---|---|---|---|
| Pro-Sftpc | Millipore (AB3786) | 1:1000 | Anti-rabbit IgG HRP Conjugate | Promega (W401B 29303401) | 1:5000 |
| β-actin | Abcam (ab8227) | 1:50.000 | Anti-mouse IgG HRP Conjugate | Promega (W401B 29303401) | 1:5000 |

### 3.11 Statistical analysis

Data were assembled using Graph Pad Prism Software (Graph Pad software, USA) and presented as average values ± S.E.M. Statistical analyses were performed using Student's t-test. Data were considered significant if $p < 0.05$. Figures were assembled using Adobe Photoshop CS6 and Adobe Illustrator CS6.

# 4. Results

## 4.1 Generation of *miR-142* KO mice

In mice, the *miR-142* gene (ENSMUSG00000065420) is located on chromosome 11 (Fig. 5). *miR-142* is positioned directly adjacent to an exon for a long non-coding RNA (A430104N18Rik ENSMUSG00000084796), which function is still unknown so far. *Benzodiazepine receptor (peripheral) associated protein 1* (*Bzrap1, ENSMUSG00000034156*) is also another gene found downstream of *miR-142*. The *miR-142* locus also contained many GC rich repeat regions, which render PCR amplification and screening difficult. The constitutive and complete deletion of the *miR-142* gene was therefore carried out and mice heterozygous for the *miR-142* KO allele were generated. Fig. 6B shows the genotyping results of E18.5 embryos arising from *miR-142* heterozygous crosses. Fig. 6C shows the validation of our primer sets to amplify either the wild-type *miR-142* allele (P2/P3), the presence of the *LoxP* site (P1/P4) or the *miR-142* KO allele (P1/P3).

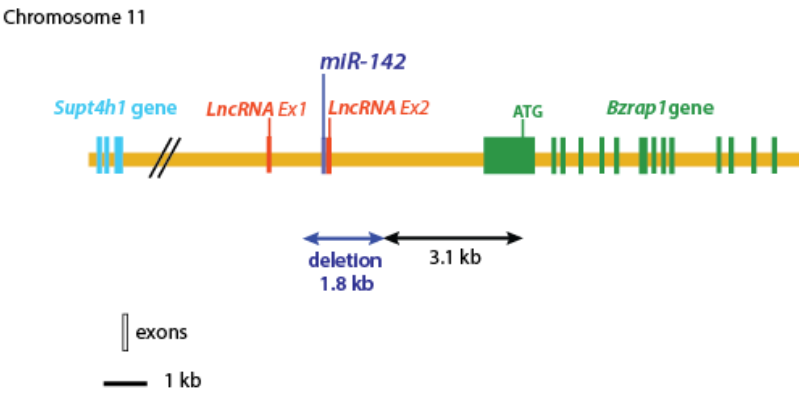


**Figure 5. Schematic representation of *miR-142* locus on the chromosome 11 of the mouse genome.** *miR-142* is located at proximity of an exon of a long non-coding RNA (LncRNA). An exon of *LncRNA* will be removed while deleting *miR-142*. *Benzodiazepine receptor (peripheral) associated protein 1* (*Bzrap1*) is also another gene found downstream of *miR-142* that could be potentially disrupted upon *miR-142* deletion.

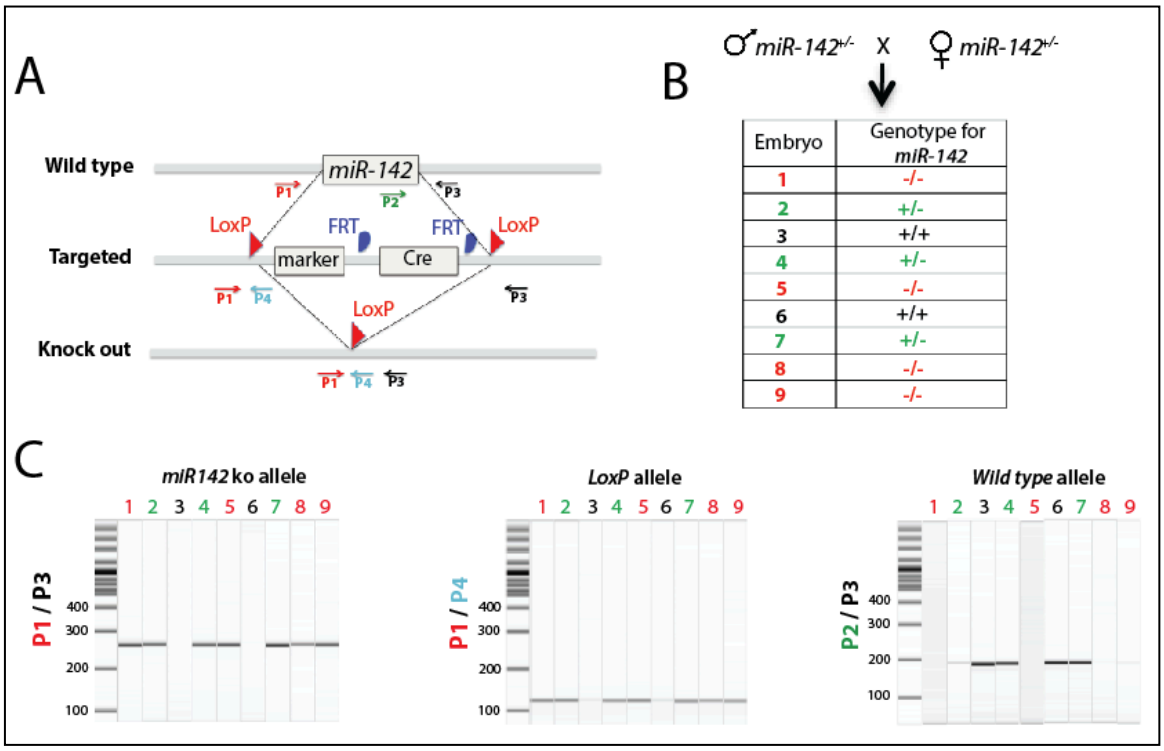


**Figure 6. Genotyping strategy for *miR-142* KO allele. A)** Schematic diagram showing WT mice *miR-142* locus, targeted allele and knock out allele. P1, P2, P3 and P4 represent the specific primers used for differentiating wild type and knock out allele. **B-C)** PCR analysis of the genomic DNA obtained from the embryos at E18.5 from *miR-142+/-* (Hets) male and female intercrossing. 254 bp band size for KO allele (Primers used: P1 and P3) and 174 bp band size for WT allele (Primers used: P2 and P3) was determined. A 105 bp band was observed using LoxP specific primers (P1 and P4).

### 4.2 *miR-142* KO pups are born alive and display no obvious abnormalities

Litters from *miR-142* heterozygous crosses were genotyped at E12.5, E18.5 and postnatally. Although the expected Mendelian ratio for generating knockout (KO) pups from crossing two hemizygous mice is 25%, this ratio appeared higher when embryos were harvested at E12.5 (39%) and E18.5 (40%) (Table 9). The likely explanation for this observation is the low number of harvested embryos (eighteen and fifteen respectively). Another important conclusion from these data is that *miR-142*-KO embryos are not dying *in utero*. In addition, individual monitoring and genotyping of all the neonates born from different litters up to 4 months of age indicate a normal representation of *miR-142*-KO mice (20% of the overall postnatal mice (n=79)). In the *miR-142*-KO group, only one 4-month-old mouse died while three animals died in the *miR-142* heterozygous group

between the ages of 3 and 4 months. None of the mice died in the control wild-type group. Overall, our data indicate very low death rate in the *miR-142*-KO group postnatally.

**Table 9. Numbers of embryos obtained at different stages of embryonic development**

| Embryonic stages | *miR142*$^{+/+}$ (WT) | *miR142*$^{+/-}$ (Hets) | *miR142*$^{-/-}$ (KO) | Total embryos |
|---|---|---|---|---|
| E12.5 | 3 (17%) | 8 (44%) | 7 (39%) | 18 |
| E18.5 | 3 (20%) | 6 (40%) | 6 (40%) | 15 |
| Post-natal | 34 (43%) | 29 (36%) # | 16 (20%) * | 79 |

(# 3 animals died at the age of 2-3 months, * 1 animal died at the age of 4 month)

### 4.3 *miR-142* deletion abolishes the expression of miR-*142-3p* and *miR-142-5p*

Our experimental approach was designed to carry out the complete deletion of *miR-142*. In the process of deleting *miR-142*, one exon for the *LncRNA*, close to *miR-142*, had also to be deleted. In addition, the expression of the *Benzodiazepine receptor (peripheral) associated protein 1* (*Bzrap1), a gene* encoding a regulator of synaptic transmission, might also be disturbed as the proposed deletion encompasses also part of the 5' region of this gene. To confirm the successful deletion of *miR-142*, RNA from E18.5 lungs from miR-*142*$^{+/+}$, *miR-142*$^{+/-}$ *and miR-142*$^{-/-}$ littermate embryos (n= 3 for each genotype) were isolated. qPCR analysis showed that the expression of *miR-142-3p* and *miR-142-5p* were reduced in *miR-142* heterozygous lungs compared to wild-type lungs. In addition, the expressions of these 2 isoforms were completely abolished in *miR-142* KO lungs (Fig. 7A-B). We also tested the expression of the *Bzrap1*, a gene, positioned 3.5kb downstream of *miR142*. *Bzrap1* expression level was unchanged in *miR-142* heterozygous or KO lungs compared to that of wild-type littermates, (Fig. 7C) confirming that the promoter region of *Bzrap1* gene was not impaired. As expected, the expression of the *LncRNA* was abrogated in both *miR-142* heterozygous and KO embryos (Fig. 7D).

*In-situ* hybridization experiments, using specific digoxygenin labeled probes for these two microRNAs showed that the *miR-142-3p* and *miR-142-5p* are expressed in both the mesenchyme as well as in the epithelium of the E18.5 lung (Fig. 8 A, B, E, F). The levels of expression of both microRNAs were significantly decreased in *miR-142* KO samples

compared to that of the WT samples (Fig. 8 C, D, G, H vs. A, B, E, F). The unbiased quantification of the expression of the respective isoforms of *miR-142* confirms the very low level of expression of both *miR-142* isoforms (Fig. 8 I, J).

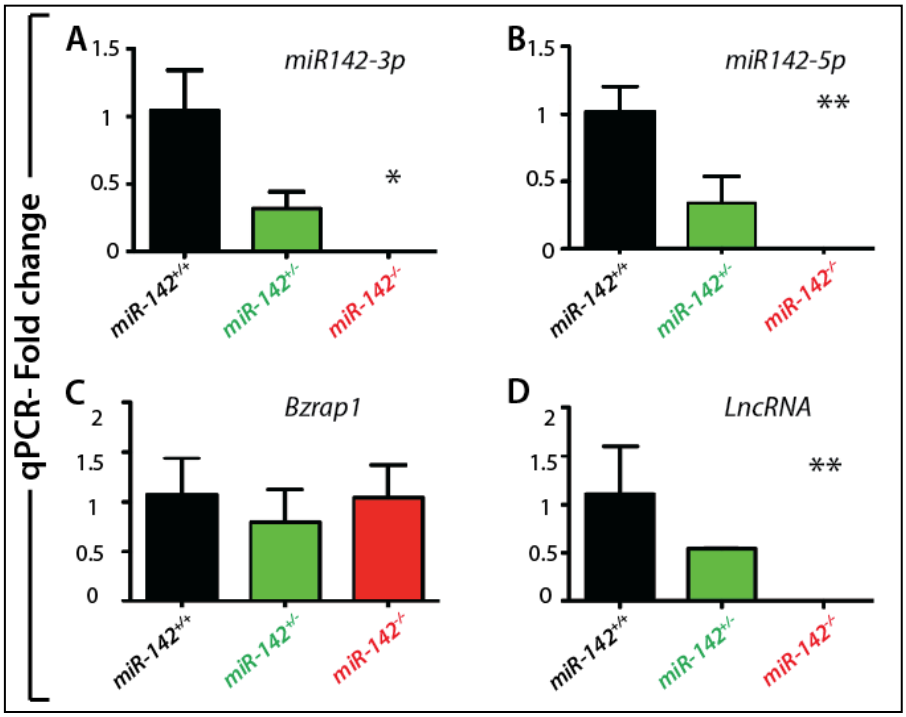


**Figure 7. Deletion of *miR-142* successfully abrogates *miR-142-3p* and *miR-142-5p* expression. A-B)** qPCR analysis on cDNA obtained from E18.5 embryonic lung sample showed that both *miR-142-3p* and *miR-142-5p* were down regulated in *miR-142*$^{+/-}$(Hets) lungs and completely absent in *miR-142*$^{-/-}$(KO) lungs as compared to *miR-142*$^{+/+}$(WT) samples. **C)** The levels of *Bzrap1* gene, positioned 3.5kb downstream of the *miR-142* gene, remain unchanged as compared to that of wild type littermates shown. **D)** Expression of LncRNA was completely abolished in *miR-142* KO lungs.

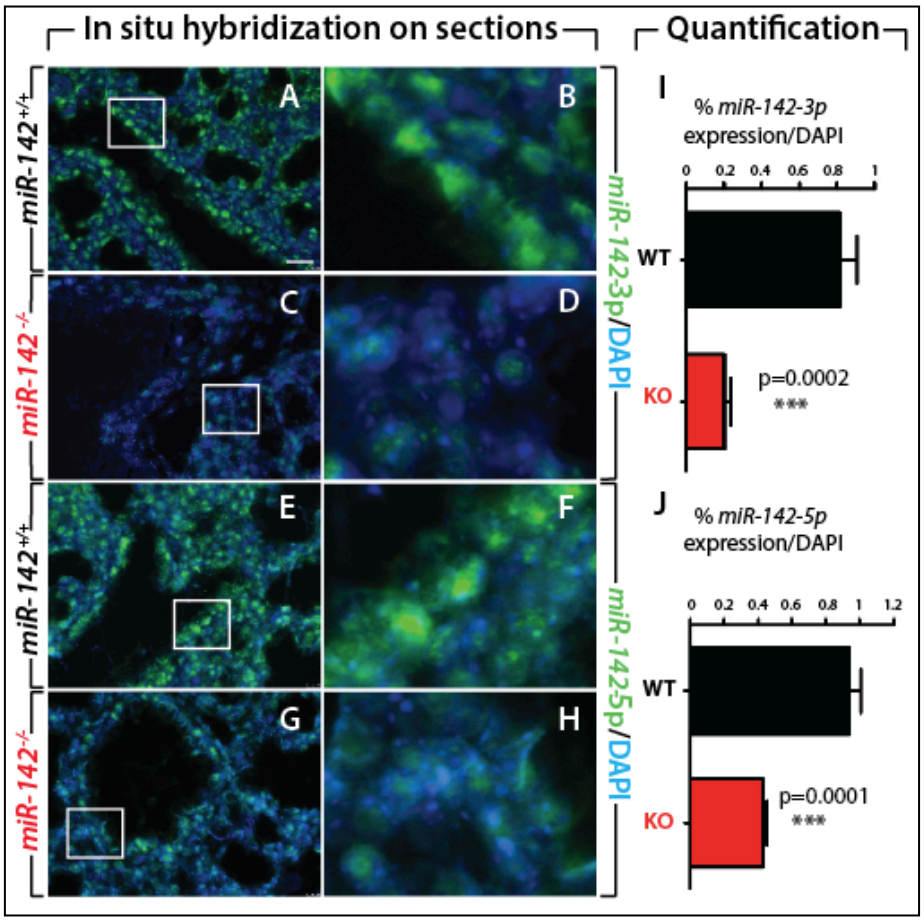


**Figure 8. *In-situ* hybridization on E18.5 *miR-142*$^{-/-}$ (KO) embryonic lung sections.** *In-situ* hybridization for *miR-142-3p* **(A-D)** and *miR-142-5p* **(E-H)** showing significant reduction of the corresponding expression levels in *miR-142*$^{-/-}$ compared to WT 18.5 embryonic lung sections. **(I-J)**. Quantification of the *in-situ* hybridization signals indicating a strong reduction of both isoforms. Scale bar represents 10µm.

### 4.4 *miR-142*-KO mice display a wide range of hematological disorder

*miR-142* is highly expressed in hematopoietic cells belonging to both the myeloid and lymphoid lineages. Using an exogenous gene trap technology, Chapnik and colleagues recently reported the phenotypic analysis of *miR-142* knockdown mice. Their mutant mice displayed an array of hematological defects (Chapnik et al., 2014). In order to validate our mouse model, we performed total blood count on 8-week-old *miR-142*$^{+/+}$(WT) and *miR-142*$^{-/-}$ (KO) mice (n=3 for each genotype). Our results also indicated a significant decrease in the number of white blood cells, lymphocytes, eosinophils, monocytes and platelets in

*miR-142* KO vs. wild-type animals (Fig. 9 B-E, G). A significant increase in mean platelet volume was also observed (Fig.9 D, F).

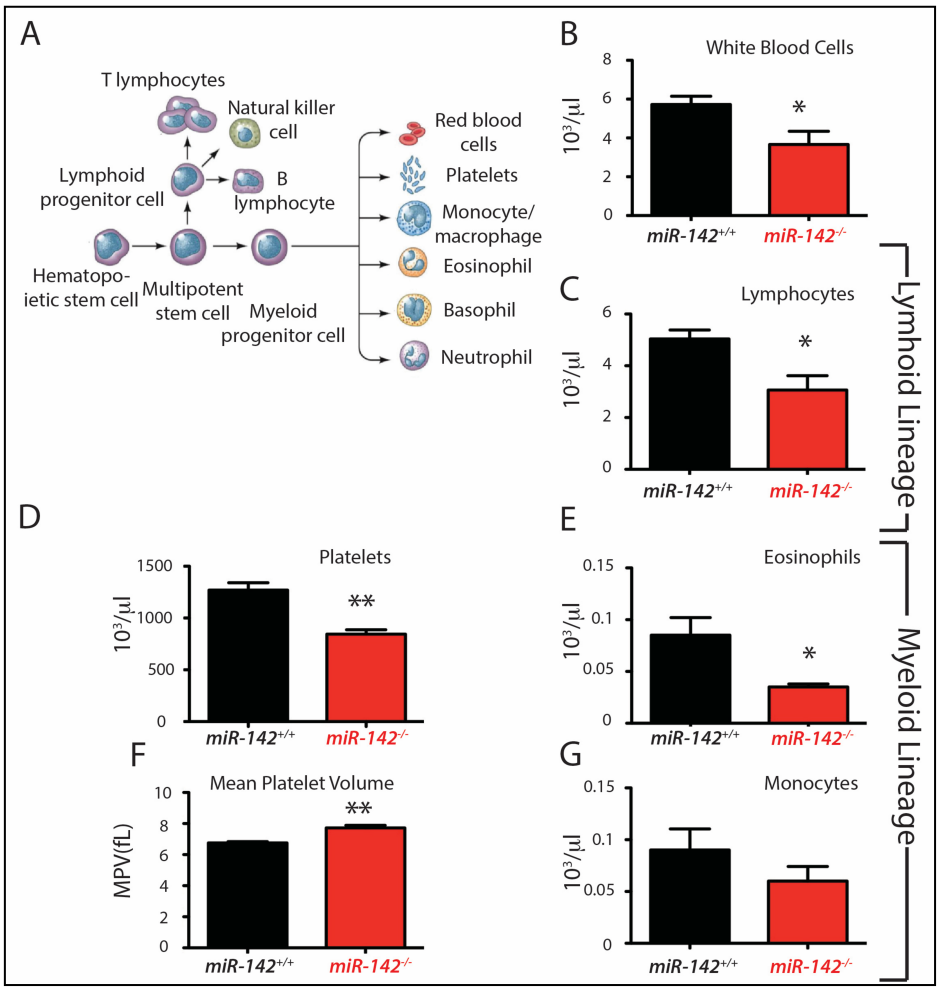


**Figure 9. *miR-142* KO mice display hematological abnormalities.**
**(A)** Schematic representation of hematopoietic stem cells differentiated into different blood cell types. Peripheral blood cell count in 8-week-old *miR-142*$^{-/-}$ mice (n=3) showing a significant decrease in circulating white blood cells (**B**), lymphocytes **(C)**, platelets (**D**), eosinophils (**E**) and monocytes (**G**) in addition to an increase in mean platelet volume (**F**)

## 4.5 Enhancement of alveolar epithelial lineage formation via the activation of the glucocorticoid pathway leads to decreased *miR-142* expression

Our *in-situ* hybridization data indicated *miR-142-3p* and *-5p* are expressed in both the epithelium and the mesenchyme at E18.5 (Shrestha et al., 2015).This suggests, in addition to its reported role in the mesenchyme (Carraro et al., 2014), *miR-142* could also play a function in the epithelium. Therefore, we hypothesized that *miR-142* could control

alveolar epithelial lineage formation during lung development. First, we took advantage of an *in vitro* model previously reported where activation of the glucocorticoid receptor pathway with dexamethasone increases alveolar epithelial lineage formation (Laresgoiti et al., 2016). Treatment of E14.5 embryonic lungs grown *in vitro* for 4 days with dexamethasone (Dex) (Fig. 10A) led to increase in the expression of both AT1 (*Aqp5, Pdpn*) and AT2 markers (*Sftpc*) (Fig. 10C). The impact of Dex treatment on Sftpc at the protein level was confirmed by immunofluorescence staining (IF) (Fig. 10E). Next, we investigated the impact of dexamethasone treatment on the expression of the specific *miR-142* isoforms. We observed a strong decrease in *miR-142-3p* and *-5p* expression upon Dex treatment (Fig. 10B) associated with a significant increase in *miR-142* targets *Apc*, *Ep300*, *gp130* but not *Kras* (Fig. 10D). These results suggested that some of the effects of dexamethasone on alveolar epithelial lineage formation could be due to decrease in *miR-142* expression.

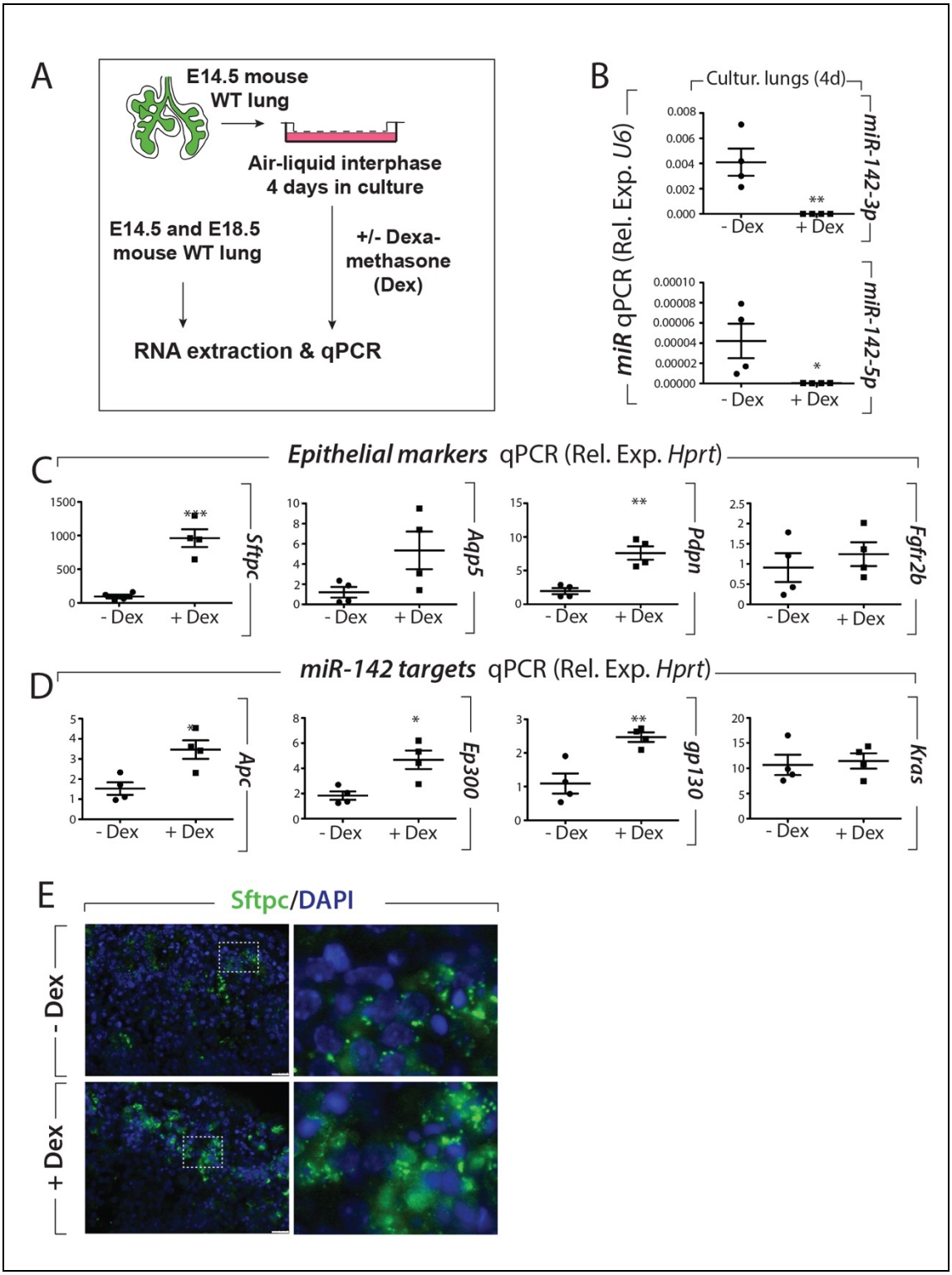


**Figure 10. Effect of dexamethasone (Dex) on E14.5 embryonic lung cultured *in vitro* for 4 days. (A)** Experimental design. **(B)** qPCR analysis showing the expression level of *miR-142-3p* and miR-142-*5p* as well as the expression of **(C)** *Sftpc*, *Aqp5*, *Pdpn* and *Fgfr2b*. **(D)** *Apc*, *Ep300*, *gp130* and *Kras* **(E)** IF staining for Sftpc on E14.5 lung explants cultured with and without Dexamethasone (100 µM). Scale bar represents 10µm.

## 4.6 *miR-142-3p* and *miR-142-5p* are expressed in both the AT1 and AT2 lineages during lung development

In order to investigate whether both *miR-142-3p* and *miR-142-5p* are expressed specifically in the AT1 and AT2 cells, we performed fluorescence *in-situ* hybridization specific to the *miR-142-3p* and *-5p*, co-stained together with either Sftpc (AT2 marker) or Pdpn (AT1 marker) at three different time points (E16.5, E17.5, and E18.5) during alveolar lineage formation (Fig. 11A). We observed the expression of the *miR-142-3p* and *-5p* in the AT1 and AT2 cells as detected by the co-expression of *miR-142-3p* and *miR-142-5p* either wtih Sftpc or Pdpn.Co-expression of *miR-142-3p* or *miR142-5p* with Sftpc was observed in all the stages considered but on the other hand, the co- expression of these miRs with Pdpn at E16.5 was not visible. However, at E17.5 and E18.5, we clearly observed cells co-expressing *miR-142-3p* or *5p* with Pdpn. These results indicate that both the microRNAs are expressed in the alveolar epithelium during development. Using FACS based approach, with a combination of antibodies like CD45 and CD31 to exclude the hematopoietic and endothelial cells as well as Epcam for capturing epithelial ($Epcam^{+ve}$) or mesenchymal ($Epcam^{-ve}$) cells, we isolated resident epithelial and mesenchymal lung cells at E14.5, E16.5 and E18.5 and examined miR expression by qPCR (Fig. 11B). The validation of this approach was carried out for known epithelial (*Cdh1*, *Epcam*, *Fgfr2b*) or mesenchymal (*Fgf10*, *Acta2*, *Vimentin*) markers (Fig. S1A-B). The expression of *miR-142-3p* is higher in the mesenchyme than in the epithelium at E16.5 and E18.5 but not at E14.5. Interestingly, between E14.5 and E18.5, *miR-142-3p* expression in the epithelium progressively decreases while the expression of its bona fide targets *Apc*, *Ep300*, *gp130,* and *Kras* were increased (Fig, S1C). Consistent with our previous observations, *miR-142-5p* was expressed at a much lower level than *miR-142-3p* (Carraro et al., 2014).

We also investigated the expression of these two microRNAs in E16.5, E17.5 and E18.5 FACS-isolated AT1 and AT2 cells (Fig. 11C). At E16.5, the captured cells for both lineages are likely to be the common bipotent progenitors(Desai et al., 2014; Treutlein et al., 2014). For the AT1 lineage, *miR-142-3p* was expressed at a similar level between E16.5 and E18.5. On the contrary, the expression of *miR-142-5p* increased as the formation of the AT1 lineage progressed. Similar expression patterns for *miR-142-3p* and *5p* were observed in the formation of the AT2 lineage. Interestingly, we noted the higher enrichment of *miR-142-5p* in AT1 compared to AT2 cells at E18.5. Furthermore, data mining analysis on the expression of *miR-142* targets using the single cell AT1 and AT2

transcriptomic data at E18.5 previously published and generated by Treutlein et al., 2014 was carried out (Fig. 11D). No differences in the expression level of *miR-142* targets were observed in AT1 vs. AT2 cells. However, we noticed a higher number of cells in the AT2 pool expressed *Apc* and *Ep300* (7/12 and 5/12, for *Apc* and *Ep300* respectively) compared to AT1 (12/41 and 10/41, for *Apc* and *Ep300* respectively) (Fig. 11D). This supports our previous result that *miR-142* expression is low in AT2 compared to AT1 cells. Interestingly, a higher number of cells in the AT1 compared to AT2 pools expressed *Kras* (19/41 and 2/12, for AT1 and AT2 respectively) suggesting that *Kras* expression level is not regulated by *miR-142* in AT1 cells. *gp130* was expressed by a low number of cells in the AT1 and AT2 pools (3/41 and 1/12, for AT1 and AT2, respectively). Altogether, the increase in these *miR-142* targets appears to occur more in AT2 than AT1, confirming the observed differential expression of *miR-142* in these cells.

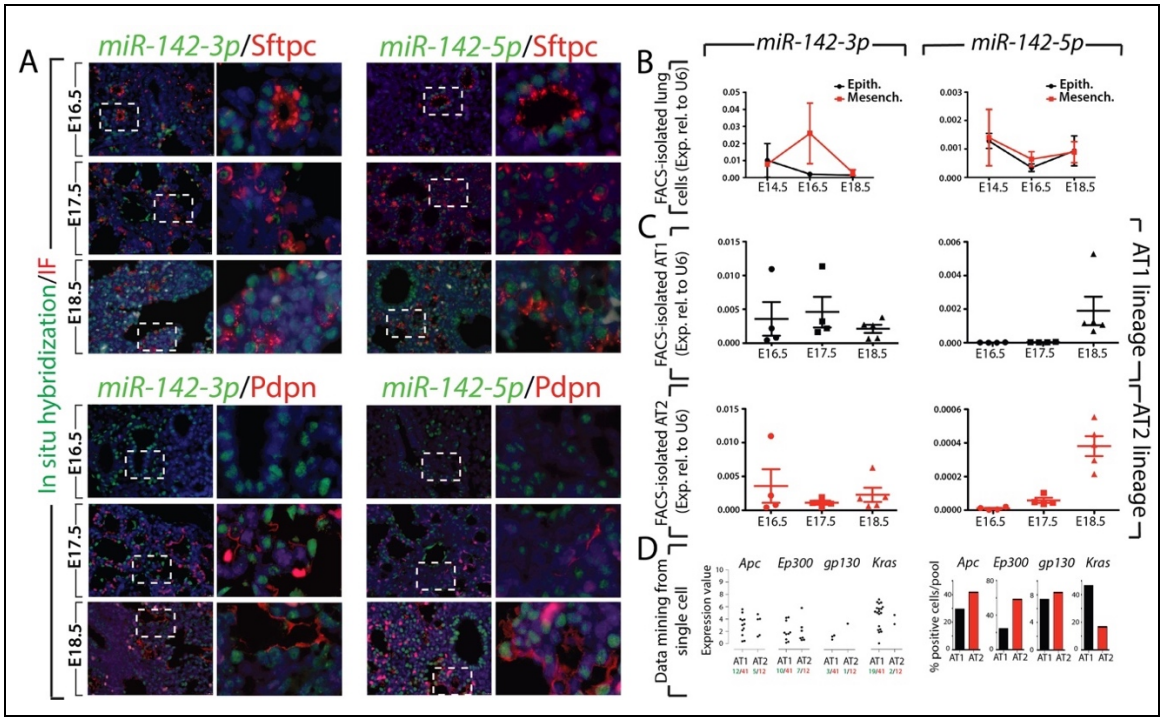


**Figure 11. Gene expression analysis during lung development of *miR-142-3p* and *miR-142-5p*.** **(A)** *In-situ* hybridization of *miR-142-3p* or *5p* and co-immunofluorescence staining for either Sftpc (AT2 marker) or Pdpn (AT1 marker). **(B)** qPCR on FACS-isolated lung epithelium and mesenchyme at E14.5, E16.5 and E18.5. **(C)** qPCR on FACS-isolated AT1 and AT2 cells at E16.5 (Bipotent cells), E17.5 and E18.5. **(D)** Mining of single cell transcriptomic data (derived from Treutlein et al., 2014) for AT1 and AT2 cells at E18.5. Scale bar represents 10µm.

## 4.7 *miR-142* KO lungs display alteration of epithelial integrity starting at the pseudoglandular stage

In order to explore further, the function of *miR-142* during lung development, we analysed the impact of loss of *miR-142* in our newly generated *miR-142* KO mice (Shrestha et al., 2015). Phenotypic analysis of the E12.5 embryonic lungs of Control and KO littermate indicated no obvious macroscopic abnormalities in terms of branching (Fig. 12A). This result was quite surprising as we reported previously that the knock down of *miR-142-3p* using morpholino specific to *miR-142-3p* in lungs grown at E11.5 *in vitro* led to impaired branching and decreased Ctnnb1 signaling in association with increased Adenomatous polyposis coli (Apc) expression and arrested proliferation in the lung mesenchyme, (Carraro et al., 2014). The lack of obvious branching phenotype in E12.5 *miR-142* KO lungs suggested that *miR-142-5p* could also play a functional role. An upregulation of *Apc* and *Ep300*, known targets for *miR142-3p* and *miR-142-5p* respectively appeared to be upregulated in KO lungs (Fig. 12B, C). Further, *in vitro* knock down experiment using morpholinos against *miR-142-3p* (mo-3p), *-5p* (mo-5p) or *(3p+5p)* (mo-(3p+5p)) indicated that the simultaneous inactivation of both isoforms leads to the rescue of the branching defects reported upon *miR-142-3p* knockdown alone (Fig. 12D). Interestingly, the expression level of *Apc*, *Ep300*, and *Kras* were not significantly altered at the RNA level from E12.5 *mir-142* KO lung samples, indicating complex gene regulation/compensation (Fig. S2A). However, an increase in Wnt signaling pathway targets like *Lef1* and *Ctnnb1* suggested increased Wnt signaling.

Careful examination of E12.5 *miR-142* KO lung epithelium, by immunofluorescence for Cdh1, suggested a disruption in the epithelial cuboidal cell morphology, and acquisition of round shape with the overall disorganization of the epithelial layer (Fig. 12B). Global transcriptomic analysis using gene arrays with RNA originating from the whole Control and KO E12.5 lungs was also carried out. The heat map (Fig. S2C) shows sets of up- or down-regulated genes selected based on their p-value in Control and KO lungs (n=3). KEGG analysis indicated perturbations in pathways involved in regulation of actin cytoskeleton, focal adhesion, and endocytosis as well as ECM receptor interaction. All these pathways, which have been shown to modulate epithelial integrity and maturation, may be involved in the observed phenotype. Interestingly, PI3K-Akt, Mapk, Ras, Hippo, and Wnt signaling were also perturbed (Fig. S2D).

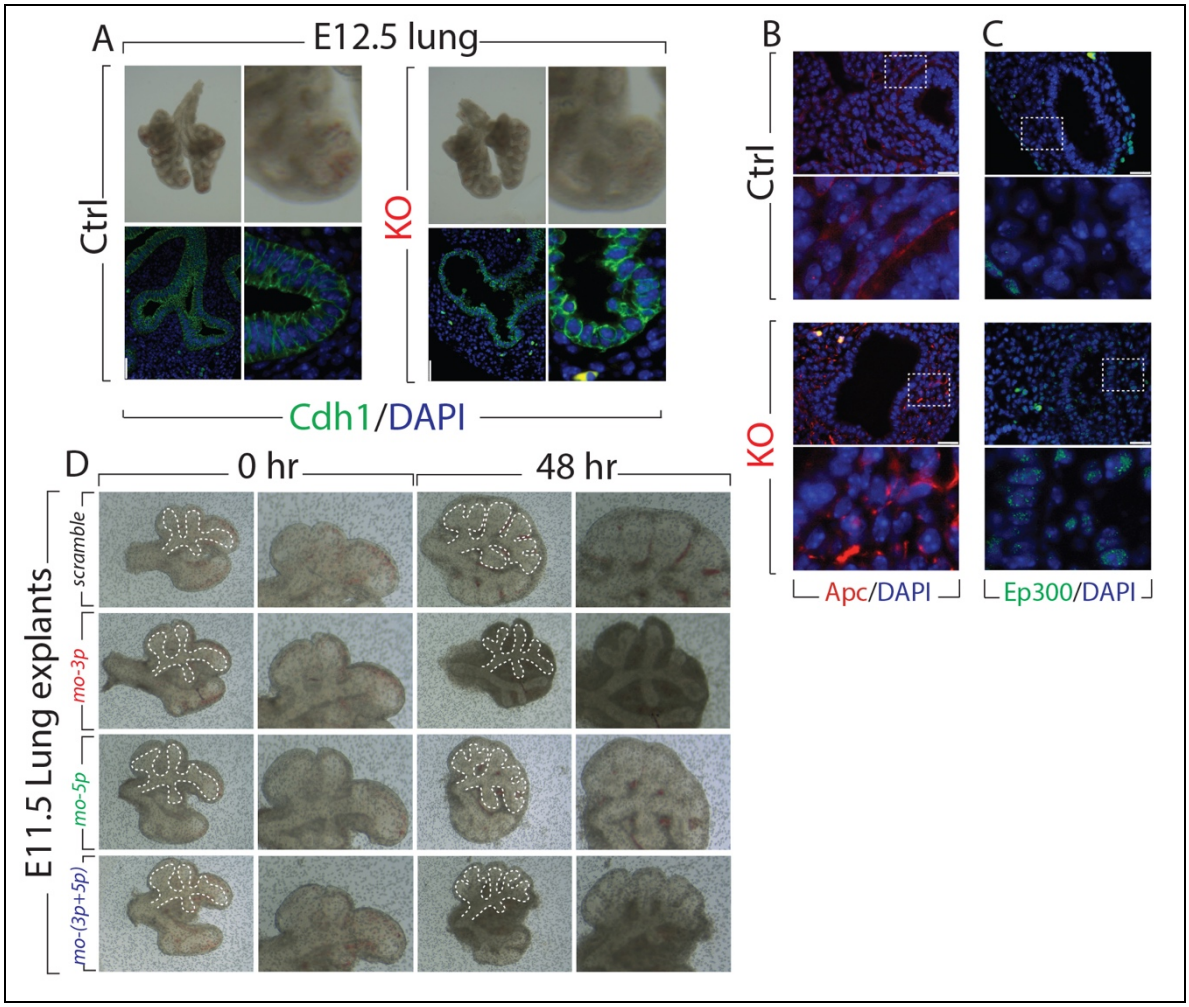


**Figure 12. Analysis of the *miR-142* KO at E12.5.** (**A**) Bright field picture and Cdh1 staining of Control (WT) littermate and *miR-142* KO lungs at E12.5. Immunofluorescence for (**B**) Apc, (**C**) Ep300 and (**D**) *In vitro* culture of E11.5 embryonic lung explants, treated with scramble, mo142-3p, mo142-5p and mo142-3p+5p. Scale bar represents 10µm.

### 4.8 The alveolar epithelial lineage is perturbed in E18.5 *miR-142* KO lungs

Macroscopic analysis of the E18.5 KO lungs indicated no obvious changes in terms of size or shape when compared to wild-type littermates. Analysis of the microscopic phenotype by H&E staining (n=3) also revealed no major structural abnormalities (Fig. 13A). Gene expression analysis by qPCR on the whole lung indicated that the AT2 marker, *Surfactant protein C* (*Sftpc*) was upregulated in KO vs. Control lungs (p=0.0074, n=3) (Fig. S3C). Both immunofluorescence and western blot analysis confirmed an increase in the number of Sftpc-positive cells (Fig. 13B and quantification). The expression of the AT1 marker

*Podoplanin* (*Pdpn*) (p=0.06, n=3) and Club cell marker *Scgb1a*1 showed a trend towards increase, however, the expression of basal cell marker *p63* was unchanged *(*Fig S3C*).* Flow cytometry analysis using Epcam, CD49f, Pdpn antibodies showed an increase in the percentage of AT2 cells (84.9% ± 0.2% vs. 79.8% ± 1.04% in KO vs. Control, respectively, p=0.002, n=3), and a decrease in the percentage of AT1 cells (9.05% ± 0.68% vs. 12.3% ± 0.66% in KO vs. Control, respectively, p=0.004, n=3) (Fig. 13C). Similar results were obtained using Epcam, Epcam, Sftpc and Pdpn antibodies (Fig. S3A,B). Analysis of Ki67 immunoreactivity, in the alveolar epithelial layer of Control and KO lungs at E18.5, indicated no changes in epithelial proliferation (Fig. S3D). Furthermore, no changes in the percentage of Epcam-positive cells ($Epcam^{+ve}$) (over total cell population) were observed (Fig. 13C), suggesting that loss of *miR-142* is not affecting overall, epithelial proliferation. Co-immunofluorescence staining for Sftpc and Pdpn further demonstrated an increased AT2 and decreased AT1 cell number in E18.5 *miR-142* KO embryos (Fig. 13D).

We also explored the status of Fibroblast growth factor 10 (Fgf10) signaling, a key pathway reported influencing alveolar epithelial lineage formation (Chao et al., 2017; Ramasamy et al., 2007). We found that the expression of *Fgf10* was not changed but a very significant increase in the expression of its receptor, *Fgfr2b,* in KO vs. Control lungs (p= 0.0018) was observed (Fig. S4A). The level of expression was also validated at the protein level by immunofluorescence staining (Fig. S4B). Analysis of *Sprouty2* and *Etv5*, two previously reported Fgf10 downstream targets (Herriges et al., 2015; Mailleux et al., 2001), showed no significant difference between Control and KO lungs, suggesting that Fgf10 signaling per se was not affected.

Next, we carried out gene arrays from Control and KO FACS-isolated AT2 cells and examined their differentiation state using the previously reported comprehensive AT1 and AT2 gene signatures (Treutlein et al., 2014). We observed a sharp difference in gene expression among the four KO samples (Fig 13E, KO vs. Control, n=4; Fig. S5A). In particular, two KO samples showed a strong upregulation of the AT1 signature and decreased AT2 signature. The other two KO samples behaved more like Control samples. Interestingly, FACS analyses of these samples were consistent with the KO phenotype (increased AT2 and decreased AT1 cell number). In addition, the heat maps (top 100 genes according to p values, Fig. S5B) shows that these samples are clustering with KO samples and not Control samples. The reason for the observed heterogeneity in the AT1 and AT2 signature between the different KO samples is not clear and could reflect differences in the penetrance of the phenotype. Alternatively, these differences could

reflect an attempt by the mutant lung to compensate for the loss of the AT1 cells. As the AT2 cells have been shown to serve as progenitors which self-renew and give rise to the AT1, an increase in the AT1 signature in the mutant AT2 cells could reflect compensatory mechanisms and would not directly be linked to an additional function of *miR-142* in AT2 alveolar differentiation. In spite of this overall variability between mutant samples, gene set analysis, which takes into consideration the four samples from each group, indicated a significant increase in the AT1 signature ($p \leq 0.01$) and a decrease in the AT2 signature ($p \leq 0.01$). In conclusion, we demonstrate increased AT2/AT1 ratio in KO vs. Control lung, as well as decreased AT2 gene signature in KO vs. Control AT2 cells.

We also examined *miR-142* targets on E18.5 *miR-142* KO lungs by qPCR. Significant changes were observed in *Apc*, *Ep300*, *gp130* and *Kras* expression. The expression of Wnt components *Lef1* and *Ctnnb1*, which are not *miR-142* targets, was not significantly affected (Fig. S2B). We further validated these observations at the protein level by immunofluorescence. Apc (Fig. 13F) and Ep300 (Fig. 13G) appeared to be up-regulated in KO lungs. The level of activated beta-catenin ($p^{S552}$Ctnnb1) was increased in KO lungs compared to Control lungs suggesting increased Wnt signaling (Fig. 13H). Finally, we observed an increased p-Erk expression (Fig. 13I), correlating with increased *Kras* mRNA levels.

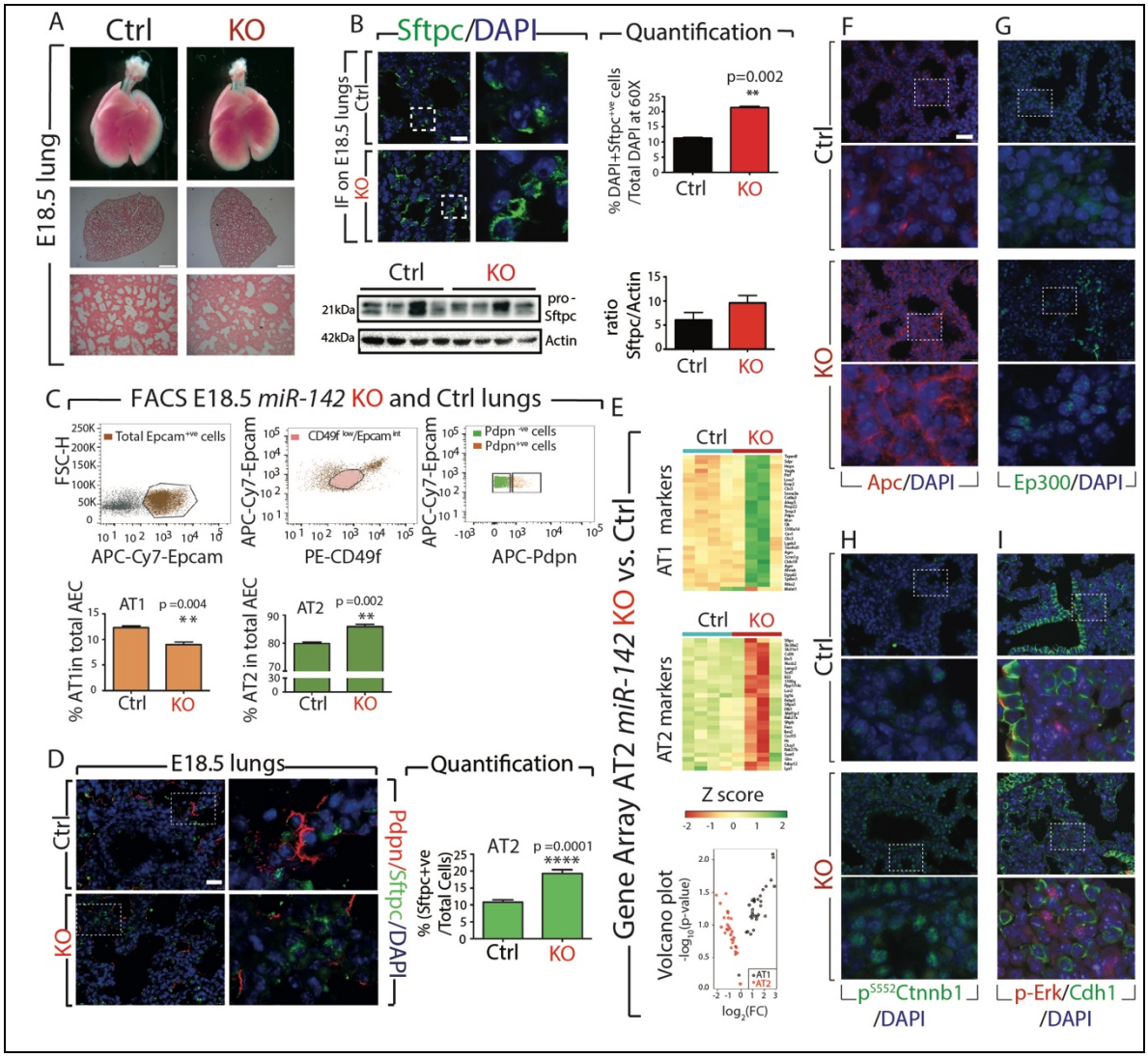


**Figure 13**. **Analysis of the alveolar epithelial lineage phenotype of the *miR-142* Control and KO lungs at E18.5**. **(A)** Bright field pictures, H & E staining of Control and *miR-142* KO lungs at E18.5. **(B)** IF and WB analysis for Sftpc expression and corresponding quantification of the number of Sftpc-positive cells. **(C)** Flow cytometry of Control and *miR-142* KO lungs for AT1 and AT2 cells. **(D)** Pdpn/Sftpc/DAPI IF staining in Control and KO E18.5 lungs. **(E)** AT1 and AT2 gene signature analysis in FACS-isolated AT2 cells from E18.5 *miR-142* KO lungs. Immunofluorescence for **(F)** Apc (**G**) Ep300 **(H)** activated beta-catenin ($p^{S522}$Ctnnb1) **(I)** p-Erk/Cdh1. Scale bar represents 10µm.

## 4.9 Impact of cell autonomous over-expression of *miR-142* in alveolar progenitors

The expression of *miR-142* in the epithelium, as well as the epithelial alveolar lineage phenotype upon global loss of function of *miR-142,* suggested that *miR-142* could play a cell-autonomous role in the epithelium. To test this possibility, we generated a knock-in of the *LoxP-Stop-LoxP-miR142* cassette in the *Rosa26* locus (*Rosa26R*$^{miR\text{-}142/miR\text{-}142}$). We crossed the *Rosa26R*$^{miR\text{-}142/miR\text{-}142}$ mice with *Sftpc*$^{CreERT2/+}$; *Tomato*$^{flox/flox}$ mice, to generate Control *Sftpc*$^{+/+;}$ *Rosa26R*$^{miR\text{-}142/+}$*; Tomato*$^{flox/+}$ and gain of function (GOF) *Sftpc*$^{CreERT2/+;}$ *Rosa26R*$^{miR\text{-}142/+}$*; Tomato*$^{flox/+}$ embryos. This Cre-based recombination allows an irreversible activation of *miR-142* expression in the epithelium. The expression of *miR-142* was induced with tamoxifen IP injection at E14.5 and E15.5. The resulting lung phenotype was analyzed at E18.5 (Fig. 14A). Experimental lungs were detected via the expression of the red fluorescent protein (RFP) in the epithelium and confirmed by genotyping. Validating our approach, we found increased *miR-142-3p* (p=0.0024) and *-5p* (p=0.0004) expression in GOF vs. Control lungs (Fig. 14B). FACS analysis of CD49f$^{low}$/Epcam$^{int}$ alveolar epithelial cells as well as AT1 (Pdpn$^{+ve}$) and AT2 (Pdpn$^{-ve}$) cells indicated no change in the percentage of AEC cells (over total cell population). However, a significant decrease in the percentage of AT2 cells (82.4% ± 1.24% vs. 86.6% ± 0.99% in GOF vs. Control, p=0.004, n=4) and an increase in the percentage of AT1 cells (10.6 ± 0.88% vs. 8.7 ± 0.38 in GOF vs. Control, p=0.001, n=4) was observed. Co-immunofluorescence staining for Sftpc and Pdpn also indicated a decrease in AT2 and an increase in AT1 cell number in E18.5 GOF embryos compared to Control (Fig. 14D).

Next, we carried out gene arrays from E18.5 Control and GOF FACS-isolated AT2 cells and examined the state of differentiation of these cells using the AT1 and the AT2 gene set signature. Fig. 14E displays the heat maps comparing the expression of the AT1 signature and the AT2 signature in Control and KO (n=4) AT2 (refer to Fig. S5D for higher magnification). Our results indicated a decrease in the AT1 signature associated with an increase in the AT2 signature in the AT2 cells. Gene set analysis indicated a small but significant decrease in the AT1 signature ($p \leq 0.001$) and an increase in the AT2 signature ($p \leq 0.001$).

In conclusion, a gain of *miR-142* expression in alveolar epithelial cells indicated a decreased AT2/AT1 cell ratio with the increased AT2 gene signature in AT2 cells, which is exactly the opposite result that was observed in the *miR-142* loss of function experiment.

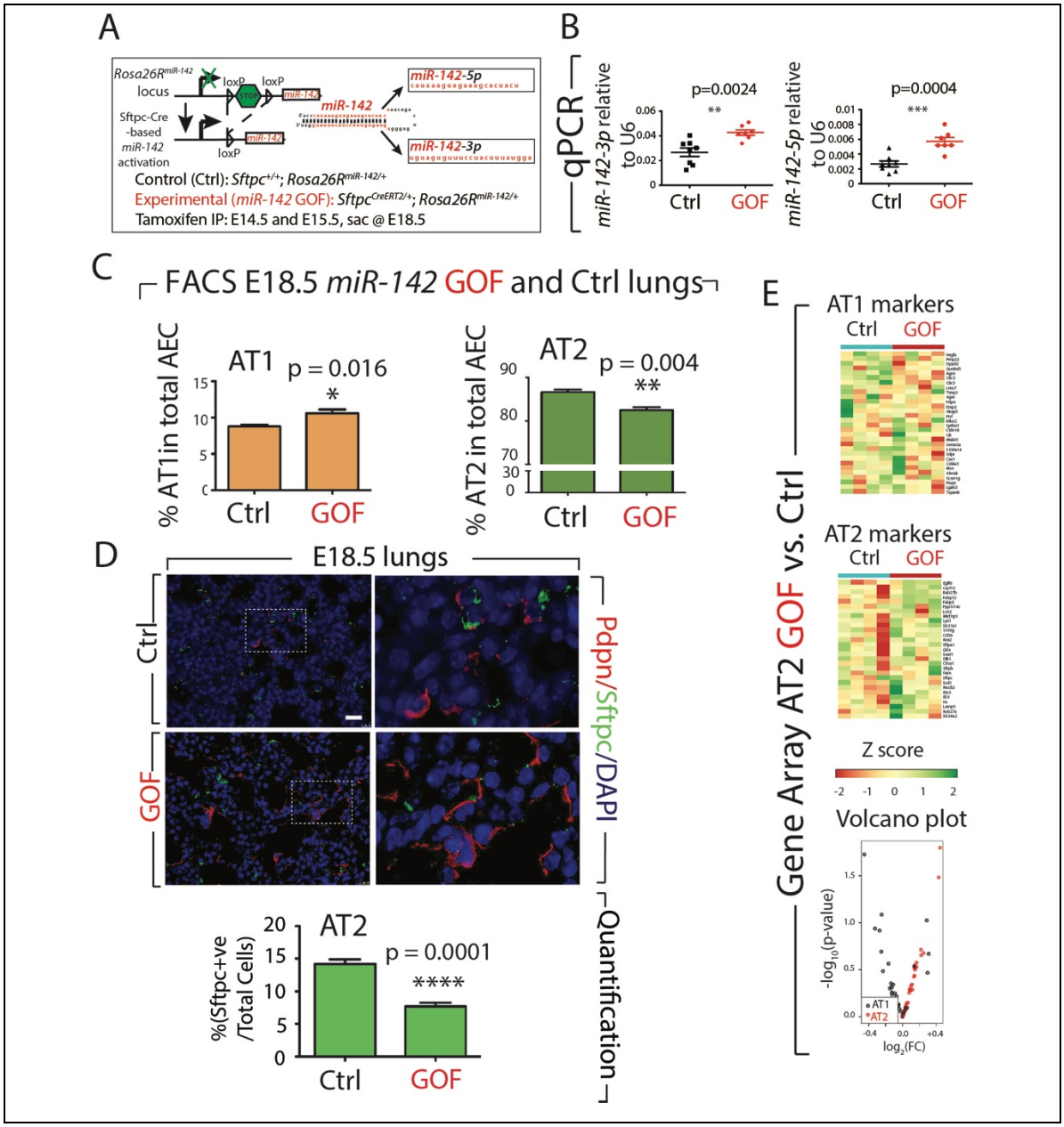


**Figure 14. Analysis of the alveolar epithelial lineage phenotype of the *miR-142* gain of function (GOF) and littermate Control lungs at E18.5. (A)** *LoxP-Stop-Loxp-miR-142* knock in mice (in the *Rosa26* locus) are crossed with *Sftpc*$^{CreERT2}$ mice. Cre activation in the alveolar epithelial progenitor cells following tamoxifen IP injection to pregnant females at E14.5 and E15.5 leads to *miR-142* overexpression in these cells. Lungs are analyzed then at E18.5. **(B)** Validation *of miR-142-3p* and *-5p* overexpression in E18.5 GOF and Control littermate lungs. **(C)** Flow cytometry analysis of Control and GOF E18.5 lungs for AT1 and AT2 cells. **(D)** Pdpn/Sftpc/DAPI IF staining in E18.5 GOF and Control littermate lungs. **(E)** AT1 and AT2 gene signature analysis in FACS-isolated AT2 cells from E18.5 *miR-142* GOF lungs. Scale bar represents 10µm.

## 4.10 Loss of *miR-142* expression *in vitro* is sufficient to increase the AT2/AT1 cell ratio.

Our results with the use of a constitutive KO for *miR-142*, leave open the possibility that the observed effect on alveologenesis may derive from secondary effects, due to early deletion of *miR-142* expressio*n*. To evaluate the impact of the *miR-142* loss of function at the time in which AT2 (*Sftpc)* and AT1 (*Pdpn*) cell markers arise, we performed *in vitro* treatment with morpholino specific for *miR-142-3p* and *-5p* on E14.5 lung explants, and cultured them for 4 days (Fig. 15A). This approach allowed to analyze the effect of *miR-142* LOF at a time when early alveolar progenitors have yet to become bipotent progenitors for the AT1 and the AT2 cells. We observed a significant decrease in the expression of *miR-142-3p* and *-5p* respectively (Fig. 15B). Treatment with both morpholinos together (mo-(3p+5p)) led to the simultaneous knock-down of both *miR-142* isoforms (Fig. 15B). The decrease in the expression of these miRNAs were further confirmed by upregulation of their respective target genes such as *Apc*, *Ep300,* and *Kras* (Fig. 15C). Interestingly, the attenuation of *miR-142-3p* and/or *5p* led to the increase in *Sftpc* expression while decreasing the expression of *Pdpn* (Fig. 15D). In accordance with our *in vivo* data, FACS analysis of AT2 and AT1 cells in these lungs grown *in vitro* demonstrated an increase in the percentage of AT2 (14.8% ± 1.33% vs. 7.9% ± 4.8% in mo-(3p+5p) vs. Scrambled, respectively, p=0.049, n=4) and a decrease in AT1 (0.86% ± 0.2% vs. 2.8%± 1.1% in mo-(3p+5p) vs. Scrambled, respectively, p=0.01, n=4) (Fig S6A-D). Therefore, our results demonstrate that *in vitro* knockdown of *miR-142* recapitulates the *in vivo* phenotype in terms of AT2/AT1 ratio. These results reinforce the concept that the observed phenotype is due to a direct effect of perturbing *miR-142* signaling, rather than to secondary effects due to the prolonged absence of *miR-142*.

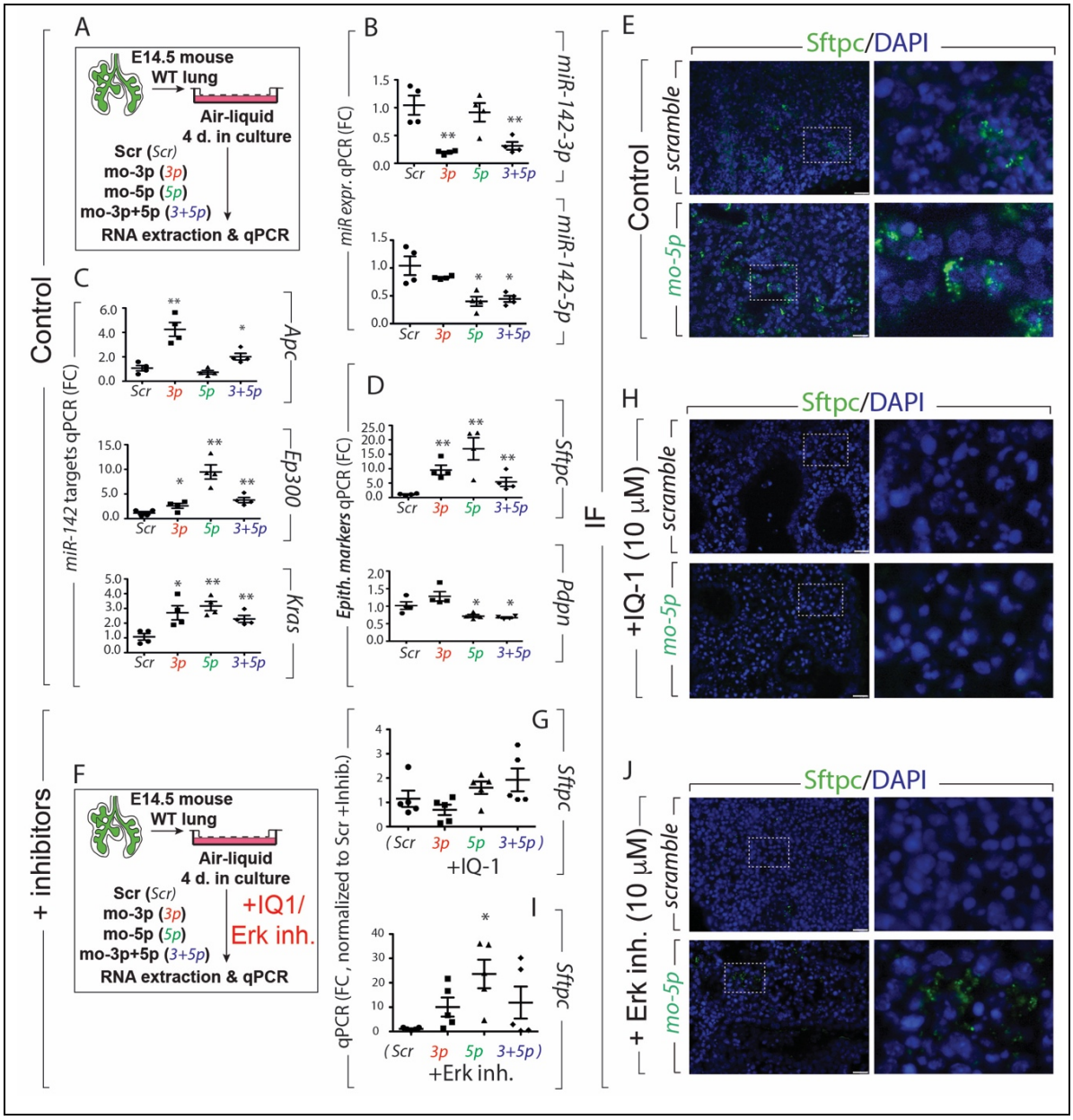


**Figure 15. *In vitro* differentiation of the alveolar epithelial progenitors. (A)** Schematic *in vitro* treatment of E14.5 WT lung explants with morpholinos specific to *miR-142-3p* and *mir-142-5p* for 4 days. Impact of morpholino treatment on **(B)** *miR-142-3p* and *-5p* **(C)** *Apc*, *Ep300*, *Kras* (**D)** *Sftpc* and *Pdpn* expression **(E)** IF staining of Sftpc on E14.5 lung explant culture treated with morpholino-*miR-142-5p* for 4 days**. (F)** Schematic *in vitro* culture of E14.5 WT lung explants with morpholinos for 4 days in presence of either IQ-1 (10µM) or SCH772984 (10µM), (a specific inhibitor of ERK1/2). qPCR analysis **(G-I)** and IF staining **(H-J)** showing the level of expression of Sftpc on E14.5 lung explant cultures in presence of either IQ-1 or SCH772984 treated with morpholino specific to *miR-142-5p*. Scale bar represents 10µm.

### 4.11 Blockade of Ep300-Ctnnb1 *in vitro* using the pharmacological inhibitor IQ-1 prevents morpholino-*miR-142*-induced increase in Surfactant Protein C (Sftpc).

In order to identify the molecular mechanism responsible for the regulation of alveolar lineage phenotype by *miR-142*, we employed the pharmacological inhibitor IQ-1 (blocks Ep300-Ctnnb1 interaction) and SCH772984, a specific inhibitor of Erk1/2 (inhibits Kras/Erk signaling). Treatment with IQ-1 (10 μm) and SCH772984 (10 μm) on E14.5 lung explants for 4 days showed that both inhibitors are efficient in reducing *Sftpc* expression (Fig. 15E, H, J and Fig. S6E, G) but do not alter the level of *Pdpn* expression (Fig. S6F, H). Next, in a rescue experiment, we evaluated the impact of these inhibitors in presence of morpholinos against *miR-142* (Fig. 15F). Silencing *miR-142* in IQ-1-treated E14.5 lung explants, led to complete downregulation of Sftpc expression indicating that knock down of *miR-142* in this experimental condition, was unable to rescue *Sftpc* expression (Fig. 15G, H). On the other hand, silencing *miR-142* in SCH772984 (Erk inhibitor) treated E14.5 lung explants led to a moderate increase in the expression of Sftpc (Fig. 15I, J). These results suggest that Ep300-Ctnnb1 rather than Kras/Erk signaling is downstream of *miR-142* to control Sftpc expression.

# 5. Discussion

## 5.1 Validation of *miR-142* KO mice

We are among the first group to report the generation and validation of classical *miR-142*-KO mice. We showed both isoforms of *miR-142*, the *3p* and *5p*, are no longer expressed in *miR-142*-KO mice. The expression of *Bzrap1*, a gene immediately flanking *miR-142,* is not altered while the expression of a LncRNA embedded within the *miR-142* gene is abolished. E18.5 *miR-142*-KO lungs display increased Wnt signaling associated with the up-regulation of *Apc* and *Ep300*, two previously reported targets of *miR-142-3p* and *-5p*, respectively. *miR-142*-KO pups are born alive and are normally represented indicating the absence of embryonic lethality. Adult *miR-142*-KO animals are viable and display impaired hematopoietic lineage formation.

A *miR-142* gene-trap allele was recently created by insertion of an exogenous gene trap sequence 50 bp upstream of the murine pre-miR-142 (Chapnik et al., 2014). In these mice, the expression of both *3p* and *5p* was reduced to very low levels but not completely abolished. The authors describe that at E14.5, embryos homozygous for the mutant allele display a normal Mendelian distribution. However, one-third of the postnatal homozygous mutant mice died within 3 weeks. Our results support these observations with the exception of the lack of perinatal death. Even though this remains to be shown, perinatal death may be associated with heart failure due to the absence of adaptive growth of the cardiomyocytes (Sharma et al., 2012). Similarly, to the homozygous *miR-142* gene-trap mice, our *miR-142*-KO mice also display decreased white blood cells, decreased platelets and increased mean platelet volume. However, we did not observe the decrease in red blood cell numbers as well as the increased level of basophils and reticulocytes (data not shown) initially reported in the homozygous *miR-142* gene-trap mice. The basis for such differences is not known so far and could be linked to the genetic background.

More recently, a conditional KO for *miR-142* was generated by deleting 900 bp of the genomic sequence that encompasses the *miR-142* precursor in the germ line (Kramer et al., 2015). The authors reported that *miR-142*-KO mice are born at the expected Mendelian ratio and appear healthy and fertile with no apparent internal organ defects, similarly to the findings described in this report. They also described a highly penetrant splenomegaly that is also observed in our *miR142*-KO mice (data not shown).

## 5.2 *miR-142-3p* and *miR-142-5p* regulate Wnt signaling by targeting *Apc* and *Ep300* respectively.

In order to predict the potential defects observed in *miR-142*-KO animals, the predicted targets for *miR-142-3p* and *5p* were characterized using Diana-MicroT (Vlachos et al., 2012) and Targetscan (targetscan.org) (Fig S7A). Among the processes and pathways potentially affected, we identified endocytosis, regulation of actin cytoskeleton, pathways in cancer, TGFβ signaling and Wnt signaling.

As the *miR-142* conventional KO leads to the deletion of both *miR-142-3p* and *miR-142-5p*, it might be challenging to tease out the activity of each isoform. Others and we have previously reported that *Apc* is a direct target of *miR-142-3p*. Fig. S7B describes the common targets (in orange) for *miR-142-3p* and *5p* as well as unique targets (yellow) for each isoform in regard to the Wnt pathway. Reduction in *Apc* leads to the activation of canonical Wnt signaling by preventing the recruitment of Ctnnb1 to the degradation complex. Increased *Apc* expression upon *miR-142-3p* silencing causes down-regulation of Wnt signaling (Carraro et al., 2014; Isobe et al., 2014). On the other hand, Sharma et al found that *Ep300* is a target of *miR-142-5p*. A mutual inhibitory loop between *Ep300* and *miR-142-5p* has also been described and under mechanical stress, Ep300 is accumulated in the cardiac cells, which results in the down-regulation of *miR-142-5p*. The loss of *miR-142-5p* expression activates genes required for myocyte survival and function (Sharma et al., 2012). Ep300 is a positive regulator of Ctnnb1, which synergistically activates Ctnnb1/TCF transcription (Sun et al., 2000). It is therefore not surprising to find that the loss of *miR-142* leads to increased expression of both Apc and Ep300 (Fig. 5). As Apc is a negative regulator and Ep300 is a positive regulator of Wnt signaling, we expect that upon deletion of *miR-142*, the balance between Apc and Ep300 will lead to either no change in Wnt signaling, an increase or a decrease in Wnt signaling. Our analysis of E12.5 and E18.5 embryonic lungs indicating that the Apc/Ep300 balance favors Wnt signaling. The regulation of the relative expression of both isoforms in specific tissues over time is still unknown. In the embryonic lung at E18.5, both the *-5p* and *-3p* isoforms are normally co-expressed in the epithelium and mesenchyme while *-3p* appears to be more abundantly expressed in the mesenchyme at E12.5 (Carraro et al., 2014). In the hematopoietic system, *-3p* is the predominant isoform expressed. In the heart, it appears that *-5p* is the major isoform. Our mouse model allows determining the overall contribution of *-3p* and *-5p* to Wnt signaling in different tissues and at different developmental stages.

### 5.3 Loss of *miR-142* leads to increased AT2/AT1 cell ratio:

The mechanisms regulating alveolar epithelial cells proliferation and differentiation as well as the advancement of distinct lung progenitor cells towards given mature alveolar cell types are poorly understood (McQualter et al., 2010; Weiss et al., 2008; Zemke et al., 2009). Recently, studies based on the use of cell-specific markers as well as single cell transcriptomic of the epithelium during lung development, have shown that AT1 and AT2 cells derive from common bipotent progenitor cells (Desai et al., 2014; Treutlein et al., 2014).

Here, using a constitutive KO mouse model, we report that in the absence of *miR-142* (abolishing both the *-3p* and *-5p* strands), there is a relative increase of AT2 and a decrease in AT1 cell number (leading to an increase in the AT2/AT1 cell number ratio). Supporting a cell-autonomous function for *miR-142* in the epithelium, increased *miR-142* from E14.5 to E18.5 in alveolar progenitor cells led to the opposite effect. Interestingly, no changes in the number of Epcam or Ki-67 positive cells were observed suggesting a direct impact of *miR-142 in* epithelial cell differentiation. Examination of the KO versus Control lungs at E18.5 revealed enhanced expression of the *miR-142* targets *Apc* and *Ep300*, associated with increased Ctnnb1 and pERK signaling. Morpholino-based knockdown of *miR-142* was sufficient to induce *Sftpc*, decrease *Pdpn,* and increase AT2/AT1 cell number ratio, as well as *Apc*, *Ep300,* and *Kras* expression. Pharmacological inhibition of Ep300-Ctnnb1 but not the Kras/Erk signaling completely prevented *miR-142* morpholino-based increase in *Sftpc* expression. Activation of the glucocorticoid pathway in an *in vitro* alveolar epithelial lineage differentiation assay was sufficient to achieve decreased *miR-142* expression, and recapitulated the increase of *Sftpc* expression. These results suggest that a novel glucocorticoid-*miR-142*-Ep300 signaling axis controls the differentiation of alveolar progenitors and maintains the balance between the AT1 and the AT2 cell number (Fig.16 Graphical abstract).

A surprising result was that the increase in AT2/AT1 cell number ratio observed in *miR-142* loss of function is associated with the AT2 cells with a global decrease in the AT2 and increased in the AT1 gene profile signature. We hypothesize the existence of a dynamic sensing mechanism during lung development, able to detect any unbalance of the AT2/AT1 cell number ratio. This sensing mechanism would take advantage of the plasticity displayed by the AT2 cells that by responding to uncharacterized compensatory mechanisms would prime them for differentiation towards the AT1 lineage. Interestingly,

during homeostasis, the AT2 cells are capable of self-renewal but do not normally give rise to the AT1 cells. However, *in vitro* assays with isolated AT2 cells, co-cultured in Matrigel with stromal cells, leads to the formation of alveolospheres containing both the AT2 and AT1 cells (Barkauskas et al., 2013). Conversely, the AT1 cells appear to be mostly terminally differentiated postnatally but can be reactivated, in the context of lung regeneration induced by pneumonectomy, to proliferate and give rise to the AT2 cells (Jain et al., 2015). It is therefore interesting that this plasticity displayed by alveolar cells postnatally can have a similar impact during embryonic lung development.

Etv5 has been recently reported to be important for the maintenance and differentiation of the AT2 cells. Conditional deletion of *Etv5* postnatally, in the differentiated AT2 cells, leads to the decrease in the AT2 and increase in the AT1 signature (Zhang et al., 2017). While globally, *Etv5* was unchanged in KO vs. control lungs, our gene array analysis showed decreased *Etv5* expression in *miR-142* KO AT2 cells, supporting the loss of AT2 signature in these cells (Fig. 5D). Recently, we showed that Fgf10 might represent a crucial molecule, controlling the differentiation of the bipotent progenitor cells towards the AT2 lineage (Chao et al., 2017). Using *Fgf10* heterozygous (*Fgf10*$^{+/-}$) lungs, we demonstrated a decrease in the AT2/AT1 cell ratio. Furthermore, a defect in epithelial differentiation and proliferation was observed in *Fgf10* hypomorphic lungs showing impairment in the AT2 lineages (Ramasamy et al., 2007). Etv5 is a known downstream target of Fgf10, and while we cannot exclude changes in a component of Fgf10 signaling, Fgf10 per se was unchanged in our model. Furthermore, the fact that pharmacological inhibition of Ep300-Ctnnb1 but not the Kras/Erk signaling completely prevented *miR-142* morpholino-based increase in *Sftpc* expression, suggest a prominent role for Wnt signaling.

Recently, a role for *histone deacetylase 3* (*Hdac3*) in the spreading of the AT1 cells and lung sacculation was reported. It was shown that *Hdac3* expressed in alveolar progenitors represses the expression of *miR-17-92* (Wang et al., 2016b). *miR-142* does not appear to impact the spreading of the AT1 cells as no such defects were detected at E18.5 or postnatally (data not shown). In addition, the adult KO lungs are functional and appear histologically normal ((Shrestha et al., 2015) and data not shown). There is no evidence so far of an organized cross talk between *miR-142* and *miR-17-92* during the late phase of lung development. During early development *miR-17-92* was shown to modulate Fgf10-Fgfr2b signaling by specifically targeting *Stat3* and *Mapk14*, hence regulating Cdh1 expression. The Cdh1 expression level, in-turn, fine-tunes Ctnnb1 signaling in the epithelium, which is critical for epithelial bud morphogenesis triggered by Fgf10 (Carraro

et al., 2009). Interestingly, mutant lungs with specific deletion of *Hdac3* in the mesenchyme also display impairment of the AT1 differentiation, correlating with decreased Ctnnb1 signaling in the epithelium. Rescue of Ctnnb1 signaling in the mutant lung partially rescues the AT1 cell differentiation defects (Wang et al., 2016a). Again, as Ctnnb1 signaling is increased in the *miR-142* KO epithelium, it is very unlikely that this leads to the perturbation of the AT1 differentiation, the conclusion that is supported by our analysis.

## 5.4 Glucocorticoids-*miR-142*-Ep300 signaling axis controls the alveolar epithelial lineage formation

To identify the molecular mechanism involved in the regulation of alveolar epithelial phenotype by *miR-142*, we employed a well-established model to activate glucocorticoid signaling using dexamethasone to stimulate the maturation of alveolar cells into functional AT1 and AT2 cells (Alanis et al., 2014; Laresgoiti et al., 2016). Interestingly, we noted a reduced expression of *miR-142-3p* and *miR-142-5p* in lung explants treated with glucocorticoid agonists, suggesting that the reduced level of *miR-142* is required for the differential of alveolar epithelial cells. Furthermore, we demonstrated two equally important pathways downstream of *miR-142* playing an important role in the formation of the alveolar lineage. Ep300/Ctnnb1 interaction has been shown to be one of the pathways involved in the differentiation of adult epithelial progenitors (Rieger et al., 2016) as well as differentiation of embryonic stem cells and regulation of proximal-distal axis during lung development (Sasaki and Kahn, 2014). *Apc* and *Ep300*, two critical targets of *miR-142*, can control Ctnnb1 pathway. Apc is part of the degradation complex for Ctnnb1 and is, therefore, a negative regulator of Ctnnb1 signaling. Conversely, Ep300 binds to Ctnnb1 and acts as a co-transcriptional activator. *In vitro* blockade of Ctnn1/Ep300 interaction with the use of IQ-1 showed complete down-regulation of Sftpc expression, suggesting impairment in the alveolar epithelial lineage, while *miR-142* LOF was unable to rescue the expression of the AT2 marker (Fig 7H). The other pathway controlled by *miR-142* is the Kras/Erk pathway. A recent report indicated that *miR-142* is highly expressed in undifferentiated mouse embryonic stem cells (mESCs) and downregulated in differentiated cells. It was also reported that overexpression of *miR-142* interrupted mESCS differentiation. A double-negative feedback loop between Kras/Erk and *miR-142* levels has been suggested. Low level of *miR-142* triggers Kras and Erk phosphorylation, which in turn induces mESC differentiation and *vice-versa* (Sladitschek and Neveu, 2015). However, evidence suggests that Kras represses the formation of the alveolar lineage as forced activation of Kras in the distal lung epithelium *in vivo* suppresses the alveolar

differentiation program (Chang et al., 2013). In our *in vitro* model, lung explants treated with Erk inhibitor alone showed reduced Sftpc expression whereas Erk inhibitor treatment in combination with morpholino specific to *miR-142* showed a moderate increase in the Sftpc expression indicating a mild rescue in the alveolar lineage phenotype (Fig. 7J).

In conclusion, we report for the first time, an important role played by both isoforms of *miR-142* in alveolar epithelial lineage formation. We show that *miR-142* governs the formation of AT1 progenitors thereby controlling the AT2/AT1 cell ratio. We propose that a glucocorticoid-*miR-142-Ep300* signaling axis controls alveolar epithelial lineage formation.

### 5.5. Future Perspective

Increased Wnt signaling has been observed in hyper proliferative diseases like Idiopathic pulmonary fibrosis (IPF), a fatal lung disease, which is characterized by, increased fibroblast proliferation, the presence of fibroblastic foci, honeycombing in lung and alveolar tissue remodeling leading to respiratory failure (Morrisey, 2003). On the other hand, increased expression of *miR-142-5p* has been seen in the macrophages of the patients with liver cirrhosis and idiopathic pulmonary fibrosis (Su et al., 2015).

In addition to this, a loss of normal alveolar architecture accompanied the loss of AT1 and AT2 cell balance and fibrotic remodeling was observed in IPF samples (Desai et al., 2014). Since we have demonstrated that *miR-142* can regulate the differentiation of alveolar epithelial cells during lung development we propose that *miR-142* can play a functional role in Idiopathic pulmonary fibrosis (IPF).

Therefore, our future goal is to understand the regulatory mechanism of *miR-142* in pulmonary fibrosis. If we could provide the molecular mechanism that mediates or regulates pulmonary via *miR-142*, it would be a one step closer to develop a therapeutic approach to reduce the severity of IPF.

Furthermore, microarray studies performed on the mouse lung infected with 2009 Pandemic H1N1 influenza A virus showed differential expression pattern of *miR-142-3p* (Wu et al., 2013).

Additionally, other studies demonstrated that insertion of *miR-142* target site into the nucleoprotein of influenza A virus (IAV) attenuates the virus replication (Langlois et al.,

2012). Considering all these data, we consider that our *miR-142* KO mice must be more susceptible to influenza A virus infection.

As influenza A virus mostly infects the epithelial cells of the upper and lower respiratory tract contributing from mild infection to more severe pneumonia associated with acute respiratory distress syndrome. It would be quite interesting to understand the link between *miR-142* and influenza virus infection that will be beneficial for the prevention and control of influenza A virus infection.

*miR-142* has been shown to be linked with various cancers including lung adenocarcinoma (Kaduthanam et al., 2013).Others and our own initial studies demonstrated that *miR-142* is significantly expressed in the mouse model of Bronchopulmonary Dysplasia (BPD), a chronic lung disease affecting mostly premature infants (Nardiello and Morty, 2016; Xing et al., 2015). Better in-depth studies need to be performed in future to understand the specific role of *miR-142* in these diseases.

# 6. Summary

*microRNA-142* (*miR-142*) is emerging as a major regulator of cell fate decision in the hematopoietic cell lineages (Chen et al., 2004) as well as in the maintenance of pluripotency of embryonic stem cells (Sladitschek and Neveu, 2015). However, *miR-142* is also expressed in many other tissues and evidence suggests that it may play a more pleiotropic role during embryonic development and disease. Therefore *miR-142* is regarded as an important regulator of many biological processes and associated signaling pathways during embryonic development, homeostasis, and disease.

The *miR-142* hairpin gives rise to the *miR-142-3p* and *miR-142-5p*. Both variants of miR-*142* are functional and can act on different independent target genes. Previously, we reported that *miR-142-3p* was critical for the control of Wnt signaling in the mesenchyme during lung development (Carraro et al., 2014). *miR-142-5p* has shown to control adaptive growth in the cardiomyocytes postnatally and its increase is associated with extensive apoptosis and cardiac dysfunction. (Sharma et al., 2012).

To understand the role of *miR-142 in vivo*, we generated *miR-142* KO mice using homologous recombination. Our validation studies showed that

- These mice showed significant decrease in both the *3p* and *5p* isoforms with impaired hematopoietic lineage formation, identical to previously reported *miR-142* gene trap knockdown mice (Chapnik et al., 2014).
- The expression of *Bzrap1*, a gene immediately flanking *miR-142* is not altered while the expression of a long non-coding RNA embedded within the *miR-142* gene is decreased.
- *miR-142* KO pups are born alive and are normally represented indicating absence of embryonic lethality.
- *miR-142* KO lungs display increased Wnt signaling associated with the up-regulation of *Apc* and *Ep300*, two previously reported targets of *miR-142-3p* and *-5p*, respectively

We further explored the significant role of *miR-142* in alveolar epithelial lineage formation during embryonic lung development. Squamous alveolar type 1 (AT1) and cuboidal alveolar type 2 (AT2) cells lining the alveolar sacs are regarded among the most important pulmonary cells allowing the lungs to function properly by mediating gaseous exchange

as well as through surfactant production. These AT1 and AT2 cells are derived from bipotent epithelial progenitor cells (Desai et al., 2014; Treutlein et al., 2014). In spite many studies, very little is known about the alveolar progenitor cells regulating the formation maturation and maintenance of AT1 and AT2 cells. Furthermore, the roles of specific microRNAs on these cells are poorly understood. Our analyses demonstrate that

- *miR-142* is expressed in the bipotent progenitors as well as in the differentiated AT1 and AT2 cells.
- *miR-142* is expressed at the much higher level in differentiated AT1 compared to AT2 cells suggesting a specific function for this miR in the formation of the AT1.
- We further demonstrate a significant decrease of AT1 and a corresponding increase of AT2 cells in the lungs of *miR-142* KO embryos.
- Increase in AT1 and the corresponding decrease in AT2 cell number is observed in a mouse model allowing over-expression of *miR-142* in alveolar epithelial progenitors. Such changes occur in absence of alterations at the level of epithelial proliferation or number of bipotent cells.

In an *in vitro* model for alveolar epithelial lineage differentiation assay using dexamethasone (Laresgoiti et al., 2016), we demonstrate that

- Activation of the glucocorticoid pathway led to increased expression of the AT2 marker Sftpc and decreased *miR-142* expression.
- Ep300-Ctnnb1 signaling and Kras/Erk signaling pathway are proposed to be two major pathways involved in the regulation of alveolar differentiation (Rieger et al., 2016; Sasaki and Kahn, 2014; Sladitschek and Neveu, 2015). Pharmacological inhibition of Ep300-Ctnnb1 but not the Kras/Erk signaling completely prevented *miR-142* morpholino-based increase in Sftpc expression.

These results therefore suggest that a critical glucocorticoid-*miR-142-Ep300* signaling axis is responsible for pneumocyte maturation during lung development.

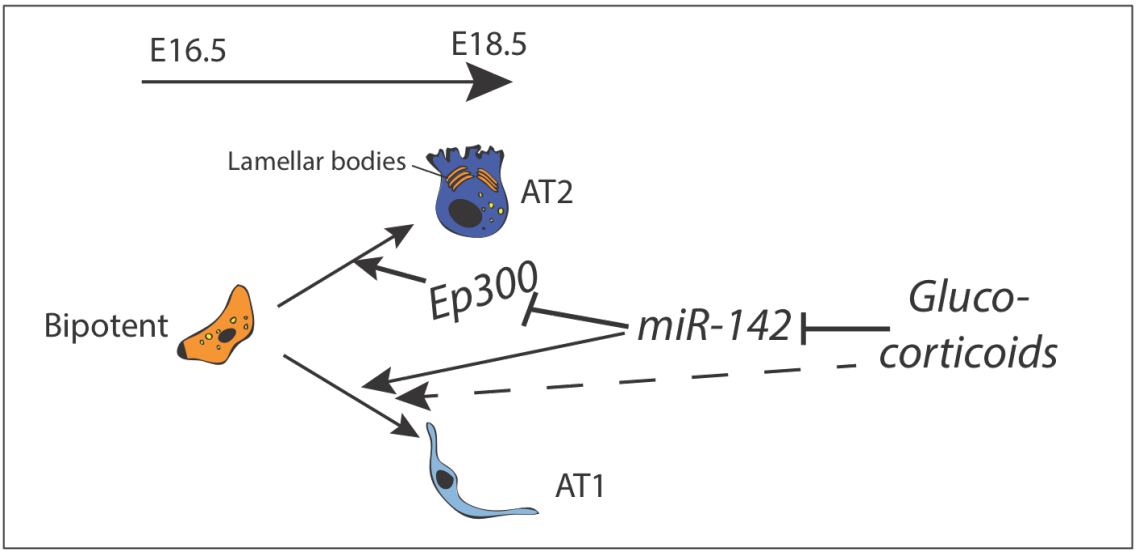


**Figure 16. Graphical abstract: A glucocorticoid-*miR-142-Ep300* signaling axis controls the formation of the alveolar epithelial lineage.** Glucocorticoids (GC) are enhancing AT1 and AT2 formation. GC inhibits *miR-142* expression. Inhibition of *miR-142* is sufficient to increase the AT2 to AT1 ratio but does not perturb the flattening of the AT1 cells. We propose that *miR-142* negatively regulates bipotent cells (BP) to AT2 differentiation while it enhances BP to AT1 differentiation. In addition, GC can also act independent of *miR-142* thereby increasing BP to AT1 differentiation.

# 7. Zusammenfassung

Die *microRNA-142* (*miR-142*) ist ein wichtiger Regulator der hämatopoetischen Zelllinie (Chen et al., 2004) und spielt eine Rolle beim Erhalt der Pluripotenz embryonaler Stammzellen (Sladitschek and Neveu, 2015).

*MiR-142* wird aber auch in anderen Geweben exprimiert; es gibt Hinweise, dass sie eine weitreichende pleiotrope Rolle in der Embryonalentwicklung und bei der Entstehung von Erkrankungen spielt. *MiR-142* gilt daher als ein wichtiger Regulator vieler biologischer Prozesse und die damit assoziierten Signalwege während der Embryonalentwicklung, der Homöostase sowie bei Erkrankungen.

Die *miR-142* kommt als *miR-142-3p* und *miR-142-5p* vor. Beide Varianten sind funktional und wirken unabhängig auf verschiedene Zielgene.
Bisher konnten wir zeigen, dass *miR-142-3p* während der Lungenentwicklung den Wnt-Signalweg im Mesenchym kontrolliert (Carraro et al., 2014). Die *miR-142-5p* steuert das postnatale, adaptive Wachstum der Kardiomyozyten; ein Anstieg der *miR-142-5p* steht in Zusammenhang mit einer vermehrten Apoptose und kardialen Dysfunktion (Sharma et al., 2012).
Zum besseren Verständnis der Rolle von *miR-142 in vivo* wurde mit Hilfe homologer Rekombination eine *miR-142* KO Maus generiert.
Die Validierungsstudien ergaben folgende Resultate:

- Diese Mäuse weisen einen signifikanten Abfall der *3p* und *5p* Isoformen mit einer gestörten Entwicklung der hämatopoetischen Zelllinie. Gleiche Ergebnisse wurden zuvor auch bei der *miR-142* Gene Trap Knockdown Maus gezeigt (Chapnik et al., 2014).
- Die Expression von *Bzrap1*, eines Gens, welches das *miR-142* Gen unmittelbar flankiert, ist unverändert. Die Expression einer im *miR-142* Gen eingebetteten non-coding RNA ist jedoch vermindert.
- Es konnten festgestellt werden. Die *miR-142*-KO Mäuse werden lebend geboren und zeigen keine Anzeichen für embryonale Sterblichkeit .
- *miR-142*-KO Lungen zeigen ein erhöhtes Wnt-Signalweg, welches mit einer Hochregulation von *Apc* und *Ep300* assoziiert ist. *Apc* und *Ep300* wurden bereits als Zielgene von miR-*142-3p* bzw. *miR-142-5p* beschrieben.

Weiterhin wurde der Einfluss von *miR-142* auf die Entwicklung der alveolaren Epithelzelllinie während der embryonalen Lungenentwicklung untersucht. Die alveolaren Zellen vom Typ I (AT1) und vom Typ II (AT2) kleiden die Alveolen aus und gelten als die wichtigsten Zellen der Lunge, da sie den Gasaustausch ermöglichen und Surfactant produzieren. Die AT1 und AT2 Zellen entwickeln sich aus bipotenten epithelialen Vorläuferzellen (Desai et al., 2014; Treutlein et al., 2014). Trotz zahlreicher Studien, ist wenig über die Bildung, die Reifung und den Erhalt der AT1 und AT2 Zellen durch die alveloaren Vorläuferzellen bekannt. Weiterhin ist die Bedeutung spezifischer microRNAs kaum untersucht.

Aus unseren Untersuchungen konnten wir ableiten:

- *miR-142* wird in den bipotenten Vorläuferzellen und in den differenzierten AT1 und AT2 Zellen exprimiert.
- Eine stärkere Expression von *miR-142* in den differenzierten AT1 Zellen als in den differenzierten AT2 Zellen weist auf eine spezifische Funktion der *miR-142* bei der Bildung der AT1 Zellen hin.
- Wir konnten eine signifikante Reduktion von AT1 und einen entsprechenden Anstieg von AT2 Zellen in den Lungen von *miR-142*-KO Embryonen zeigen.
- Im Mausmodell der induzierbaren Überexpression von *miR-142* in alveolaren epithelialen Vorläuferzellen beobachteten wir einen Anstieg von AT1 Zellen und einen entsprechenden Abfall von AT2 Zellen. Dabei konnten keine Veränderungen der epithelialen Proliferation oder der Anzahl der bipotenten Zellen festgestellt werden.

In einem *in-vitro* Modell zur Differenzierung der alveolaren epithelialen Zelllinie mit Dexamethason konnten wir folgendes zeigen (Laresgoiti et al., 2016):

- Eine Aktivierung des Glukokortikoid Signalweg führt zu einer erhöhten Expression des AT2 Markers Sftpc und eine verminderten Expression von *miR-142*.
- Die Ep300-Ctnnb1 und Kras/Erk Signalwege gelten als zwei wichtige Signalwege zur Regulation der alveolaren Differenzierung (Rieger et al., 2016; Sasaki und Kahn, 2014; Sladitschek und Neveu, 2015). Die pharmakologische Inhibition des Ep300-Ctnnb1, aber nicht des Kras/Erk Signalweges, verhindert die durch Morpholino gegen *miR-142* induzierte erhöhte Expression von Sftpc.

Diese Ergebnisse deuten darauf hin, dass die Glukokortikoid-miR-142-*Ep300* Signalachse für die Reifung der Pneumozyten während der Lungenentwicklung von Bedeutung ist.

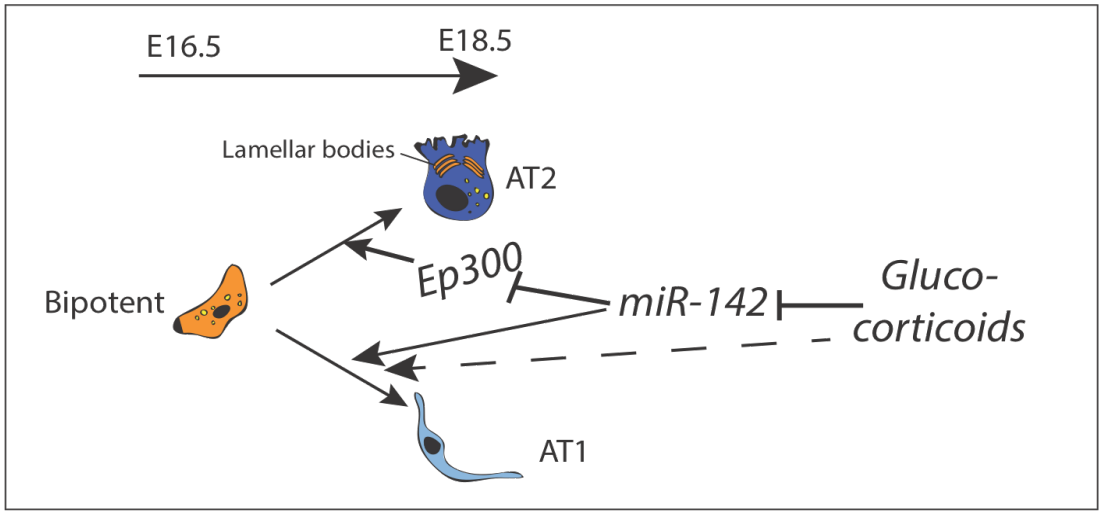


**Fig. 16: Graphische Darstellung: Eine Glukokortikoid-*miR-142-Ep300* Signalachse steuert die alveolare Epithelzelllinie:** Glukokortioide (GC) verstärken die AT1 und AT2 Bildung. GC hemmen die *miR-142* Expression. Diese Hemmung ist ausreichend, das Verhältnis von AT2 zu AT1 zu erhöhen, ohne die Streckung der AT1 zu stören. Wir gehen davon aus, dass *miR-142* ein negativer Regulator der Differenzierung von bipotenten Zellen (BP) zu AT2 Zellen ist, während es die Differenzierung von BP zu AT1 verstärkt. Darüber hinaus können Glukokortikoide - unabhängig von *miR-142* - die Differenzierung von AT1 Zellen aus den BP fördern.

# 8. References

Alanis, D.M., Chang, D.R., Akiyama, H., Krasnow, M.A., and Chen, J. (2014). Two nested developmental waves demarcate a compartment boundary in the mouse lung. Nat Commun *5*, 3923.

Ambros, V. (2004). The functions of animal microRNAs. Nature *431*, 350-355.

Ambros, V., and Lee, R.C. (2004). Identification of microRNAs and other tiny noncoding RNAs by cDNA cloning. Methods Mol Biol *265*, 131-158.

Ameres, S.L., and Zamore, P.D. (2013). Diversifying microRNA sequence and function. Nat Rev Mol Cell Biol *14*, 475-488.

Angulo, M., Lecuona, E., and Sznajder, J.I. (2012). Role of MicroRNAs in lung disease. Arch Bronconeumol *48*, 325-330.

Annoni, A., Brown, B.D., Cantore, A., Sergi, L.S., Naldini, L., and Roncarolo, M.G. (2009). In vivo delivery of a microRNA-regulated transgene induces antigen-specific regulatory T cells and promotes immunologic tolerance. Blood *114*, 5152-5161.

Barkauskas, C.E., Cronce, M.J., Rackley, C.R., Bowie, E.J., Keene, D.R., Stripp, B.R., Randell, S.H., Noble, P.W., and Hogan, B.L. (2013). Type 2 alveolar cells are stem cells in adult lung. J Clin Invest *123*, 3025-3036.

Bartel, D.P. (2004). MicroRNAs: genomics, biogenesis, mechanism, and function. Cell *116*, 281-297.

Bhaskaran, M., Wang, Y., Zhang, H., Weng, T., Baviskar, P., Guo, Y., Gou, D., and Liu, L. (2009). MicroRNA-127 modulates fetal lung development. Physiol Genomics *37*, 268-278.

Calin, G.A., and Croce, C.M. (2006). MicroRNA signatures in human cancers. Nat Rev Cancer *6*, 857-866.

Cardoso, W.V., and Lu, J. (2006). Regulation of early lung morphogenesis: questions, facts and controversies. Development *133*, 1611-1624.

Carraro, G., El-Hashash, A., Guidolin, D., Tiozzo, C., Turcatel, G., Young, B.M., De Langhe, S.P., Bellusci, S., Shi, W., Parnigotto, P.P.*, et al.* (2009). miR-17 family of microRNAs controls FGF10-mediated embryonic lung epithelial branching morphogenesis through MAPK14 and STAT3 regulation of E-Cadherin distribution. Dev Biol *333*, 238-250.

Carraro, G., Shrestha, A., Rostkovius, J., Contreras, A., Chao, C.M., El Agha, E., Mackenzie, B., Dilai, S., Guidolin, D., Taketo, M.M.*, et al.* (2014). miR-142-3p balances proliferation and differentiation of mesenchymal cells during lung development. Development *141*, 1272-1281.

Chang, D.R., Martinez Alanis, D., Miller, R.K., Ji, H., Akiyama, H., McCrea, P.D., and Chen, J. (2013). Lung epithelial branching program antagonizes alveolar differentiation. Proc Natl Acad Sci U S A *110*, 18042-18051.

Chao, C.M., El Agha, E., Tiozzo, C., Minoo, P., and Bellusci, S. (2015). A breath of fresh air on the mesenchyme: impact of impaired mesenchymal development on the pathogenesis of bronchopulmonary dysplasia. Front Med (Lausanne) *2*, 27.

Chao, C.M., Yahya, F., Moiseenko, A., Tiozzo, C., Shrestha, A., Ahmadvand, N., El Agha, E., Quantius, J., Dilai, S., Kheirollahi, V.*, et al.* (2017). Fgf10 deficiency is causative for lethality in a mouse model of bronchopulmonary dysplasia. J Pathol *241*, 91-103.

Chapnik, E., Rivkin, N., Mildner, A., Beck, G., Pasvolsky, R., Metzl-Raz, E., Birger, Y., Amir, G., Tirosh, I., Porat, Z.*, et al.* (2014). miR-142 orchestrates a network of actin cytoskeleton regulators during megakaryopoiesis. Elife *3*, e01964.

Chen, C.Z., Li, L., Lodish, H.F., and Bartel, D.P. (2004). MicroRNAs modulate hematopoietic lineage differentiation. Science *303*, 83-86.

Chen, C.Z., Schaffert, S., Fragoso, R., and Loh, C. (2013). Regulation of immune responses and tolerance: the microRNA perspective. Immunol Rev *253*, 112-128.

Chiou, G.Y., Chien, C.S., Wang, M.L., Chen, M.T., Yang, Y.P., Yu, Y.L., Chien, Y., Chang, Y.C., Shen, C.C., Chio, C.C.*, et al.* (2013). Epigenetic regulation of the miR142-3p/interleukin-6 circuit in glioblastoma. Mol Cell *52*, 693-706.

Danger, R., Pallier, A., Giral, M., Martinez-Llordella, M., Lozano, J.J., Degauque, N., Sanchez-Fueyo, A., Soulillou, J.P., and Brouard, S. (2012). Upregulation of miR-142-3p in peripheral blood mononuclear cells of operationally tolerant patients with a renal transplant. J Am Soc Nephrol *23*, 597-606.

Deng, B., Zhang, Y., Zhang, S., Wen, F., Miao, Y., and Guo, K. (2015). MicroRNA-142-3p inhibits cell proliferation and invasion of cervical cancer cells by targeting FZD7. Tumour Biol *36*, 8065-8073.

Desai, T.J., Brownfield, D.G., and Krasnow, M.A. (2014). Alveolar progenitor and stem cells in lung development, renewal and cancer. Nature *507*, 190-194.

El Agha, E., and Bellusci, S. (2014). Walking along the Fibroblast Growth Factor 10 Route: A Key Pathway to Understand the Control and Regulation of Epithelial and Mesenchymal Cell-Lineage Formation during Lung Development and Repair after Injury. Scientifica (Cairo) *2014*, 538379.

Esteller, M. (2011). Non-coding RNAs in human disease. Nat Rev Genet *12*, 861-874.

Fan, H.B., Liu, Y.J., Wang, L., Du, T.T., Dong, M., Gao, L., Meng, Z.Z., Jin, Y., Chen, Y., Deng, M.*, et al.* (2014). miR-142-3p acts as an essential modulator of neutrophil development in zebrafish. Blood *124*, 1320-1330.

Friedman, R.C., Farh, K.K., Burge, C.B., and Bartel, D.P. (2009). Most mammalian mRNAs are conserved targets of microRNAs. Genome Res *19*, 92-105.

Harris, K.S., Zhang, Z., McManus, M.T., Harfe, B.D., and Sun, X. (2006). Dicer function is essential for lung epithelium morphogenesis. Proc Natl Acad Sci U S A *103*, 2208-2213.

He, L., and Hannon, G.J. (2004). MicroRNAs: small RNAs with a big role in gene regulation. Nat Rev Genet *5*, 522-531.

Herriges, J.C., Verheyden, J.M., Zhang, Z., Sui, P., Zhang, Y., Anderson, M.J., Swing, D.A., Zhang, Y., Lewandoski, M., and Sun, X. (2015). FGF-Regulated ETV Transcription Factors Control FGF-SHH Feedback Loop in Lung Branching. Dev Cell *35*, 322-332.

Herriges, M.J., Swarr, D.T., Morley, M.P., Rathi, K.S., Peng, T., Stewart, K.M., and Morrisey, E.E. (2014). Long noncoding RNAs are spatially correlated with transcription factors and regulate lung development. Genes Dev *28*, 1363-1379.

Huntzinger, E., and Izaurralde, E. (2011). Gene silencing by microRNAs: contributions of translational repression and mRNA decay. Nat Rev Genet *12*, 99-110.

Isobe, T., Hisamori, S., Hogan, D.J., Zabala, M., Hendrickson, D.G., Dalerba, P., Cai, S., Scheeren, F., Kuo, A.H., Sikandar, S.S.*, et al.* (2014). miR-142 regulates the tumorigenicity of human breast cancer stem cells through the canonical WNT signaling pathway. Elife *3*.

Iwasaki, K., Yamamoto, T., Inanaga, Y., Hiramitsu, T., Miwa, Y., Murotani, K., Narumi, S., Watarai, Y., Katayama, A., Uchida, K.*, et al.* (2016). MiR-142-5p and miR-486-5p as biomarkers for early detection of chronic antibody-mediated rejection in kidney transplantation. Biomarkers, 1-10.

Jain, R., Barkauskas, C.E., Takeda, N., Bowie, E.J., Aghajanian, H., Wang, Q., Padmanabhan, A., Manderfield, L.J., Gupta, M., Li, D.*, et al.* (2015). Plasticity of Hopx(+) type I alveolar cells to regenerate type II cells in the lung. Nat Commun *6*, 6727.

Johar, D., Siragam, V., Mahood, T.H., and Keijzer, R. (2015). New insights into lung development and diseases: the role of microRNAs. Biochem Cell Biol *93*, 139-148.

Jonas, S., and Izaurralde, E. (2015). Towards a molecular understanding of microRNA-mediated gene silencing. Nat Rev Genet *16*, 421-433.

Kaduthanam, S., Gade, S., Meister, M., Brase, J.C., Johannes, M., Dienemann, H., Warth, A., Schnabel, P.A., Herth, F.J., Sultmann, H.*, et al.* (2013). Serum miR-142-3p is associated with early relapse in operable lung adenocarcinoma patients. Lung Cancer *80*, 223-227.

Kee, H.J., Park, S., Kwon, J.S., Choe, N., Ahn, Y., Kook, H., and Jeong, M.H. (2013). B cell translocation gene, a direct target of miR-142-5p, inhibits vascular smooth muscle cell proliferation by down-regulating cell cycle progression. FEBS Lett *587*, 2385-2392.

Kimura, J., and Deutsch, G.H. (2007). Key mechanisms of early lung development. Pediatr Dev Pathol *10*, 335-347.

Kotton, D.N., and Morrisey, E.E. (2014). Lung regeneration: mechanisms, applications and emerging stem cell populations. Nat Med *20*, 822-832.

Kramer, N.J., Wang, W.L., Reyes, E.Y., Kumar, B., Chen, C.C., Ramakrishna, C., Cantin, E.M., Vonderfecht, S.L., Taganov, K.D., Chau, N.*, et al.* (2015). Altered lymphopoiesis and immunodeficiency in miR-142 null mice. Blood *125*, 3720-3730.

Krol, J., Loedige, I., and Filipowicz, W. (2010). The widespread regulation of microRNA biogenesis, function and decay. Nat Rev Genet *11*, 597-610.

Langlois, R.A., Varble, A., Chua, M.A., Garcia-Sastre, A., and tenOever, B.R. (2012). Hematopoietic-specific targeting of influenza A virus reveals replication requirements for induction of antiviral immune responses. Proc Natl Acad Sci U S A *109*, 12117-12122.

Laresgoiti, U., Nikolic, M.Z., Rao, C., Brady, J.L., Richardson, R.V., Batchen, E.J., Chapman, K.E., and Rawlins, E.L. (2016). Lung epithelial tip progenitors integrate glucocorticoid- and STAT3-mediated signals to control progeny fate. Development *143*, 3686-3699.

Lei, Z., Xu, G., Wang, L., Yang, H., Liu, X., Zhao, J., and Zhang, H.T. (2014). MiR-142-3p represses TGF-beta-induced growth inhibition through repression of TGFbetaR1 in non-small cell lung cancer. FASEB J *28*, 2696-2704.

Lin, R.J., Xiao, D.W., Liao, L.D., Chen, T., Xie, Z.F., Huang, W.Z., Wang, W.S., Jiang, T.F., Wu, B.L., Li, E.M.*, et al.* (2012). MiR-142-3p as a potential prognostic biomarker for esophageal squamous cell carcinoma. J Surg Oncol *105*, 175-182.

Liu, X., Sempere, L.F., Galimberti, F., Freemantle, S.J., Black, C., Dragnev, K.H., Ma, Y., Fiering, S., Memoli, V., Li, H.*, et al.* (2009). Uncovering growth-suppressive MicroRNAs in lung cancer. Clin Cancer Res *15*, 1177-1183.

Lu, X., Li, X., He, Q., Gao, J., Gao, Y., Liu, B., and Liu, F. (2013). miR-142-3p regulates the formation and differentiation of hematopoietic stem cells in vertebrates. Cell Res *23*, 1356-1368.

Lu, Y., Thomson, J.M., Wong, H.Y., Hammond, S.M., and Hogan, B.L. (2007). Transgenic over-expression of the microRNA miR-17-92 cluster promotes proliferation and inhibits differentiation of lung epithelial progenitor cells. Dev Biol *310*, 442-453.

Ma, Z., Liu, T., Huang, W., Liu, H., Zhang, H.M., Li, Q., Chen, Z., and Guo, A.Y. (2016). MicroRNA regulatory pathway analysis identifies miR-142-5p as a negative regulator of TGF-beta pathway via targeting SMAD3. Oncotarget.

Maes, T., Cobos, F.A., Schleich, F., Sorbello, V., Henket, M., De Preter, K., Bracke, K.R., Conickx, G., Mesnil, C., Vandesompele, J.*, et al.* (2016). Asthma inflammatory phenotypes show differential microRNA expression in sputum. J Allergy Clin Immunol *137*, 1433-1446.

Mailleux, A.A., Tefft, D., Ndiaye, D., Itoh, N., Thiery, J.P., Warburton, D., and Bellusci, S. (2001). Evidence that SPROUTY2 functions as an inhibitor of mouse embryonic lung growth and morphogenesis. Mech Dev *102*, 81-94.

McCulley, D., Wienhold, M., and Sun, X. (2015). The pulmonary mesenchyme directs lung development. Curr Opin Genet Dev *32*, 98-105.

McQualter, J.L., Yuen, K., Williams, B., and Bertoncello, I. (2010). Evidence of an epithelial stem/progenitor cell hierarchy in the adult mouse lung. Proc Natl Acad Sci U S A *107*, 1414-1419.

Morimoto, T., Sunagawa, Y., Kawamura, T., Takaya, T., Wada, H., Nagasawa, A., Komeda, M., Fujita, M., Shimatsu, A., Kita, T.*, et al.* (2008). The dietary compound curcumin inhibits p300 histone acetyltransferase activity and prevents heart failure in rats. J Clin Invest *118*, 868-878.

Morrisey, E.E. (2003). Wnt signaling and pulmonary fibrosis. Am J Pathol *162*, 1393-1397.

Morrisey, E.E., and Hogan, B.L. (2010). Preparing for the first breath: genetic and cellular mechanisms in lung development. Dev Cell *18*, 8-23.

Nardiello, C., and Morty, R.E. (2016). MicroRNA in late lung development and bronchopulmonary dysplasia: the need to demonstrate causality. Mol Cell Pediatr *3*, 19.

Nimmo, R., Ciau-Uitz, A., Ruiz-Herguido, C., Soneji, S., Bigas, A., Patient, R., and Enver, T. (2013). MiR-142-3p controls the specification of definitive hemangioblasts during ontogeny. Dev Cell *26*, 237-249.

Nishiyama, T., Kaneda, R., Ono, T., Tohyama, S., Hashimoto, H., Endo, J., Tsuruta, H., Yuasa, S., Ieda, M., Makino, S.*, et al.* (2012). miR-142-3p is essential for hematopoiesis and affects cardiac cell fate in zebrafish. Biochem Biophys Res Commun *425*, 755-761.

Ornitz, D.M., and Yin, Y. (2012). Signaling networks regulating development of the lower respiratory tract. Cold Spring Harb Perspect Biol *4*.

Qian, S., Ding, J.Y., Xie, R., An, J.H., Ao, X.J., Zhao, Z.G., Sun, J.G., Duan, Y.Z., Chen, Z.T., and Zhu, B. (2008). MicroRNA expression profile of bronchioalveolar stem cells from mouse lung. Biochem Biophys Res Commun *377*, 668-673.

Ramasamy, S.K., Mailleux, A.A., Gupte, V.V., Mata, F., Sala, F.G., Veltmaat, J.M., Del Moral, P.M., De Langhe, S., Parsa, S., Kelly, L.K.*, et al.* (2007). Fgf10 dosage is critical for the amplification of epithelial cell progenitors and for the formation of multiple mesenchymal lineages during lung development. Dev Biol *307*, 237-247.

Rawlins, E.L., Clark, C.P., Xue, Y., and Hogan, B.L. (2009). The Id2+ distal tip lung epithelium contains individual multipotent embryonic progenitor cells. Development *136*, 3741-3745.

Rieger, M.E., Zhou, B., Solomon, N., Sunohara, M., Li, C., Nguyen, C., Liu, Y., Pan, J.H., Minoo, P., Crandall, E.D.*, et al.* (2016). p300/beta-Catenin Interactions Regulate Adult Progenitor Cell Differentiation Downstream of WNT5a/Protein Kinase C (PKC). J Biol Chem *291*, 6569-6582.

Rock, J.R., and Hogan, B.L. (2011). Epithelial progenitor cells in lung development, maintenance, repair, and disease. Annu Rev Cell Dev Biol *27*, 493-512.

Sasaki, T., and Kahn, M. (2014). Inhibition of beta-catenin/p300 interaction proximalizes mouse embryonic lung epithelium. Transl Respir Med *2*, 8.

Schulte, C., and Zeller, T. (2015). microRNA-based diagnostics and therapy in cardiovascular disease-Summing up the facts. Cardiovasc Diagn Ther *5*, 17-36.

Sessa, R., and Hata, A. (2013). Role of microRNAs in lung development and pulmonary diseases. Pulm Circ *3*, 315-328.

Sharma, S., Liu, J., Wei, J., Yuan, H., Zhang, T., and Bishopric, N.H. (2012). Repression of miR-142 by p300 and MAPK is required for survival signalling via gp130 during adaptive hypertrophy. EMBO Mol Med *4*, 617-632.

Shrestha, A., Carraro, G., El Agha, E., Mukhametshina, R., Chao, C.M., Rizvanov, A., Barreto, G., and Bellusci, S. (2015). Generation and Validation of miR-142 Knock Out Mice. PLoS One *10*, e0136913.

Sladitschek, H.L., and Neveu, P.A. (2015). The bimodally expressed microRNA miR-142 gates exit from pluripotency. Mol Syst Biol *11*, 850.

Su, S., Zhao, Q., He, C., Huang, D., Liu, J., Chen, F., Chen, J., Liao, J.Y., Cui, X., Zeng, Y.*, et al.* (2015). miR-142-5p and miR-130a-3p are regulated by IL-4 and IL-13 and control profibrogenic macrophage program. Nat Commun *6*, 8523.

Sun, Y., Kolligs, F.T., Hottiger, M.O., Mosavin, R., Fearon, E.R., and Nabel, G.J. (2000). Regulation of beta -catenin transformation by the p300 transcriptional coactivator. Proc Natl Acad Sci U S A *97*, 12613-12618.

Treutlein, B., Brownfield, D.G., Wu, A.R., Neff, N.F., Mantalas, G.L., Espinoza, F.H., Desai, T.J., Krasnow, M.A., and Quake, S.R. (2014). Reconstructing lineage hierarchies of the distal lung epithelium using single-cell RNA-seq. Nature *509*, 371-375.

Tsang, F.H., Au, S.L., Wei, L., Fan, D.N., Lee, J.M., Wong, C.C., Ng, I.O., and Wong, C.M. (2015). MicroRNA-142-3p and microRNA-142-5p are downregulated in hepatocellular carcinoma and exhibit synergistic effects on cell motility. Front Med *9*, 331-343.

Vegter, E.L., van der Meer, P., de Windt, L.J., Pinto, Y.M., and Voors, A.A. (2016). MicroRNAs in heart failure: from biomarker to target for therapy. Eur J Heart Fail *18*, 457-468.

Ventura, A., Young, A.G., Winslow, M.M., Lintault, L., Meissner, A., Erkeland, S.J., Newman, J., Bronson, R.T., Crowley, D., Stone, J.R.*, et al.* (2008). Targeted deletion reveals essential and overlapping functions of the miR-17 through 92 family of miRNA clusters. Cell *132*, 875-886.

Vlachos, I.S., Kostoulas, N., Vergoulis, T., Georgakilas, G., Reczko, M., Maragkakis, M., Paraskevopoulou, M.D., Prionidis, K., Dalamagas, T., and Hatzigeorgiou, A.G. (2012). DIANA miRPath v.2.0: investigating the combinatorial effect of microRNAs in pathways. Nucleic Acids Res *40*, W498-504.

Wang, X., Wang, Y., Snitow, M.E., Stewart, K.M., Li, S., Lu, M., and Morrisey, E.E. (2016a). Expression of histone deacetylase 3 instructs alveolar type I cell differentiation by regulating a Wnt signaling niche in the lung. Dev Biol *414*, 161-169.

Wang, X.S., Gong, J.N., Yu, J., Wang, F., Zhang, X.H., Yin, X.L., Tan, Z.Q., Luo, Z.M., Yang, G.H., Shen, C.*, et al.* (2012). MicroRNA-29a and microRNA-142-3p are regulators of myeloid differentiation and acute myeloid leukemia. Blood *119*, 4992-5004.

Wang, Y., Frank, D.B., Morley, M.P., Zhou, S., Wang, X., Lu, M.M., Lazar, M.A., and Morrisey, E.E. (2016b). HDAC3-Dependent Epigenetic Pathway Controls Lung Alveolar Epithelial Cell Remodeling and Spreading via miR-17-92 and TGF-beta Signaling Regulation. Dev Cell *36*, 303-315.

Warburton, D., El-Hashash, A., Carraro, G., Tiozzo, C., Sala, F., Rogers, O., De Langhe, S., Kemp, P.J., Riccardi, D., Torday, J.*, et al.* (2010). Lung organogenesis. Curr Top Dev Biol *90*, 73-158.

Wei, J.Q., Shehadeh, L.A., Mitrani, J.M., Pessanha, M., Slepak, T.I., Webster, K.A., and Bishopric, N.H. (2008). Quantitative control of adaptive cardiac hypertrophy by acetyltransferase p300. Circulation *118*, 934-946.

Weiss, D.J., Kolls, J.K., Ortiz, L.A., Panoskaltsis-Mortari, A., and Prockop, D.J. (2008). Stem cells and cell therapies in lung biology and lung diseases. Proc Am Thorac Soc *5*, 637-667.

Whitsett, J.A., Wert, S.E., and Weaver, T.E. (2010). Alveolar surfactant homeostasis and the pathogenesis of pulmonary disease. Annu Rev Med *61*, 105-119.

Williams, A.E., Moschos, S.A., Perry, M.M., Barnes, P.J., and Lindsay, M.A. (2007). Maternally imprinted microRNAs are differentially expressed during mouse and human lung development. Dev Dyn *236*, 572-580.

Winter, J., Jung, S., Keller, S., Gregory, R.I., and Diederichs, S. (2009). Many roads to maturity: microRNA biogenesis pathways and their regulation. Nat Cell Biol *11*, 228-234.

Wu, L., Cai, C., Wang, X., Liu, M., Li, X., and Tang, H. (2011). MicroRNA-142-3p, a new regulator of RAC1, suppresses the migration and invasion of hepatocellular carcinoma cells. FEBS Lett *585*, 1322-1330.

Wu, Z., Hao, R., Li, P., Zhang, X., Liu, N., Qiu, S., Wang, L., Wang, Y., Xue, W., Liu, K.*, et al.* (2013). MicroRNA expression profile of mouse lung infected with 2009 pandemic H1N1 influenza virus. PLoS One *8*, e74190.

Xing, Y., Fu, J., Yang, H., Yao, L., Qiao, L., Du, Y., and Xue, X. (2015). MicroRNA expression profiles and target prediction in neonatal Wistar rat lungs during the development of bronchopulmonary dysplasia. Int J Mol Med *36*, 1253-1263.

Zemke, A.C., Teisanu, R.M., Giangreco, A., Drake, J.A., Brockway, B.L., Reynolds, S.D., and Stripp, B.R. (2009). beta-Catenin is not necessary for maintenance or repair of the bronchiolar epithelium. Am J Respir Cell Mol Biol *41*, 535-543.

Zhang, Z., Newton, K., Kummerfeld, S.K., Webster, J., Kirkpatrick, D.S., Phu, L., Eastham-Anderson, J., Liu, J., Lee, W.P., Wu, J.*, et al.* (2017). Transcription factor Etv5 is essential for the maintenance of alveolar type II cells. Proc Natl Acad Sci U S A *114*, 3903-3908.

# 9. Supplementary Material

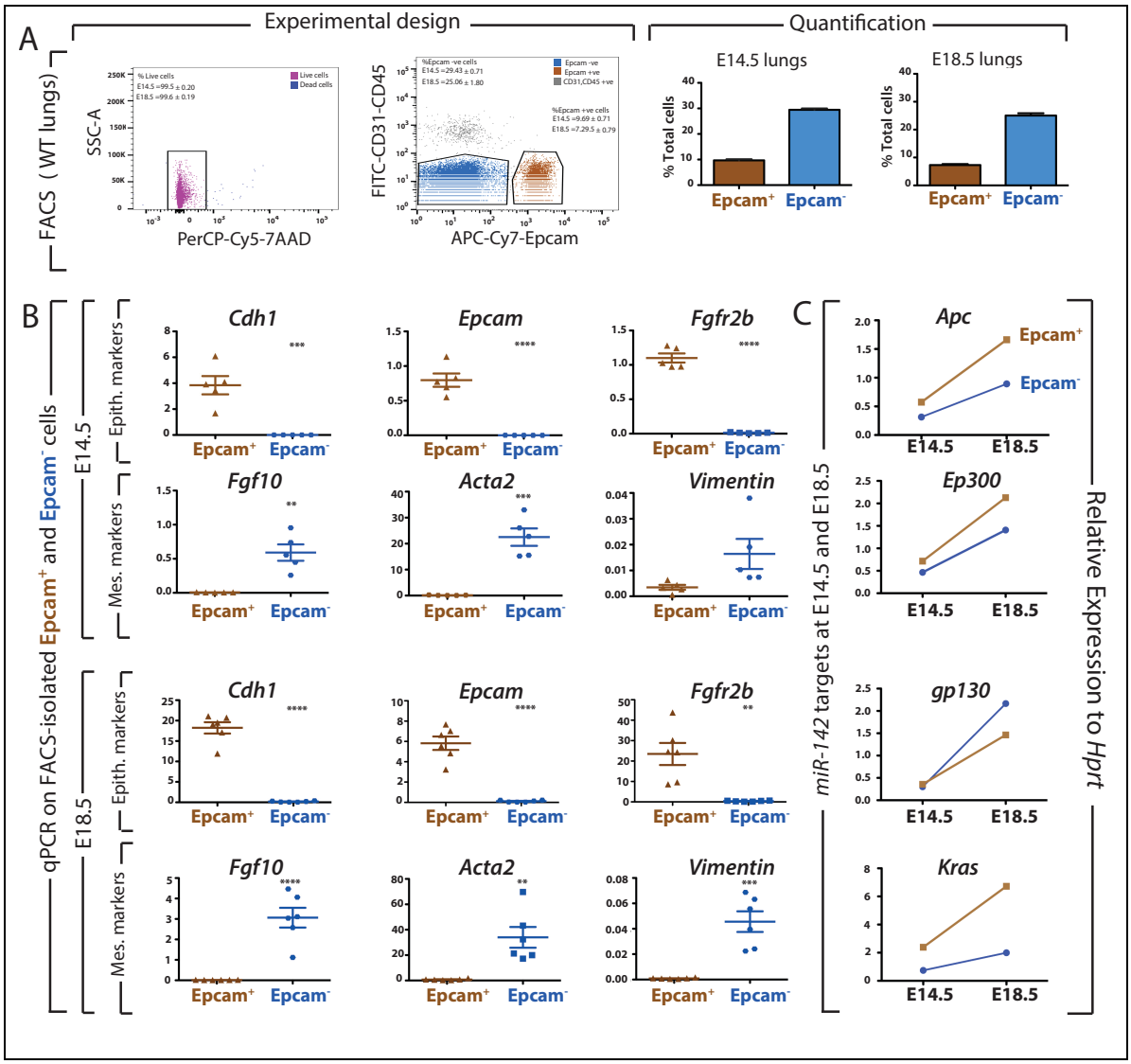


**Figure S1. FACS-based isolation of resident epithelial and mesenchymal cells and validation of gene expression. (A)** FACS-based isolation of CD31$^{-ve}$ CD45$^{-ve}$ Epcam$^{+ve}$ (resident epithelium) and Epcam$^{-ve}$ (resident mesenchyme). Quantification showing the epithelial to mesenchymal ratio at E14.5 and E18.5. **(B)** qPCR validation of the isolated epithelial and mesenchymal cells using epithelial (*Cdh1*, *Epcam*, *Fgfr2b*) and mesenchymal (*Fgf10*, *Acta2*, *Vimentin*) markers at these two time points. **(C)** Expression analysis of *miR-142* targets *Apc, Ep300, gp130* and *Kras* in the mesenchyme as well as in the epithelium. *Hprt* used as a housekeeping gene.

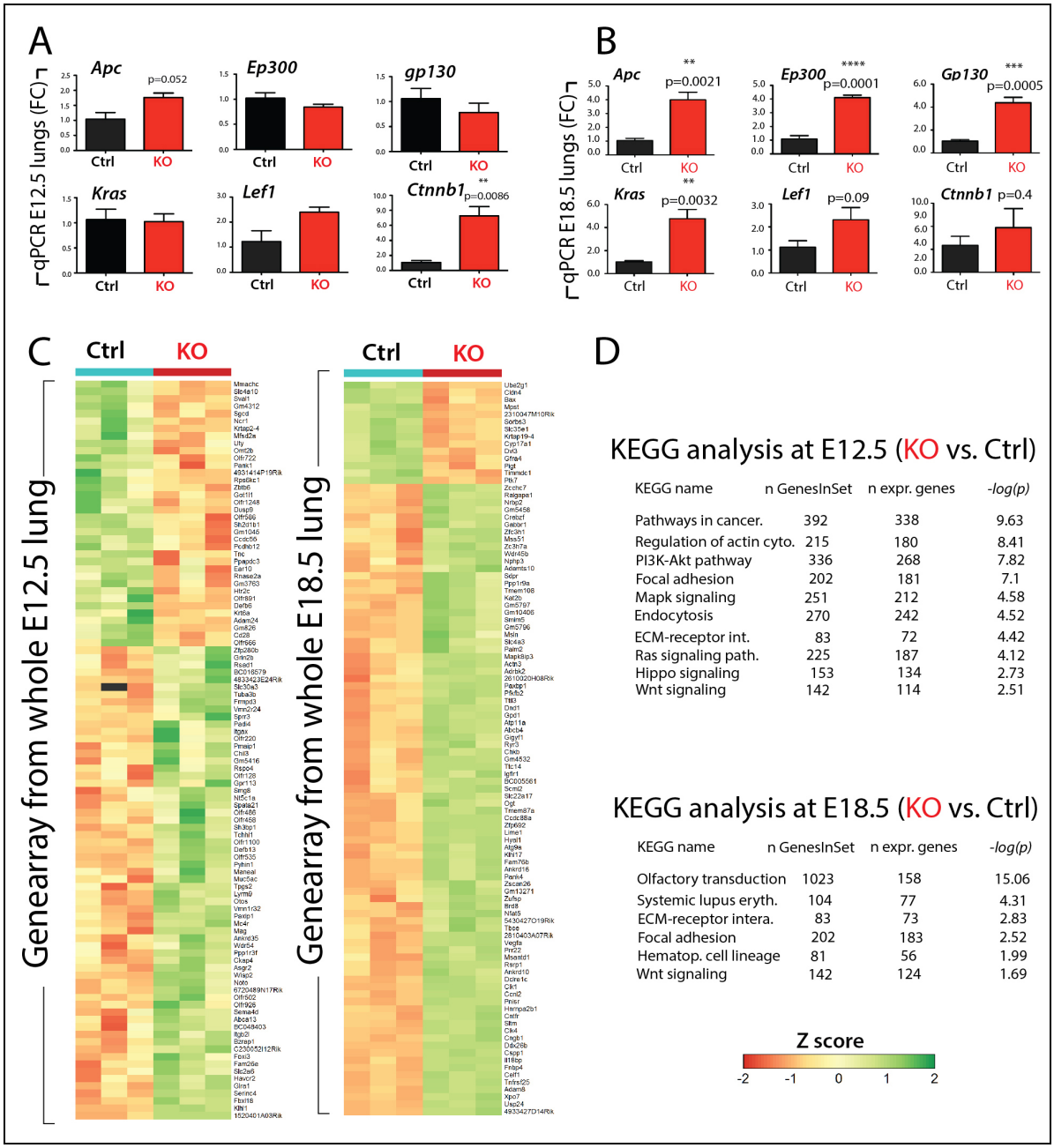


**Figure S2. Gene Array and KEGG pathway analysis on E12.5 and E18.5 Control and KO lungs. A)** Gene expression analysis of *miR-142* target genes by qPCR in E12.5 and **B)** E18.5 Control and *miR-142* KO lungs **C)** Gene array analysis (n=3). **D)** Corresponding KEGG pathway analysis.

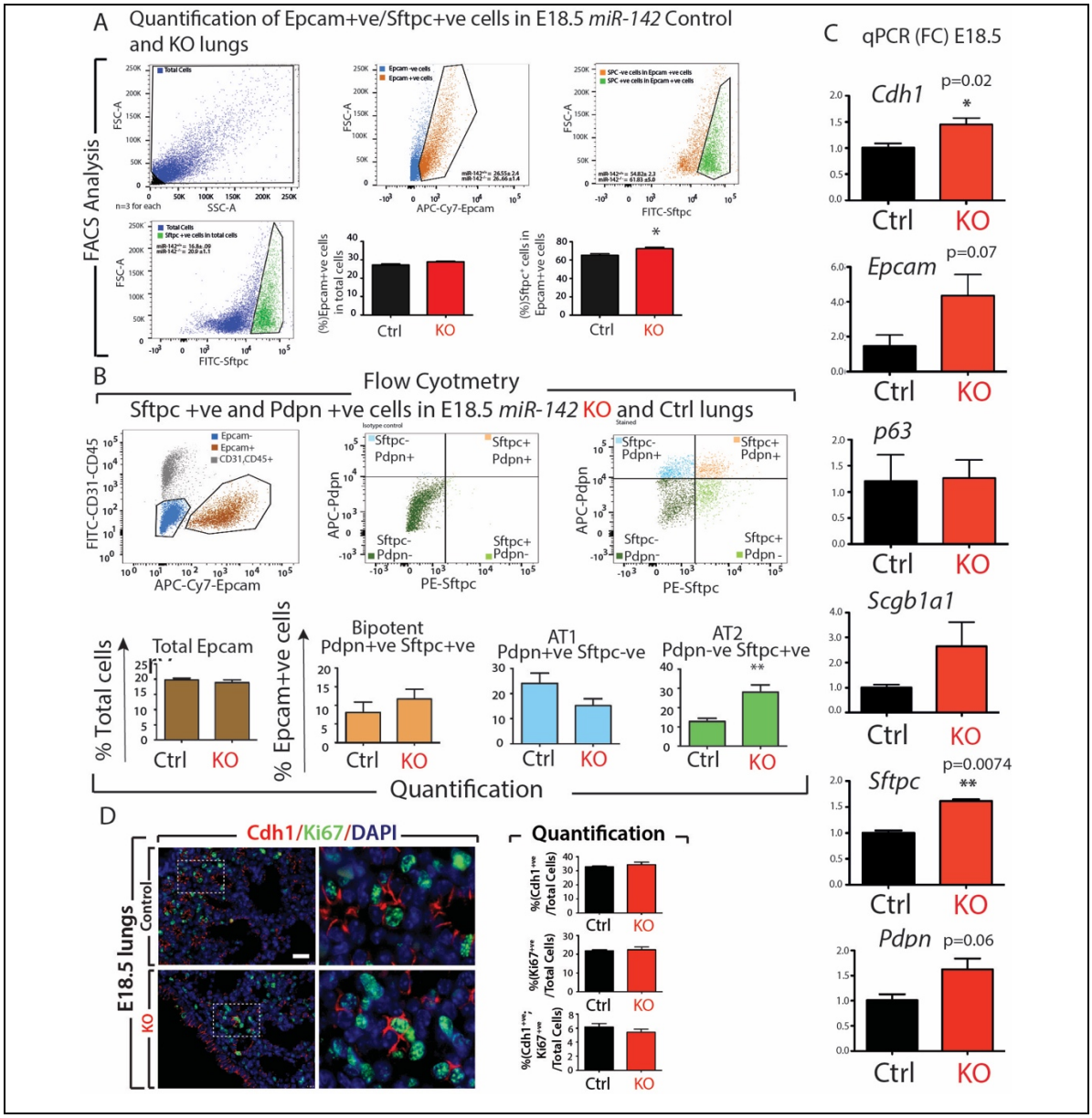


**Figure S3. Quantification of the number of Epcam as well as AT2 cells in Control and Experimental *miR-142* KO lungs at E18.5. Analysis of proliferation (A)** Flow cytometric analysis using Epcam and Sftpc antibodies in E18.5 *miR-142* KO showed an increase in the percentage of AT2 cells compared to the wild type littermate controls**. (B)** Flow cytometry analysis using Epcam, Sftpc and Pdpn antibodies in E18.5 *miR-142* KO lungs showed a decrease in Pdpn+ve (AT1) and increased in Sftpc +ve (AT2) cells compared to the wild type littermate controls. Quantification of Pdpn+ve and Sftpc +ve cells. **(C)** qPCR analysis for general epithelial markers (*Cdh1*, Epcam) as well as for markers of the conducting (*p63*, *Scgb1a1*) and respiratory (*Sftpc*, *Pdpn*) airways. **(D)** Cdh1/Ki67 double IF staining in E18.5 Control and KO lungs showed no significant difference in proliferation between Control and KO lungs. Scale bar represents 10µm.

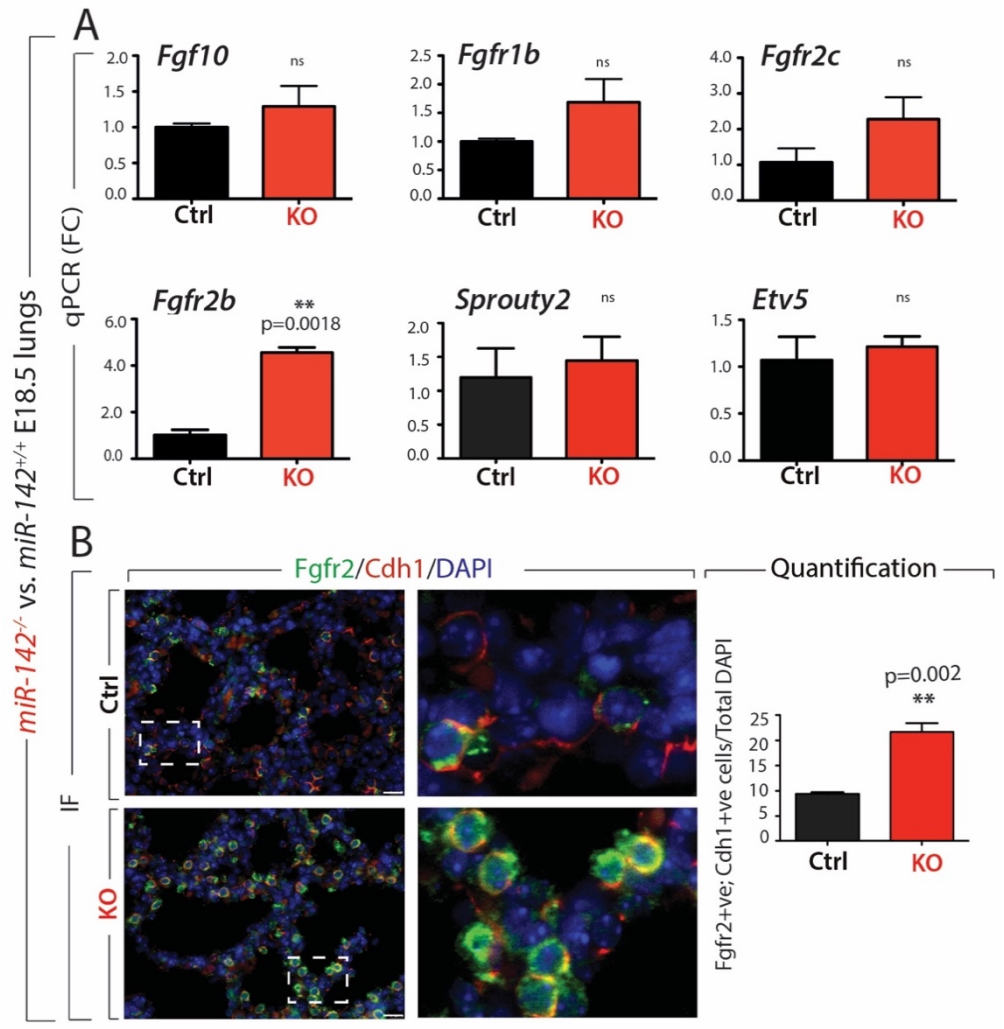


**Figure S4. Examination of Fgf signaling in E18.5 *miR-142* Control and KO lungs. (A)** qPCR analysis of *Fgf10*, *Fgfr1b*, *Fgfr2b Fgfr2c, Sprouty2* and *Etv5* in E18.5 Control and KO lungs. **(B)** Fgfr2 expression in the epithelium is validated by immunofluorescence with Fgfr2 and Cdh1 antibodies. Quantification indicating increased number of $Fgfr2^{+ve}$ cells in KO vs. control lungs. Scale bar represents 10μm.

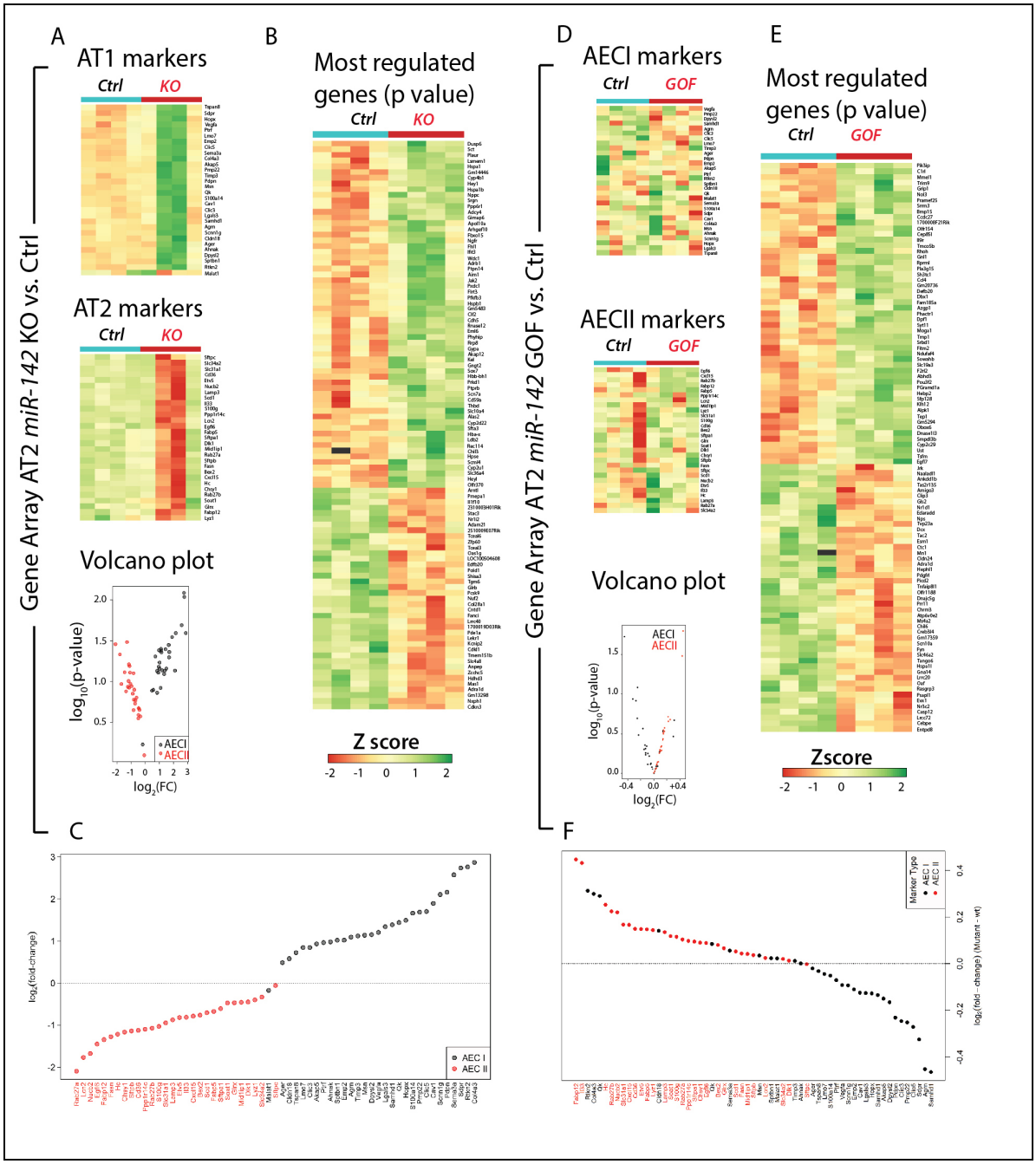


**Figure S5. High magnification of the heatmaps shown in Figure 3 and 5. (A-C)** Gene array analysis on FACS-isolated AT2 cells from E18.5 Controls and *miR-142* KO mice (n=4). **(D-F)** Gene array analysis on FACS-isolated AT2 cells from E18.5 Controls and *miR-142* GOF mice (n=4).

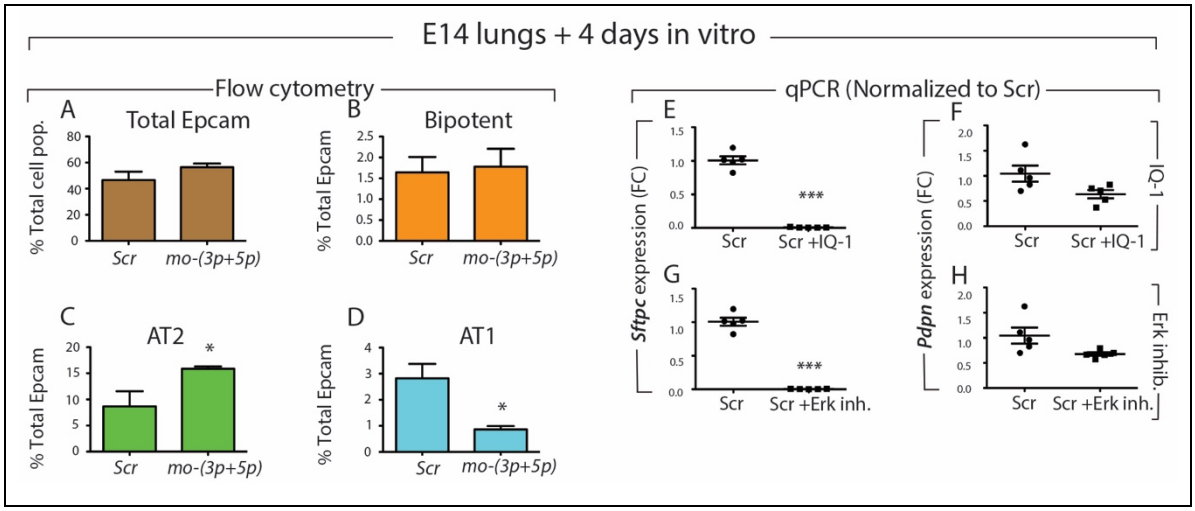


**Figure S6. *In vitro* alveolar epithelial lineage formation.** Flow cytometry analysis on the number of Epcam **(A)**, bipotent **(B)**, AT2 **(C)** and AT1 **(D)** cells in lungs cultured with morpholino *miR-142-3p* and *-5p* (*mo-(3p +5p)*) together. Expression of Sftpc and Pdpn upon IQ-1 treatment **(E, F)** or Erk inhibitor **(G, H)** treatment in E14.5 lungs grown *in vitro* with scramble and morpholino specific to *miR-142-3p* and *miR-142-5p*.

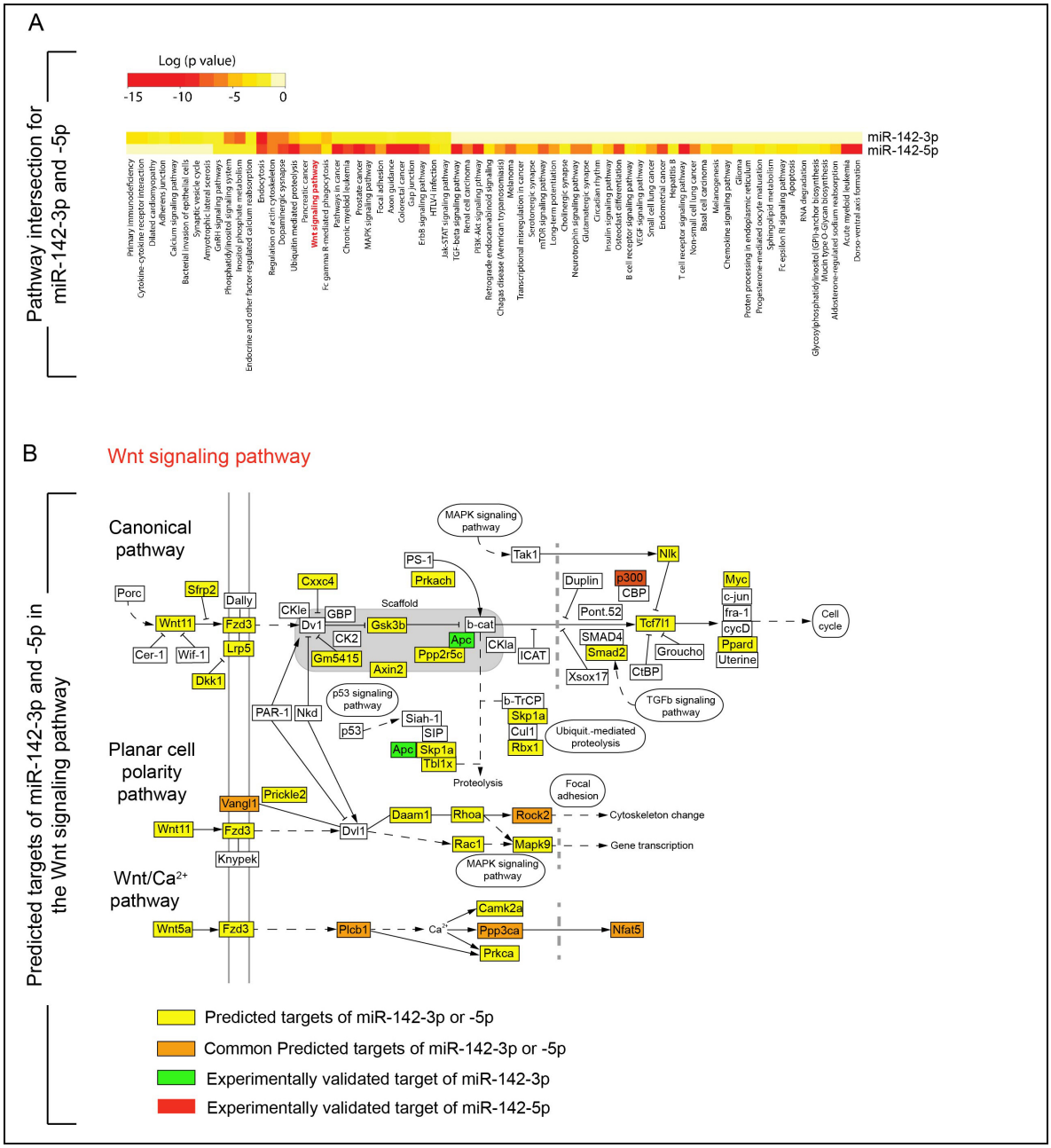


**Figure S7. Predicted targets of *miR-142-3p* and *miR-142-5p* using Diana-MicroT and Target Scan software prediction tools**. **(A)** Pathway intersection between miR-*142-3p* and *miR-142-5p.* **(B)** Predicted targets of *miR-142-3p* and *miR-142-5p* in the Wnt signaling pathway. Orange boxes: common predicted targets for both isoforms; yellow boxes: predicted targets for both isoforms; green boxes: experimentally validated target of *miR-142-3p*; red box: experimentally validated targets for *miR-142-5p.*

# 10. Acknowledgements

First and foremost, I would like to express my sincere gratitude to Prof. Dr. Saverio Bellusci for providing me an opportunity to carry out the research project in his lab. His suggestions and guidance on scientific research, encouragement and moral support are highly appreciated. He has been very kind and patient to teach me all the lab skills that is required to carry out my research project which made it possible to complete my Doctoral Thesis. His enthusiasm and passion for his work have always been a great source of inspiration throughout my doctoral studies.

It would be ungrateful on my part not to mention about the nice, friendly nature and supportive behavior of all the lab members and staff of Bellusci lab.

I am very much grateful to Heike Habermann who is always been kind, loving and supportive. Her assistance in every single administrative work is highly appreciated. I also would like to thank our Lab Manager Kerstin Goth who is also been highly supportive and caring. She has been always helpful in managing administrative as well as lab problems. We students have always benefited from her efficient lab management skills. Special thanks to Dr. Thomas Sontag for his valuable scientific suggestions and helping me in getting approval for my animal experiment protocols. I also appreciate the help of Jana Rostkovios especially for the technical support throughout my studies.

I am very much obliged to Dr. Gianni Carraro, who taught me most of the valuable techniques during my first my year of study. He has always been so generous to offer me his direct or indirect supervision and guidance throughout my Doctoral thesis. I am very much grateful to Dr. Elie El Agha, for his critical comments and guidance.

I would also like to offer my deepest gratitude to fellow students and other lab members in the Bellusci lab, Dr. Cho-Ming Chao, Dr. Alena Moiseenko, Vahid Kheirollahi, Salma Dilai, Mathew Jones, Negha Ahmadvand, Sara Taghizadeh, Arun Lingampally, Xuran Chu, Sirisha Bagari and Volker Zimmerman. You people are great and have always enjoyed working together. I wish you all best in your future endeavor.

I especially would like to thank Cho, Alena, and Vahid for being a very nice colleague and friend with whom, I cherish most of the memorable moments spent together inside and outside of the lab.

Special thanks to Ana Ivonne Vazquez-Armendariz for helping me with FACS measurements and Dr. Jochen Wilhem for Gene Array data analysis.
I would also like to thank Dr. Guillermo Barreto, for his valuable advice and constructive criticism.

I also acknowledge Dr. Daniel Zahner and animal caretakers Christian Eng, Sabrina Schick and Martin Stellwagen for their support in breeding the animals.
Finally, I would like to express my deep love and gratitude to my parents, for their kind support, patience, and their unconditional love.

Last but not the least, I would like to show my deepest gratitude to all the mice that were sacrificed for the completion of my study.